The Mousty Formation (Brabant Massif, Belgium): state of the art

ALAIN HERBOSCH

Université Libre de Bruxelles, Département Géosciences, Environnement et Société, Avenue F.D. Roosevelt 50, 1050 Bruxelles, Belgium; alain.herbosch@ulb.be.

I dedicate this article to T.N. Debacker for his outstanding contribution to the geological knowledge of the Brabant Massif and in gratitude for all the teachings he offered me during 25 years of friendly and fruitful collaboration.

ABSTRACT

The Mousty Formation has unique and particularly interesting lithological, mineralogical, sedimentological, metamorphic and tectonic characteristics which have been the subject of much research in connection with the new geological map of Wallonia, but also within the framework of a large amount of academic research, sometimes unpublished. An effort to synthesise and upgrade it in an updated framework seemed necessary. After a history of its definition, mapping and outcrop areas, the following topics are successively addressed in detail and illustrated with diagrams and photos: its lithostratigraphy with the probable discovery of its base near the Court-St-Etienne anticline, its well-constrained biostratigraphy and chronostratigraphy, a new estimate of its minimum thickness, its sedimentology—a subject little addressed until now—, and the resulting depositional sedimentary environment. Its geochemistry, never addressed, is comparable to black shale international standards, except for abnormally high manganese and very low calcium contents; high radon levels in buildings are related to the black slate presence in outcrops. Its mineralogy is rich in manganese-bearing metamorphic minerals, its metamorphism in which we go beyond the strict framework of the formation to deal with the entire southern outcropping rim of the Brabant Massif. Finally, the relationship between the Mousty Formation and the tectonic is discussed, with additional field data, in the context of the innovative and unifying concept of a low-angle extensional detachment called the Asquempont Detachment System. All these observations, some old and some very recent, discussed in the updated framework of the geology of the Caledonian basement of Brabant and in the global stratigraphy and palaeogeography of the lower Palaeozoic, allow us to renew in depth the vision we had of the Mousty Formation and of its place in the Brabant Massif.

1. Introduction

Multidisciplinary research has been undertaken on the Brabant Massif (Belgium) since the early 1980s under the instigation of L. André, W. De Vos, A. Herbosch, M. Vanguestaine and J. Verniers to mention only the initiators. Numerous publications, master and Ph.D. theses result from this research. They were then relayed by the program of the new geological map of Wallonia. These researches have brought a considerable amount of new data, sometimes unpublished, modified in the course of research progress, or drowned among other information. This justifies the present synthesis, which should make it possible to rectify some errors and inconsistencies and to considerably improve our knowledge of the Mousty Formation (MF) and its geological relationships with the Brabant Massif as a whole.

Why this formation in particular? There are many reasons: first because MF occupies a key tectonic position at the boundary between the core of the Brabant Massif and its periphery. Secondly, because its black shale lithology, often manganiferous, is almost unique in Belgium and shows a large variety of metamorphic minerals. Then, it is a fairly thick formation that occupies significant outcrop areas in the Dyle basin, where it appears on four of the new 1/25 000 geological maps of Wallonia. Some special features are worth mentioning, such as the "Terres noires" formerly exploited, the lydite (phtanite) used for tool making by the Neanderthals, and

significant radon anomalies. And finally, because I have acquired a deep knowledge of this formation as a result of the direction of several end-of-study dissertations and the survey of all the maps where it crops out.

2. History and definition of the Mousty Formation

The name of this formation comes from the hamlet of Mousty at the bottom of the Dyle valley, between Court-Saint-Etienne and Ottignies. The black shales of Mousty were described by Malaise in a descriptive way that was refined over time: "Between Mousty and Franquenies we find pyritiferous black phyllades, passing to a black graphitic schist… They contain beds of black quartzite with a mammillary surface" (Malaise, 1873, p. 27; translated from French as the following citations); in 1883a (p. 21), he wrote: "black layers of Mousty" and in 1883b, (p. 202): "Blackish-grey to bluish-grey ampelite and graphitic schists, phtanites". Later, Malaise (1909, p. M38) made it a Cambrian *assise*: "Sl1c Black phyllades and black graphitic and pyrite-bearing slates with lydite, and compact anthracitic limestone with *Primitia Solvensis*". Then he gave a detailed description (p. M33): "L'assise de Mousty est formée de schistes et quartzite stratoïde noirâtres, ampélite graphique, noire et pyriteuse, véritable schiste alunifère, avec blocs et amas de phtanite noirâtre compacte, à surface mamelonnée, souvent veiné de calcite et de calcédoine avec enduits de cette dernière substance; calcaire compact, noirâtre, anthraciteux, également en amas, mais moins fréquent que le phtanite" (The Mousty assise consists of blackish stratoid slates and quartzites, black and pyritic graphic ampelite, a genuine aluminiferous slate, with blocks and heaps of compact black lydites, with a hilly surface, often veined with calcite and chalcedony with coatings of the latter substance; compact, blackish, anthracitic limestone, also in heaps, but less common than the lydite). This description is very accurate and still relevant, except for the limestones associated with lydite which, despite unsuccessful research, we have never observed. And for good reason, recent investigations on the collections of Malaise show that there was a sampling error (F. Tourneur, pers. comm., 2000) and that there is thus no limestone associated with lydite. Historically, the remarkable and exhaustive description of the MF by Anthoine & Anthoine (1943) must be highlighted, even if their stratigraphic and tectonic speculations are not of the same quality.

3. Mapping and outcropping areas

The MF only outcrops in the Dyle basin where it has been mapped on numerous occasions: from the end of the 19th century the 1/40 000 scale maps by Mourlon (1893), then by Fourmarier (1920), de la Vallée Poussin (1930), Anthoine & Anthoine (1943), Legrand (1968), Michot (1977), De Vos et al. (1993) and more recently four 1/25 000 scale maps surveyed in the framework of the new Walloon geological map (Herbosch & Lemonne, 2000; Delcambre et al., 2002; Herbosch & Blockmans, 2012; Blockmans et al., in press). Finally, a larger-scale synthetic subcrop-map of the entire Brabant Massif outcrop area was published by Herbosch & Debacker (2018). The eastern half of this map is shown in Figure 1. The MF, in a shade of pink, can be seen on the western half of the map, where it forms a wide embayment that narrows towards the North and moulds the Central Brabant Domain. To the East, it continues under the Cenozoic cover to the SE of Perwez where it disappears.

3.1. Dyle and Orneau basins

As observed on the simplified geological map of Figure 2, MF outcrops over fairly large areas. Indeed, towards the NW

(Nivelles - Genappe map, Herbosch & Lemonne, 2000), this formation is observed along the Ri Cala River, from Château du Ruart to its confluence with the Dyle River (Noirhat), and in the Dyle valley, from Thy to its confluence with the Thyle River at Court-St-Etienne. In the SW, in the valley of the Ri d'Hé, from Fosty to Tangissart, and in the Ri de la Falise rivulet, the MF continues and passes to the younger Chevlipont Formation (Fm) (Fig. 2). In the Thyle valley, the outcrops continue to the N as far as Court-St-Etienne via La Roche and Faux, then along the Dyle as far as Mousty and a little further to the N (Chastres - Gembloux map, Delcambre et al., 2002; Wavre - Chaumont-Gistoux map, Herbosch & Blockmans, 2012). It is also observed to the E of Court-St-Etienne along the Orne River and E of Mousty in the Ri Angon brook until the E of the railway line in the Bois des Rêves Domain.

Towards the N, E and NW, the contact with the older formations of the Brabant Massif (Blanmont and Tubize formations) is faulted (Fig. 2). One can observe from the NW towards the NE: (1) the Genappe Fault (Anthoine & Anthoine, 1943; Herbosch & Lemonne, 2000) in the Ri Cala River as well as in the Dyle valley (Genappe), (2) the Orne Fault (Anthoine & Anthoine, 1943; de Magnée & Raynaud, 1944) in the Orne, Ri Angon and Dyle valleys (S of Ottignies), (3) the E-W Noirmont-Baudecet Fault (Delcambre et al., 2002) in the upper Orne valley (Noirmont). These faults are currently being interpreted as part of the Asquempont Detachment System (see § 14.1).

Still in the Dyle basin, the MF continues under the cover to the NW (Figs 1, 2; Waterloo - La Hulpe map, Blockmans et al., in press), in the triangle formed by the extension of the Orne Fault to the NW and the Genappe Fault to the NNW. Several boreholes have recognised the MF on the basis of its black shale facies (BGS (Belgian Geological Survey) boreholes 39/4-64, -149, -162, 39/8-418, -419). This triangle is clearly visible on the aeromagnetic map (Fig. 3) where it forms a zone of low magnetism flanked by two strongly magnetic ridges (Sintubin, 1997, figs 1B and C; Everaerts, 2000, fig. 7.12; Debacker et al., 2005a, fig. 13; Herbosch & Debacker, 2018, figs 7, 10). The MF also continues under the cover between the valleys of Ri Cala, Dyle, Ri d'Hé and Thyle, restricted to the E by the Orne Fault (Fig. 2). It continues again towards the S and SE along this fault which is extended by the Noirmont-Baudecet Fault where several boreholes intersected the black shale facies just S of Noirmont (Fig. 2, Orne valley, BGS 40/5-515, -516, -127; Delcambre & Pingot, 2002), then SE of Baudecet towards the Sauvenière farm (BGS 40/6-002; Fourmarier, 1920). Of all these boreholes, only the Noirmont borehole (BGS 40/5-515) has been identified by acritarchs. This is the easternmost point where this formation has been physically recognised. It continues even further E on the Perwez - Eghezée map (Fig. 1, S of Perwez; Pingot & Delcambre, 2006; Herbosch & Debacker, 2018, figs 8, 10).

3.2. Senne basin and other regions

The MF is totally absent in the Senne basin (Herbosch & Debacker, 2018, fig. 9), even in boreholes. The Oisquercq Fm, which outcrops in the Senne basin, was long thought to be a lateral variation of the MF (Fourmarier, 1920; Vanguestaine, 1977; Michot, 1980). The discovery of acritarchs in the Lessines and Oudenaarde boreholes dating the Oisquercq Fm from the former lower–middle Cambrian boundary (Vanguestaine, 1992; Herbosch et al., 1991; Herbosch & Verniers, 2013), definitively eliminated this hypothesis (Fig. 4). Moreover, MF is eliminated in the Senne basin by the Asquempont Fault, which belongs to an early detachment in extension called the "Asquempont Detachment System" (Debacker, 2001; Debacker et al., 2003, 2004a; Herbosch & Debacker, 2018). This is an important topic to which we will return later (§ 14.1). The MF has also been
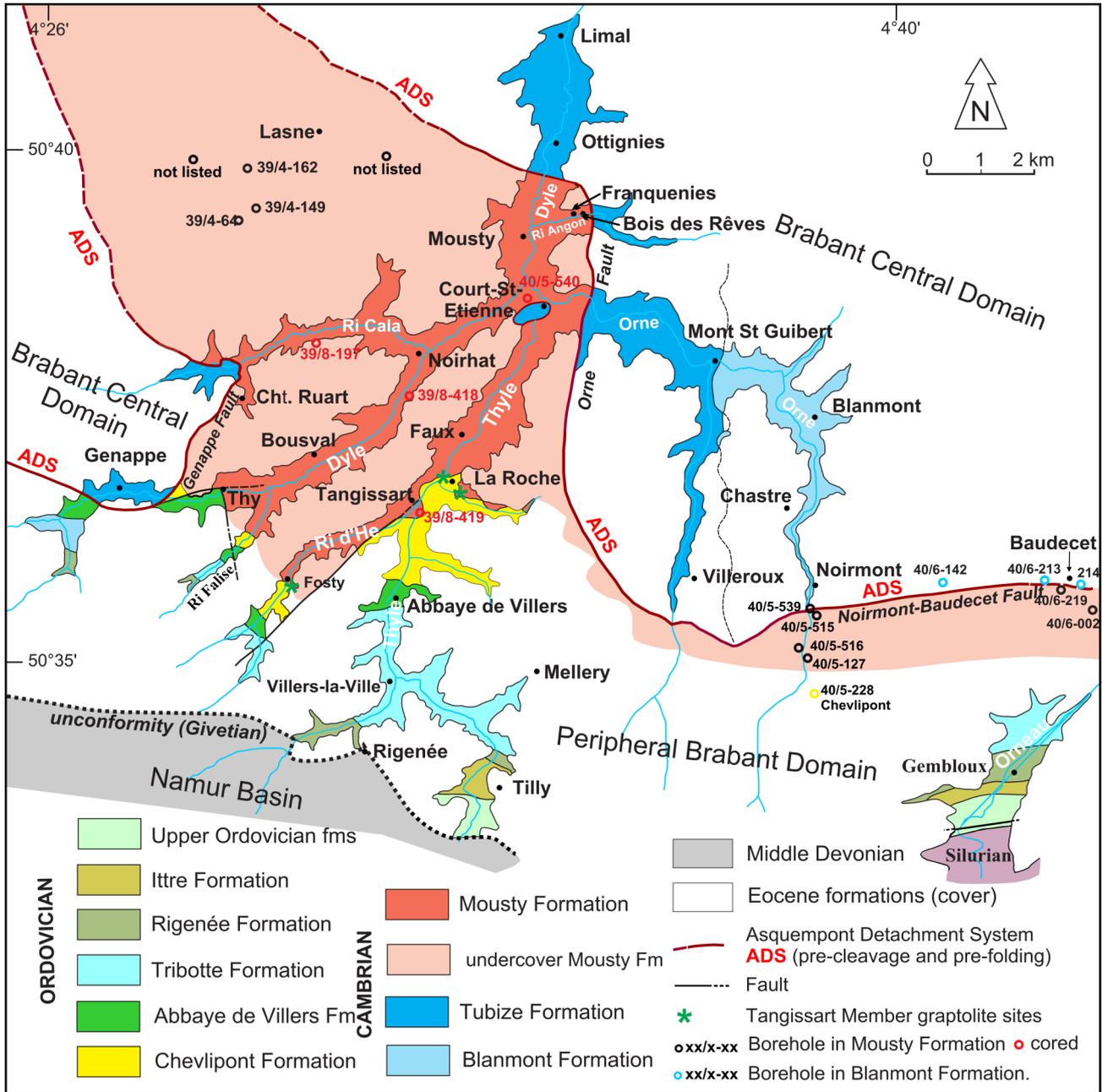
Figure 1. E-Brabant Massif map at ~1/200 000 scale showing the Palaeozoic geology from the Dyle basin outcrop area in the W to the Mehaigne outcrop area in the E. Geological formations were extrapolated under the Cenozoic cover where possible and represented in paler shades of the same colours as the outcropping zones. The position of the cross-sections A-A'-A'' and B-B' is indicated in red. The black rectangle shows the position of Fig. 2. Modified from Herbosch & Debacker (2018).

Figure 2. Schematic geological map of the Cambrian, Ordovician and Silurian basement from the Dyle and Orneau basins. Traces of the Orne, Noirmont-Baudecet and Genappe faults correspond to a low-angle extensional detachment called the Asquempont Detachment System (ADS, Debacker et al., 2003, 2004a). The ADS trace is only partly visible on the field and has been completed with the aeromagnetic and gravimetric maps (Fig. 3; Debacker et al., 2004a, fig. 13; Herbosch & Debacker, 2018, fig. 7).

erroneously described in other boreholes but only on the basis of the black shale facies criterion. It is in fact indistinguishable on this criterion alone, notably from the Jodoigne Fm and many Silurian formations.

3.3. Cross-section

Of the rare cross-sections that intersect the MF, that of Michot (1977, fig. 4) follows the Thyle valley between Rigenée to the S and La Roche to the N (Fig. 2). Unfortunately, it only shows the MF at its southern end where it undulates subhorizontally and is almost completely hidden by the Chevlipont Fm. The cross-section A–A'–A" of Figure 1 is very schematic due to the lack of sufficient outcrops between A and A' and the Cenozoic cover that hides the formations between A' and A".

4. Type of outcrops and major lithology

4.1. Type of outcrops and illustrated examples

Generally speaking, the MF comprises numerous but very small outcrops: road and railway embankments, bottoms and sides of sunken roads, disused quarries, temporary excavations, and ploughed fields on the edges of the plateau. These outcrops are still strongly altered, an alteration that is marked in the geomorphology by a significant widening of the Thyle, Ri Cala and Dyle valleys as the MF passes (Fig. 2). The cleavage is marked in a very variable way, sometimes very clear and sometimes barely visible, which is probably linked to the very important alteration of these slates. Some particularly extensive outcrops or outcrops with special characteristics are worth mentioning:
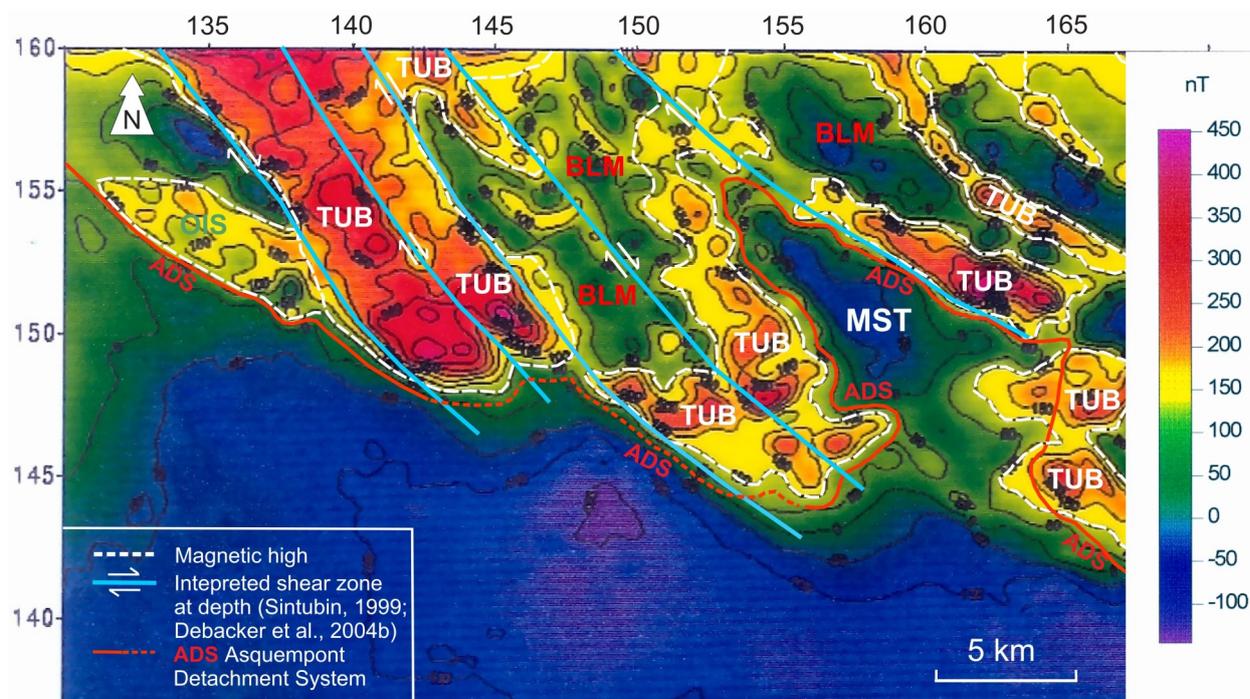
Figure 3. Aeromagnetic map (aeromagnetic field reduced-to-the-pole, de-corrugated flight line) of the southern part of the aeromagnetic high of the core of the Brabant Massif (after Everaerts, 2000, fig.1.12). Structural interpretations based on new geological maps and publications of Sintubin (1999) and Debacker et al. (2004a). In the centre right the non-magnetic triangle (blue) framed by a strong magnetic ridge (orange) corresponds to the Mousty Fm. Abbreviations: BLM = Blanmont Fm, TUB = Tubize Fm, OIS = Oisquercq Fm, MST = Mousty Fm, ADS = Asquempont Detachment System. Modified from Herbosch & Debacker (2018, fig. 5).

- The disused Franquenies quarry (N 50°39'32"/E 4°34'27"; Photo 8) presented one of the best outcrops in the lower part of the formation (see § 5.3).
- The E side of the former railway line 141 Ottignies - Genappe (now Ravel) at Court-St-Etienne, shows sub-continuous outcrops over 80 m to the SW (Photo 6; Delcambre & Pingot, 2002, fig. 8; from N 50°38'39.11"/E 4°33'43.37" to N 50°38'37.07"/4°33'37.46") (see § 5.2).
- The E slope of the railway line Ottignies - Charleroi km 37.2–37.3 near Tangissart (N 50°36'49"/4°32'32"E) shows sub-continuous outcrops of the upper part of the formation (Photo 7).
- The western slope of the N-S road down to the Thy Castle (Photo 2; N 50°36'46"/E 4°29'14") shows a discontinuous section about 150 m long.
- There is also a series of sunken roads that cut the SE slope of the Dyle valley such as those of Basse Lalou (Photo 4; N 50°37'05"/E 4°31'62") and Bois de la Tassenière (N 50°36'35" / E 4°29'65").
- At Court-St-Etienne, two outcrops are worth mentioning: a small but important near the Thyle (Photo 1; Rue Coussin Ruelle, N 50°38'31"/E 4°34'14"), a footpath up the N slope of the Orne (N of Rue de Tienne; N 50°38'39"/E 4°34'34").
- At Basse-Hutte, along a tributary of the Ri Cala, sandstone beds with a rarely seen high-density turbidite structure can be observed in an old excavation (Photo 5; N 50°38'07"/E 4°28'56").
- Finally, a typical temporary outcrop at Mousty hamlet is shown in Photo 3.

4.2. Main lithology

The only way to get a clear idea of the lithology is to take the largest possible samples and to saw them in the laboratory. Boreholes are few and cores are often weathered and fragmented and still little studied, except for the Bousval, Court-Saint-Etienne and Tangissart boreholes which have been described succinctly (location in Fig. 2; see Appendix 1).

This formation, at first glance rather monotonous, essentially consists of grey-blue to grey-black slates, graphitic and/or pyritic. Pyrite is rarely visible at the outcrop due to its alterability and the presence of graphitized organic matter gives these slates a more or less dark colour that stains the fingers. These mudrocks (>50% of grains less than 62 µm) usually show a silt content of less than 1/3 and are therefore clayslate if they have a laminar structure or claystone if they do not. The silt content is sometimes higher, and these are then mudslate (field classification of Lundegard & Samuels, 1980). The structure is sometimes massive without laminations but is more often laminar as in typical black shales with rhythmic variations in clay/silt and organic matter contents (Photos 11, 16, 19). The bedding is quite often marked by silty laminae (Photos 18, 19).

Episodically, graded siltstone or more often graded siltstone-mudstone are observed. They show plane parallel, oblique or convoluted laminations, characteristic structures of high-density turbidites (Bouma, 1962; Photos 5, 17) or most frequently of low-density turbidites (Photos 15, 18; Stow & Piper, 1984; Stow & Smillie, 2020). In the uppermost Tangissart Member which marks the transition to the Chevlipont Fm, fine laminae (mm) of wavy siltites appear within the grey slates and become more and more numerous (Photo 14; see § 5.4).

The presence of manganese, already reported by Dumont (1848, p. 421), seems to be quite frequent and randomly distributed throughout the formation. It is frequently marked on the outcrop by black to red alteration coatings with an iridescent look, clearly visible for example in the sunken path of Basse-Laloux or towards Thy. The Mn is expressed in thin sections by the presence of spessartine and other Mn metamorphic minerals (see Chap. 11). These minerals are small in size and therefore difficult to see even with a hand lens. Sometimes ilmenite sticks and garnet can be distinguished, for example near the Ferme du Cocq (N 50°63'86"/E 4°54'98").

Age (Ma)	Series	Stages	Brabant Massif lithostratigraphy	
			Groups	Formations

Figure 4. Stratigraphy of the Brabant Massif from Cambrian to Middle Ordovician (chronostratigraphy after Gradstein et al., 2020). Modified from Herbosch & Verniers (2013).

In the old Franquenies quarry (location Fig. 2; Photos 8 to 11; see § 5.3), the very graphitic and pyritic slates (with or without garnet) contain some extremely hard, siliceous lenses or beds previously described as "phtanite" (Photos 9, 10) by Malaise (1909). Nearby, very characteristic lydite in beds with a conchoidal structure (radiolarite?) were observed (Photo 12) in a small quarry located in the Bois des Rêves Domain (location Fig. 2; see § 5.3; Anthoine & Anthoine, 1943; Van Tassel, 1986; Herbosch & Blockmans, 2012).

4.3. Some clarifications on the use of terminology: phtanite, radiolarite, lydite

We will use these lithological terms in the following sense (e.g. Michel & Fairbridge, 1992):
- phtanite: black siliceous rocks observed in ancient series (Precambrian or Palaeozoic). They are made up of very small quartz crystals, organic matter and radiolarian remains. Term used in this sense in the old Belgian literature.
- radiolarite: rocks in which silica has been supplied by radiolarian tests. The radiolarites sensu stricto, red in colour (coloured by Fe and Mn), classically refer to the sedimentary cover of ophiolites, while the lydian are entirely black radiolarites where the remains of radiolarians are more difficult to identify.
- lydite: rock similar to radiolarites sensu stricto but grey or black in colour due to the presence of finely dispersed organic matter. Pyrite and some phosphate grains are also found, and radiolarians are rarely preserved.

5. Lithostratigraphy

5.1. Introduction

What is fundamental from the lithostratigraphic point of view in

the description of a formation is the definition of its base and its summit. In the present case, the lower contact of the MF to the N, NE and SW is everywhere with the Tubize Fm (Fig. 2), which is abnormal from the point of view of the stratigraphic succession. Indeed, the Jodoigne and Oisquercq formations, which should normally lie between the Mousty and Tubize formations (Fig. 4), are obviously absent. This is not a thrusting contact, as many authors thought (e.g. Fourmarier, 1920; Anthoine & Anthoine, 1943; Herbosch et al., 2001), but a low-angle extensional detachment called "Asquempont Detachment System" (ADS Figs 1, 2) which predates the Brabantian cleavage and folding (e.g. Debacker et al., 2004a; Herbosch et al., 2008, fig. 11; explanations in § 14.1). This early detachment brings the black slates of the MF into contact with the green siltstone and quartzite of the Tubize Fm or more to the SE with the massive quartzite of the Blanmont Fm (Fig. 2). In contrast, the top is well exposed in the Thyle valley where it has been named the Tangissart Member (Mbr) (Herbosch & Lemonne, 2000; Verniers et al., 2001). The transition is gradual and brings the black slates of the MF into contact with the grey wavy laminated siltstones of the Chevlipont Fm (Fig. 4; see § 5.4).

The geologists of the map of Wallonia (Herbosch & Lemonne, 2000; Delcambre et al., 2002; Herbosch & Blockmans, 2012) have not been able to find field criteria that allow this thick and monotonous formation to be subdivided and mapped into several members as Anthoine & Anthoine (1943) did. In the explanatory notes of the new maps of the Brabant Massif as well as in the synthesis concerning the MF (Verniers et al., 2001; Herbosch & Verniers, 2013) we had introduced, in addition to the upper Tangissart Mbr, the Franquenies Mbr we thought to be located towards the base of the formation, which is no longer correct as we will see below.

5.2. Identification of the base of the formation

A 161 m deep core hole drilled in the MF on the northern flank

Plate 1. Photo 1. Small outcrop of black slate to the E of Court-St-Etienne, Rue Coussin Ruelle just at the corner before the bridge over the Thyle (N 50°38'31"/E 4°34'14"). The hammer gives the scale. Precise location in Fig 5. Photo A. Herbosch, 2020. **Photo 2.** Outcrops on the W bank of the Rue Ferme del Wastez, 100 m NE of the Château de Thy (location on Fig. 27: 400 m E of the Château de Thy; N 50°36'46"/E 4°29'14"). Photo A. Herbosch, 2020. **Photo 3.** Temporary outcrop at Mousty. The unconformity with the Eocene cover sands is clean without conglomerate. The dark slate in cm beds shows a pronounced moving of the bank heads. Photo A. Herbosch, 2005. **Photo 4.** Outcrop in the sunken road to the S of Rue du Château, Basse Lalou (N 50°37'05"/E 4°31'62"). Genappe, Dyle valley E slope. Photo A. Herbosch, 2021. **Photo 5.** High-density turbidite beds in an old excavation. The siltstone beds are surrounded by well-cleaved slates (S1). Basse-Hutte brook, 50 m W of Chapelle du Ruart (location Fig 27; N 50°38'07"/E 4°28'56"). Details in Photo 17. Photo A. Herbosch, 2022. **Photo 6.** Sandstone bed dissected by the cleavage (S1), embedded in black slate. Lowermost part of the Mousty Fm in the E bank of the former Ottignies - Nivelles railway (now Ravel). SW of Court-St-Etienne, Dyle valley. Precise location in Figs 5, 6. Photo A. Herbosch, 2021. **Photo 7.** Black slate of the upper part of the Mousty Fm on the E bank of the Ottignies - Charleroi railway line km 37.2, level crossing of Tangissart (N 50°36'49"/E 4°32'32"). Thyle valley E slope. Photo A. Herbosch, 2020.
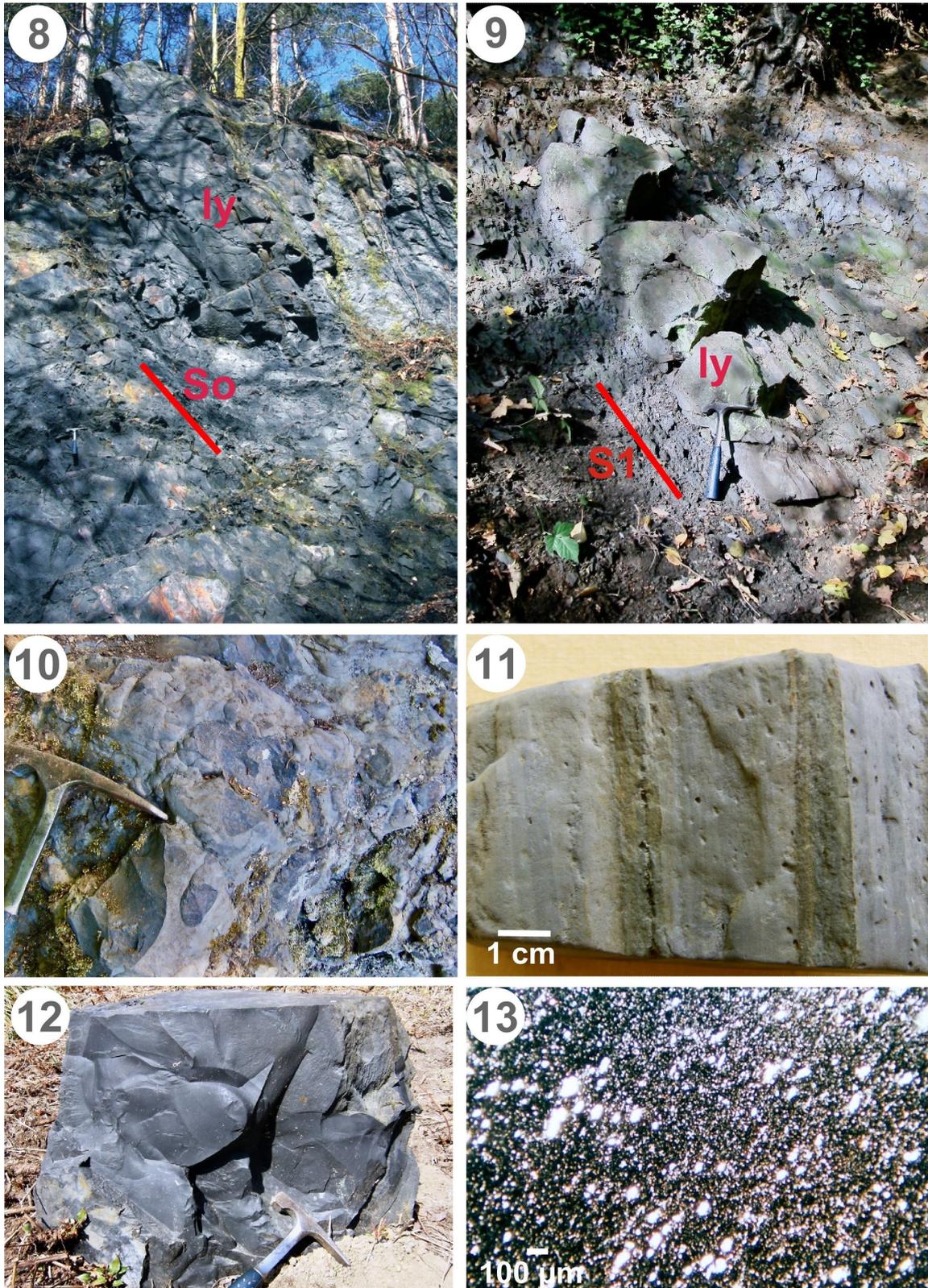
Plate 2. Photo 8. General view of the northern front of the Franquenies quarry in 2010. The black slates are graphitic and pyritic and sometimes contain garnets. The stratification (S0) is subvertical and the cleavage parallel to the wall. The upper part of the wall (Ly) shows a lydite level (phtanite). Exact location in Fig. 8. The hammer gives the scale. Photo A. Herbosch, 2010. **Photo 9.** Discontinuous and elongated lydite (ly) levels parallel to the cleavage (S1) which are embedded in black slate. West wall of the quarry in 2010. Exact location in Fig. 8. Photo A. Herbosch, 2010. **Photo 10.** Macrophoto of a lydite block fallen at the foot of the N wall of the quarry. It shows a botryoidal to reniform structure, a blue-black colour and a conchoidal break. Exact location in Fig. 8. Photo A. Herbosch, 2010. **Photo 11.** Macrophoto of a clayshale with a laminar structure marked by rhythmic variation in silt and organic matter. The holes in the two very brown levels and their colour probably correspond to the oxidation of the pyrite. Natural surface of an altered sample from the garden W of the Franquenies quarry. Exact location in Fig. 8. Photo A. Herbosch, 2010. **Photo 12.** Lydite slab observed in the garden of the "Bois des Rêves" Provincial Domain from the now disappeared stratified lydite quarry. The slab is jay-black, very hard, with conchoidal breaks, but does not show any mameliform or reniform structure. Photo A. Herbosch 2022. **Photo 13.** Sample of lydite from the stratified lydites of the "Bois des Rêves". The black matrix is formed by graphite, quartz, muscovite and the white elongated holes filled with microquartz underlining the stratification, are interpreted as phantoms of radiolarians (see text for explanation). Thin section, normal light. Photo A. Herbosch, 2010.
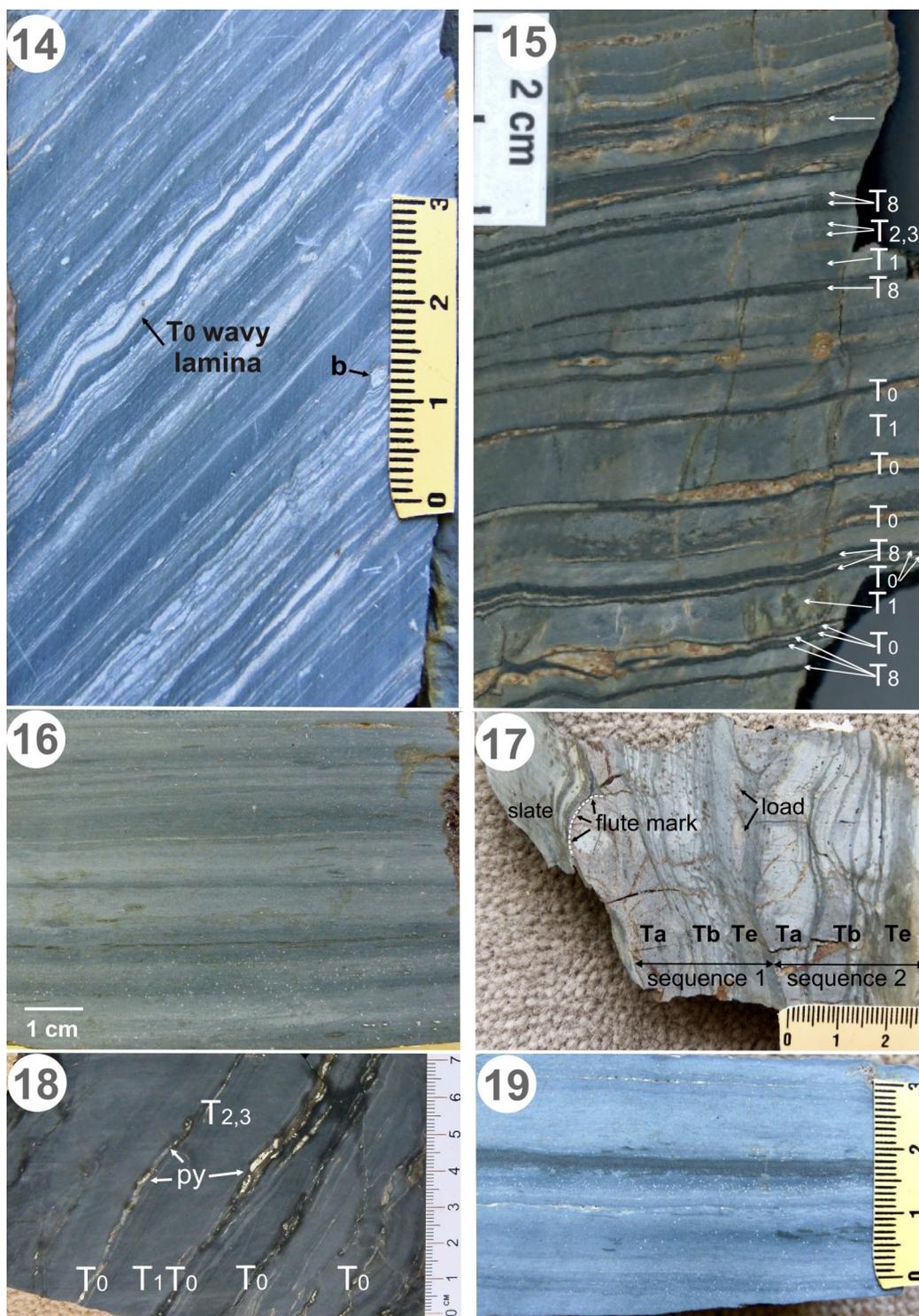
Plate 3. Photo 14. Laminar siltstone-mudstone with a wavy structure. Uppermost Tangissart Member of the Mousty Fm marking the progressive transition to the Chevlipont Fm. La Roche, E railway embankment, km 36.2 (N 50°36'48"/E 4°32'32"). The slates correspond to the hemipelagic sedimentation and the wavy siltstones are interpreted as episodic low-density mud-silt turbidites (see Fig. 11). b = bioturbation. T0 = basal lenticular wavy laminae. Sawn and polished sample. Photo A. Herbosch, 2022. **Photo 15.** Black slates with fine wavy siltstone layers from the W bank of the Rue Ferme del Waste near Thy (N 50°36'46"/E 4°29'14"; outcrop of Photo 2), Dyle valley. Facies interpreted as silt-mud low-density turbidites (Stow model), each basal silty lenticular laminae corresponds to the T0 division, base of the sequence model. The basal laminae are coloured orange by the alteration of pyrite formed by diagenesis due to the high porosity of the silt layers. See text. Sawn and polished sample. Photo A. Herbosch, 2010. **Photo 16.** Typical black slate, more precisely clayslate with a laminar structure marked by variations in clay/silt ratio and graphite content. Tangissart level crossing km 37.2 of the railway to Charleroi. Thyle valley, upper part of the formation. Sawn and polished sample. Photo A. Herbosch, 2022. **Photo 17.** Two sequences of high-density turbidites (Bouma model). The sequences are incomplete, the terms Ta, Tb and Te of the model can be observed. At the base of the first sequence, the trace of a flute mark in cross-section is underlined. Sample from Photo 5. Basse-Hutte brook, 200 m NW of the Chapelle du Ruart (location Fig. 27; N 50°38'07"/E 4°28'56"). Sawn and polished sample. Photo A. Herbosch, 2022. **Photo 18.** Laminar black slate, the silty laminae are filled with pyrite (py). Interpreted as mud-silt turbidites, the silty laminae formed the base of the T0 sequences. Noirhat borehole 39/8-418, 32.9 m, Thyle valley (location Fig. 2). Sawn and polished sample. Photo A. Herbosch, 2020. **Photo 19.** Typical black slate, more precisely clayslate with a laminar structure marked by variations in clay/silt ratio and graphite content. The bedding is marked by millimetre-sized silty laminae, in the centre a lamina with a high organic matter content. Franquenies quarry, Ri Angon valley (location Fig. 2). Sawn and polished sample. Photo A. Herbosch, 2022.
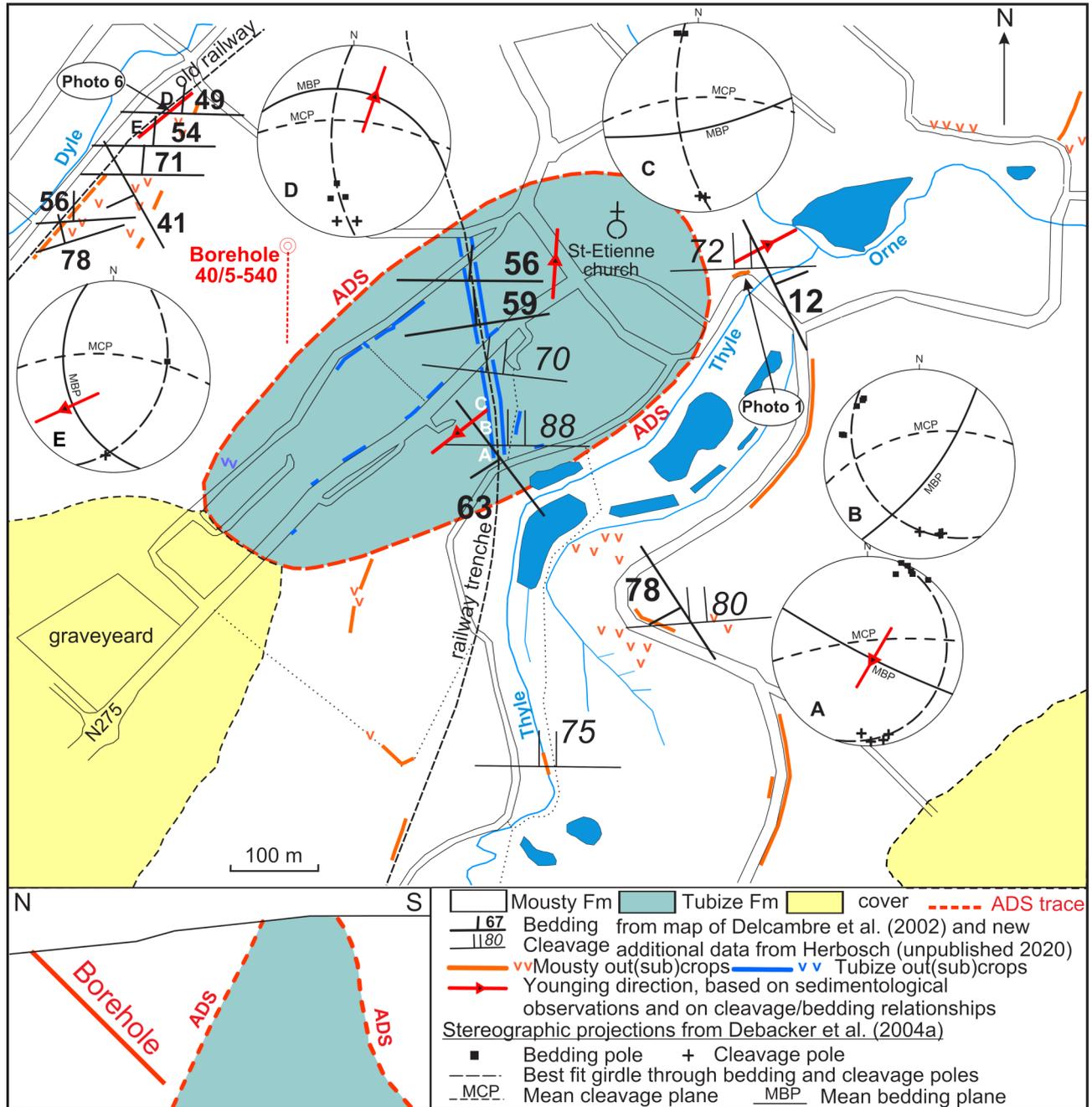
Figure 5. Detailed map of the Tubize Fm which is entirely surrounded by the Mousty Fm at Court-St-Etienne. This structure was formerly interpreted as a klippe. Mapping data revised in 2021 by Herbosch, cleavage and bedding partly from Delcambre et al. (2002) and Herbosch (unpublished data, 2002). The younging directions are based on sedimentological observations, cleavage/bedding relationship and stereographic projections by Debacker et al. (2004a, fig. 7). The data suggest a dome-like anticlinal structure, younging outwards (red arrows). Modified from Debacker et al. (2004a, fig. 7).

of the Court-St-Etienne anticline uplift (location in Fig. 5 borehole BGS 40/5-540) shows pyritic black slate and grey slate interbedded with thin siltstone and sparse sandstone which quickly changes to pyritic siltstone and sandstone levels and then to abundant sandstone (log in Fig. 6B) The siltstone and sandstone levels show no turbiditic structure. These lithologies, in particular the significant presence of siltstone and sandstone levels, are not known in the other drill holes or in the outcrops of the MF.

The wooded slope on the E side of the former railway line 141 Ottignies - Genappe (now Ravel), from 19 m after its NE junction with the Avenue des Prisonniers de Guerre (point 0 m of the section) to about 95 m SW (location NW corner of Fig. 5), shows sub-continuous outcrops with lithologies comparable to those of the upper half (above 70 m) of the Court-St-Etienne

borehole (Fig. 6B). This section is located about 250 m NW of the drill hole, roughly parallel to the direction of the strata. Despite the poor quality of this outcrop, we were able, after pruning and cleaning, to make a schematic log covering a distance of 76 m (from N 50°38'39.11"/E 4°33'43.37" to N 50° 38'37.07"/E 4°33'37.46"). The section shows mainly black graphitic slates with some thin beds of greyish siltstone and yellowish sandstone. The direction of the few layers is fairly constant with a slope of 45–60° S while the cleavage is always N-S with a very steep (>75°) slope to the N (Fig. 6A).

With regard to the comparison between the two logs in Figure 6, we have to realise that there is a big difference between the description of a poor-quality field section like the Ravel and the much easier and detailed description of the cores. In particular, it was not possible to distinguish in the field
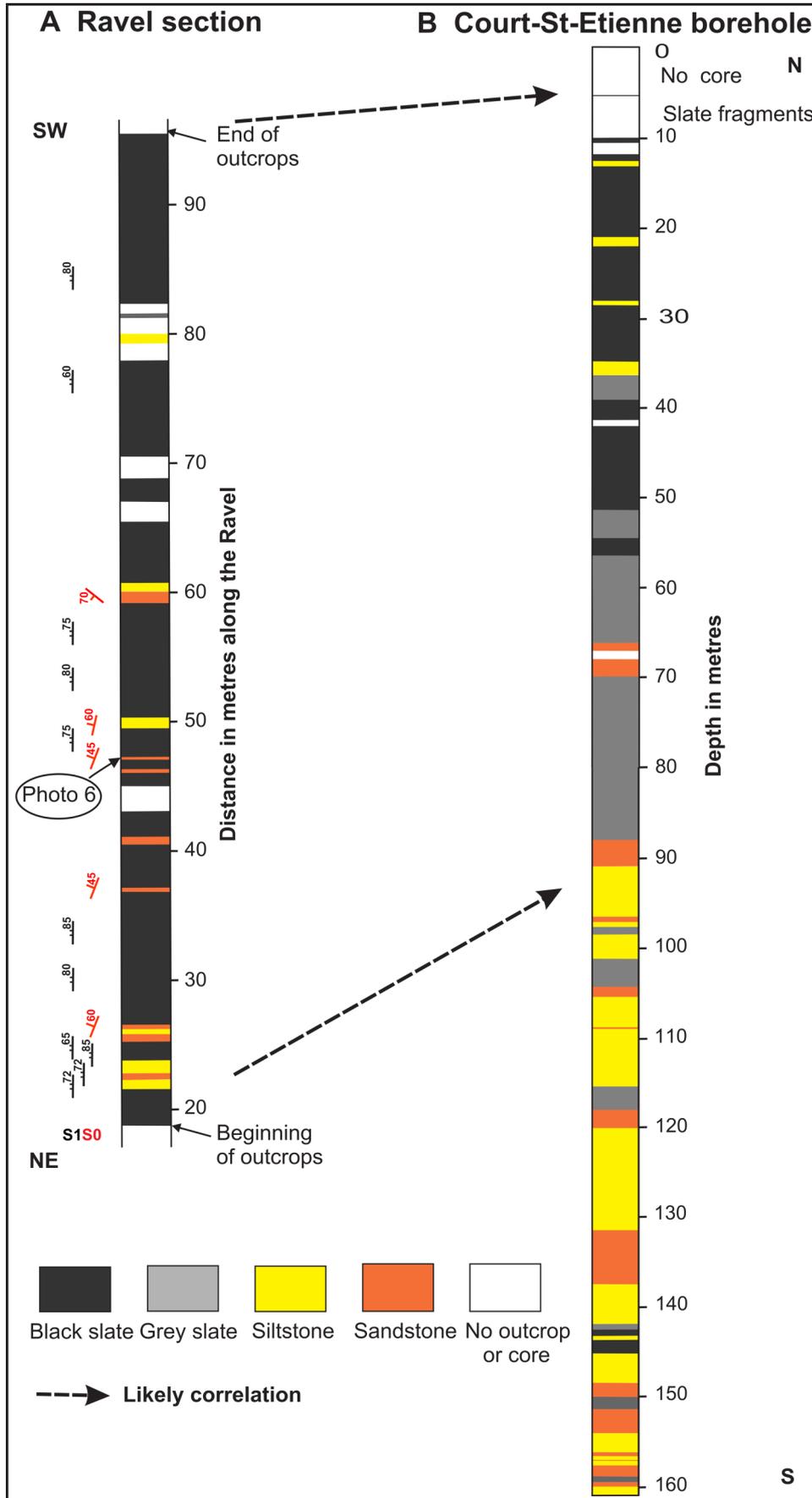
Figure 6. Comparison between: **A.** lithological section of the Ravel to the SW of Court-St-Etienne (old railway line), and **B.** simplified section of the Court-St-Etienne borehole described by Delcambre, Pingot & Herbosch (unpublished). The 0 m point of the Ravel section is at its intersection with the Rue des Prisonniers de Guerre. See text for explanation.

between black slate and grey slate as for the borehole. Therefore, the correlation in Figure 6 is made in a global way considering that the Ravel section is mainly formed by black slate, with siltstone and sandstone levels decreasing progressively from the beginning (19 m) to the top of the section (65 m). This allowed us to propose a global correlation of the Ravel section with the part above 70 m of the borehole. This correlation may even extend beyond the beginning of the Ravel outcrops. Indeed, below 70–80 m, siltstone and sandstone layers increase strongly in the borehole, which is not the case in

the Ravel section (Fig. 6).

Given the omnipresence of black slate facies and the absence of thick siltstone or sandstone levels in all the outcrops of the MF (except for a few sequences of fine-grained turbidite), it would be quite plausible that the Court-St-Etienne borehole and the homologous Ravel section partially cover not only the lowest part of the MF but also the highest part of the stratigraphically underlying Jodoigne Fm. Indeed, the upper unit of the Jodoigne Fm (Jodoigne Unit; Fig. 4) shows metric to decametric black slates alternating with rhythmic decimetric sequences of sandstone, siltstone and black slates (Herbosch et al., 2008, fig. 5). The comparison between the two lithologies seems compatible with this hypothesis. However, it should be born in mind that the Jodoigne Fm lies on the northern flank of the Brabant Anticline (Gette River, NE of Fig. 1), which is located several tens of kilometres away, and that consequently lateral facies variations are very likely.

It can therefore be concluded that the outcrops located between 19 and 95 m of the Court-St-Etienne Ravel most probably show the base of the MF, which is in excellent agreement with the anticlinal rise affecting the southern part of Court-St-Etienne (Fig. 5; see § 14.6). Nevertheless, this Ravel section could also partly be located in the upper part of the Jodoigne Unit of the Jodoigne Fm, as the lithologies are quite similar. A definitive answer to these hypotheses can only be given by the micropalaeontological analysis of the borehole. Another consequence is that, given this uncertainty, we cannot make it the base member of the MF, so we have informally called it the Court Unit (Fig. 7).

5.3. The Franquenies quarry and its surroundings: the presence of lydite within the black slate

This former quarry has been described many times in the literature (de Burtin, 1788; Malaise, 1883b; De Windt, 1897;

Leriche, 1921; Anthoine & Anthoine, 1943; Michel & Haesaerts, 1975; Van Tassel, 1986; Haulotte, 2002; Debacker et al., 2004a) because it shows one of the largest outcrops of the MF and also because of the quite exceptional presence of siliceous levels assimilated to lydite (phtanite). These lydites were well known to the Neandertals who used them to make tools. Highly graphitic slates from Franquenies even seem to have been traded as pigments, since they were found in the Scladina cave near Andenne and are known as the "Black Pigment of Sclayn" (Bonjean et al., 2015a, 2015b). Based on detailed drawings and investigations in the quarry (Anthoine & Anthoine,1943, fig. 2), bedding observations made during excavation work in nearby streets (Van Tassel, 1986, fig. 7), and new observations of bedding and cleavage, Debacker et al. (2004a, fig. 10) were able to construct a geometrical interpretation of the bedding trace (Fig. 8). The interpretation of these data shows the presence of steeply plunging folds, with a steeply plunging cleavage/bedding intersection lineation (type B folds, see § 14.2).

The quarry shows mainly very black slates which mostly contain pyrite, only visible on broken samples, and sometimes garnet and ilmenite in thin sections. The subvertical stratification and the cleavage, parallel to the outcrop, are difficult to observe due to the strong alteration. Blacker and more massive lydite levels are observed high up in the middle of the N wall (Photo 8) as well as on the W side where they form oblong metric lenses elongated in the cleavage within the black slates (location Fig. 8, Photo 9). These lenses aligned in the cleavage suggest a recrystallisation under tectonic stresses. At the foot of the N wall, very hard, black metric blocks could be found with a conchoidal fracture whose surface shows botryoidal and reniform structures also characteristic of recrystallisation (Photo 10).

In contrast, in a small quarry located at the NW end of the Bois des Rêves Provincial Domain, 160 m to the E of the
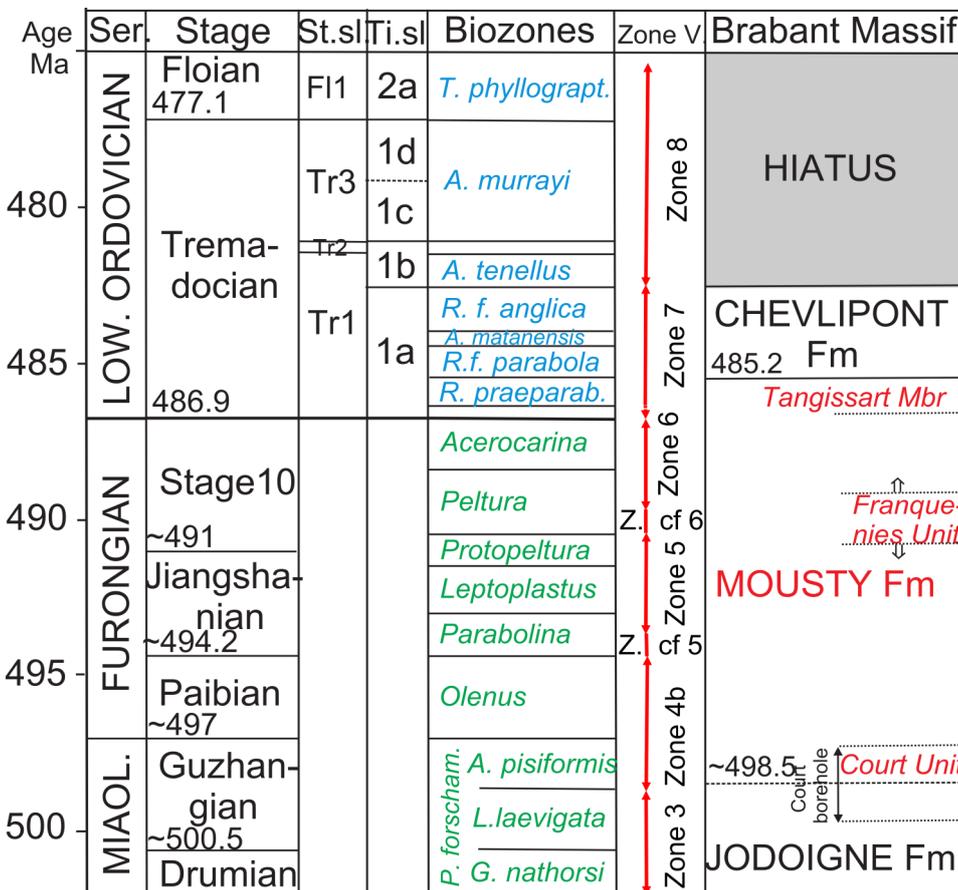
Figure 7. Detailed stratigraphy of the Mousty Fm and adjacent formations. Chronostratigraphy, trilobite and graptolite biozones after Peng et al. (2020) for the Cambrian and Goldman et al. (2020) for the Ordovician. Time Slice (Ti. sl.) after Webby et al. (2004) and Stage Slice (St. sl.) after Bergström et al. (2009). Vanguestaine informal acritarchs biozones (Zone V.) reinterpreted by Herbosch (2021, fig. 5). See text concerning Franquenies Unit and Court Unit.
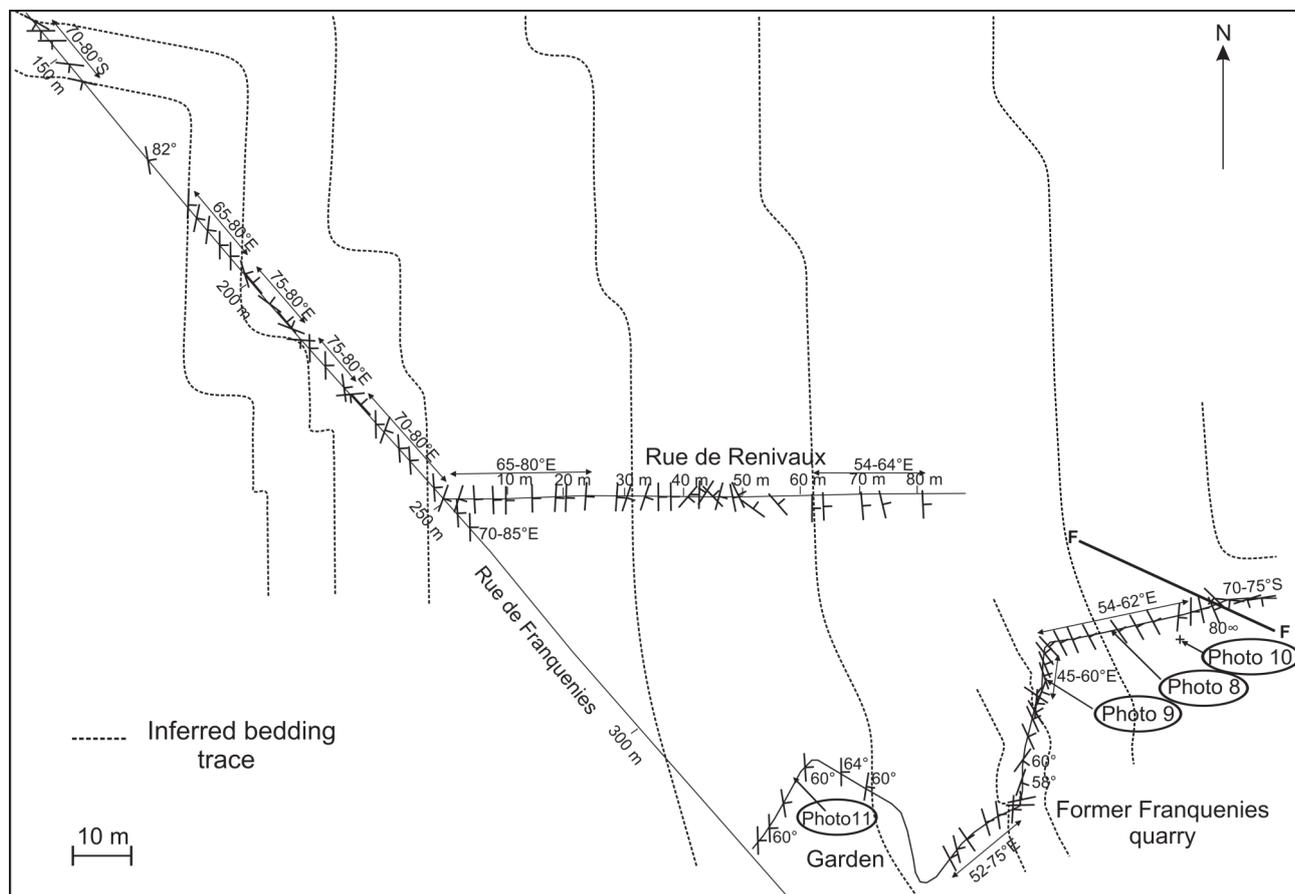
Figure 8. Former Franquenies quarry redrawn from the map of Anthoine & Anthoine (1943, fig. 2), bedding observations made in two nearby streets (Van Tassel, 1986, fig. 7) and new observations of bedding and cleavage by Debacker et al. (2004a). Probable bedding trace was constructed using the king band method. Modified from Debacker et al. (2004a, fig. 10).

Franquenies quarry, the lydian rocks appear in regular decimetric seamless beds that continue regularly over a thickness of three metres with a direction of N20–30°W and a dip of 70–80° E (location Fig. 2; Anthoine & Anthoine, 1943, p. M73; Van Tassel, 1986; Herbosch & Blockmans, 2012; N 50° 39'32"/E 4°34'37"). They are jay black in colour, very hard, with conchoidal breaks, but do not show any mammillated or reniform structure. This unique outcrop has disappeared since 1996 when we last observed it. Nevertheless, we have observed in the gardens of the Bois des Rêves Domain some lydian slabs which come from this quarry (Photo 12). We will see later (§ 8.4) that the sample from this quarry presents a microscopic structure with small-elongated holes of microquartz (Photo13) which is not found in the various varieties of lydites from the Franquenies quarry (Herbosch, unpublished; E. Goemaere, pers. comm., 2020).

Interestingly Anthoine & Anthoine (1943, p. M73) have described lydite in the vicinity of the Franquenies quarry and also in some other places. During the survey of the geological maps of the Brabant Massif we observed lydite blocks scattered on the surface of the ground and in outcrops not only in the Franquenies quarry, the small quarry of Bois des Rêves and the bed of the Ri Angon, but also towards the S in an area extending into the Bois de Franquenies to its southern limit near Brûlotte (about 1 km S of Franquenies). A block of about two cubic metres is located in the back garden of the Brûlotte Music School. We did not observe anything on the W bank of the Dyle, where outcrops are very scarce. A facies very close to these lydites also crops out in the Ri Cala valley, near a pond 200 m E of the Chapelle du Ruart (location Fig. 2; Walraevens,

1982; Herbosch, unpublished; N 50°63'44"/E 4°49'05"). This facies had already puzzled Anthoine & Anthoine (1943, p. M94): ".... we find aligned kidneys of a rock resembling a blue phtanite with fine paste whose surface becomes green by alteration". Although the internal stratigraphy of the MF is not well known, it is highly unlikely that we are at the same stratigraphic level as the Franquenies quarry. These same authors report fragments of these same hard rocks in the upper part of the formation near Tangissart, which we confirm. These observations seem to show that lydites can be found everywhere in the MF, although they are much more frequent in the Franquenies quarry and its surroundings, which has sedimentological consequences as we shall see in Chapter 8.

The Franquenies quarry is located about 2 km N of the Ravel section that shows most probably the base of the MF and 500 m S of the Asquempont Detachment Fault which marks the transition to the Tubize Fm (Fig. 2; see § 5.3). It is therefore highly probable that we are stratigraphically within the first third of the formation. However, we do not know the extent of the folds affecting the MF or the place where the detachment cuts it towards its base. So, we cannot predict the exact position of the Franquenies area within the formation. Therefore, we cannot make it a member, so we have informally called it the Franquenies Unit (Fig. 7).

5.4. The uppermost Tangissart Member

The uppermost part of the formation, named the Tangissart Mbr (Fig. 4; Herbosch & Lemonne, 2000; Verniers et al., 2001; Delcambre & Pingot, 2002), is characterized by the progressive

and recurrent development of clearer millimetre-sized silty laminae within the black slate. These laminae show a wavy structure and when they are thicker, they show oblique laminations at their base (Photo 14, see § 8.2). It was in this member that Lecompte (1948, 1949) discovered dendroid graptolites (location Fig. 2; see Chap. 6). The disappearance of the last thick interval of black slates without silty laminae marks the top of this transitional member and the beginning of the Chevlipont Fm (Fig. 4). The thickness of this member is not known precisely due to the lack of continuous outcrops, but it should not exceed a few hundred metres.

5.5. Contact with the Eocene cover

The contact with the Eocene cover has rarely been observed. It is of course in angular unconformity (Photo 3) and sometimes underlined by a conglomerate a few centimetres thick made up of sandstone centimetric debris or at the Franquenies quarry, by debris of black slate perforated by marine organisms (already noted by Dupréel, 1937).

5.6. Synthesis

Although we have not been able to subdivide this thick formation into members, we have nevertheless succeeded in identifying a section where its base is most likely present. Its summit, the Tangissart Mbr, has been recognised since the 1990s. The base of the MF, identified thanks to the Court-St-Etienne borehole, is most likely located in the outcrop approximately 80 m long on the E slope of the Ravel (former railway line) located 250 m to the N of the borehole (Fig. 5). Moreover, given the unusual presence for the MF of a few levels of siltstone and sandstone in this section, the hypothesis of its partial belonging to the Jodoigne unit of the upper part of the Jodoigne Fm is not impossible. As a result, we could only make an informal unit, the Court Unit (Fig. 7).

The area around the Franquenies quarry situated in the lower part of the MF could be described with particularly interesting occurrence of lydite, but the impossibility of locating it stratigraphically with precision led us to make it an informal unit, the Franquenies Unit (Fig. 7). An important part of the formation, which occupies large areas to the S and SW of Court-St-Etienne in the Ri Cala, Dyle, Ri d'Hé and Thyle valleys (Fig. 2), is very poorly known due to a lack of good or continuous outcrops. Nevertheless, the present work represents a real improvement on the previous situation where only the top of the MF was known and the Franquenies quarry was erroneously set as the lower member (Verniers et al., 2001; Herbosch & Verniers, 2013). Only palaeontological investigations, in particular on the Court-St-Etienne borehole, will confirm these preliminary hypotheses.

6. Bio- and chronostratigraphy

No macrofossils have ever been observed in the MF except in its very upper part, the Tangissart Mbr, where Lecompte (1948) found dendroid graptolites and poorly preserved trilobites (identified as cf. *Platypeltis croftii* Callaway by Dr C.J. Stubblefield). Other discoveries of graptolites and trilobites were made in the 1950s, as reported by Van Tassel (1986), who also found poorly diverse linguliformean brachiopods (see Laibl et al., 2023). The discovery, initially made in the railway embankments between La Roche and Faux (spot 72 = km ~37.4 and spot 74 = km ~36.5; spot 74 is described in detail in figure 8 of Van Tassel, 1986), was later extended (Lecompte, 1949, fig. 1) to two other sites in the same member: one in the Ri de Ste-Gertrude 700 m NE of the La Roche railway station (spot 95

Ch.), and the other on the right bank of the Ri d'Hé near Fosty (spot 26G.; see asterisk in Fig. 2). This author and Van Tassel (1986) described many other graptolites occurrences in the Chevlipont Fm. These graptolites have been identified by Bulman (in Lecompte, 1949) as belonging to a single species *Dictyonema flabelliformis*, probably *sociale var.* (now *Rhabdinopora flabelliformis*). In summary, these early works enabled a rough correlation between the Belgian *R. flabelliformis* fauna and the British *R. socialis-flabelliformis* biozones which were used until recently (Verniers et al., 2001; Herbosch & Verniers, 2013). Trilobites from the Tangissart Mbr collected by Lecompte (1948) and those reported by Van Tassel (1986) were recently studied by Laibl et al. (2023), who identified *Platypeltoides* cf. *croftii*, confirming Stubblefield's (in Lecompte, 1948) preliminary identification, and an unidentified asaphid species.

Wang & Servais (2015) have taken up the exhaustive study of the *R. flabelliformis* of the Brabant Massif and the Condroz Inlier (Wépion borehole; Graulich, 1961) stored in collections. They have shown that the graptolites of the Tangissart Mbr belong to the *Rhabdinopora praeparabola* Biozone which is found at the extreme base of the Tremadocian, precisely the lower half of the time slice 1a of Webby et al. (2004) which extends from 486.5 to 485.2 Ma using the graptolite biozonation of Goldman et al. (2020, fig. 20.4) (Fig. 7). Other graptolites collected in the Chevlipont Fm belong to the *R. f. parabola* and *R. f. anglica* biozones forming the upper part of time slice 1a which extends to the middle of Tremadocian, c. 482 Ma (Herbosch, 2021).

The MF was difficult to date by acritarchs because the outcrop samples were always sterile (Vanguestaine, 1974; Martin, 1977; extensive personal trials with Vanguestaine). It should be noted that neither the Franquenies quarry nor the Court-St-Etienne borehole have been dated palaeontologically. Finally, it was dated by acritarchs in boreholes located in the western part of the Brabant Massif. They gave an age from the lower and middle part of the upper Cambrian for the Eine (BGS 84E1372, 62 m) and the Vollezele (BGS 100E010, 50 m) boreholes (Vanguestaine et al., 1989a, b; Vanguestaine, 1992, figs 6, 8). The biostratigraphic extension of acritarchs observed in these two boreholes ranges from the informal Zone 4b (*Agnostus pisiformis* Biozone) to the upper part of the Zone cf 6 (*Peltura* Biozone; Fig. 9) using the Vanguestaine acritarch zones reviewed by Herbosch (2021, fig. 5). These biozones correspond to the uppermost part of the Guzhangian, the entire Paibian and Jiangshanian stages as well as the lower part of Stage 10 (Fig. 7; Peng et al., 2020).

The destructive borehole of Court-St-Etienne 40/5-539 drilled along the northern side of the Asquempont Detachment System in the Orne valley (Fig. 2: Noirmont-Beaudecet Fault) penetrated the Bruxelles Fm to a depth of 19.5 m, then the Blanmont Fm to 43.5 m, and finally the MF to 69 m. This latter formation can be seen in its classic black slate facies. Cuttings yielded abundant and relatively poorly preserved acritarchs. According to Vanguestaine (written comm, 1998) the assemblage is characterized by "the relative abundance of Prismatomorphitae (*Timofeevia*, *Cristallinium* / *Vulcanisphaera*) compared to Diacromorphitae (*Acanthodiacrodium* / *Arbusculidium* / *Ladogella*) and Galeates (*Cymatiogalea* / *Stelliferidium*), a ratio which is characteristic of the former upper Cambrian". He added that this assemblage suggests a correlation with the top of Rv4 and Rv5 from the Stavelot Inlier which corresponds to the whole of Stage 10 (zones cf 6 and 6; Fig. 7). This together with the presence of several specimens of ?*Lusatia* sp. as in the late Cambrian from Montcornet-en-Ardennes (Rocroi Inlier; Ribecai & Vanguestaine, 1993) and the absence of Tremadocian markers, lead to a late Cambrian age.
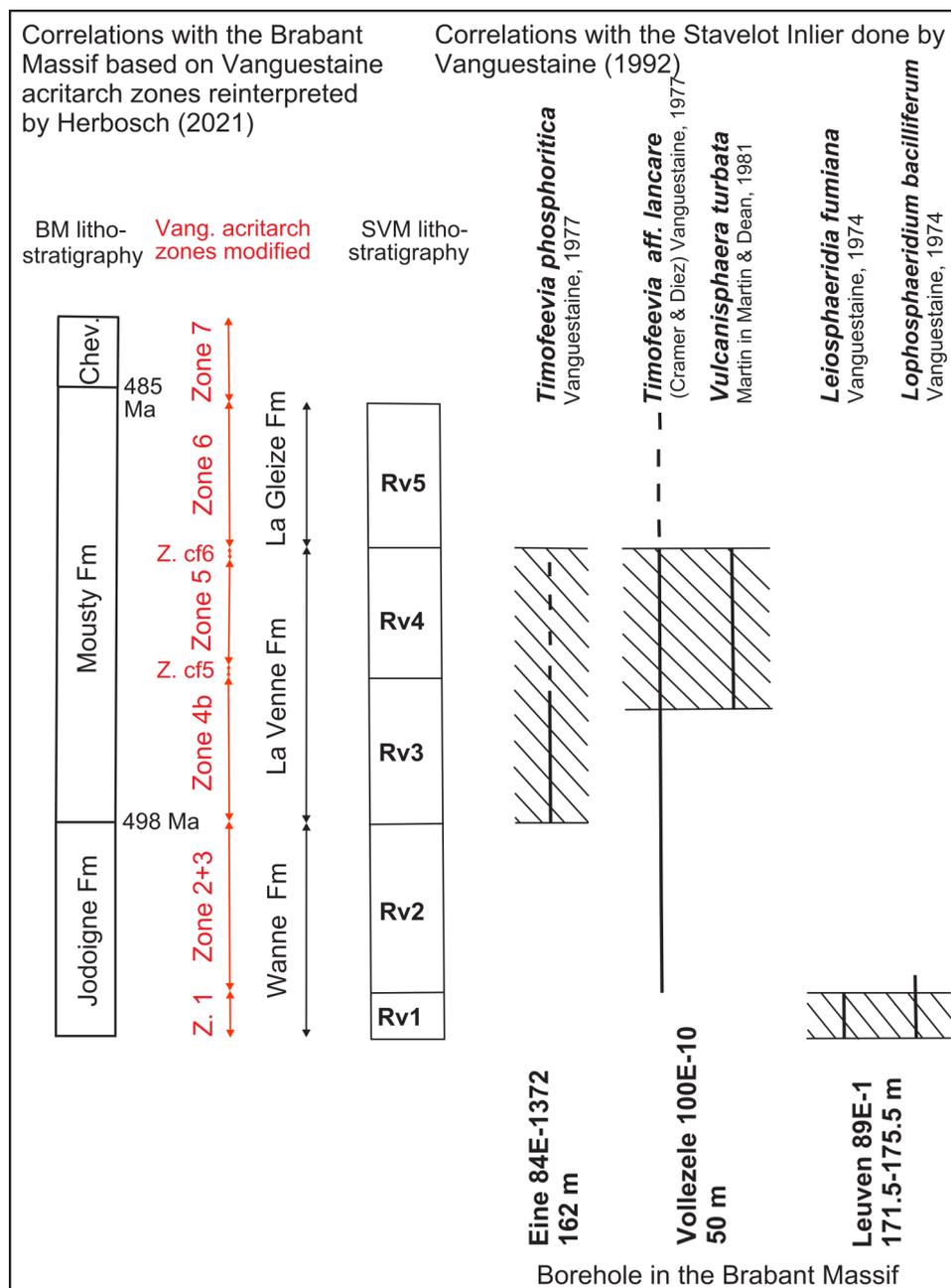
Figure 9. Biostratigraphic correlations for the dating of the Mousty Fm from the acritarchs found by Vanguestaine (1992, fig. 8) in the Eine, Vollezele and Leuven boreholes, which are compared with the litho- and biostratigraphy of the Stavelot Inlier (right part). Correlations with the Vanguestaine acritarch zones reinterpreted by Herbosch (2021, fig. 5) (left part). The Leuven borehole shows turbidite sequences and has therefore been assigned to the Jodoigne Fm (Herbosch et al., 2008).

The attribution of borehole 40/5-539 to a late Cambrian age must currently be considered with caution as none of the taxa mentioned are restricted to the late Cambrian and the absence of Tremadocian marker is not significant (T. Servais, pers. comm., 2023). Consequently, we will ignore this observation, which does not affect the conclusions of this chapter, as the top of the formation is extremely well dated by graptolites.

In the global Cambrian stratigraphy (Peng et al., 2020), these ages correspond to the uppermost Guzhangian and the Paibian, Jiangshanian and Stage 10 from the Furongian Series (Fig. 4). The graptolites of the Tangissart Mbr belong to the *Rhabdinopora praeparabola* Biozone which proves the earliest Tremadocian age of that upper member (Wang & Servais, 2015). It can be concluded, with caution, that the age of the MF extends from the upper Guzhangian to the earliest Tremadocian (Figs 7 and 9), which corresponds to a time interval of about 13 m.y. This formation thus includes the basal part of about 1 m.y. of the Tremadocian and, consequently, crosses the Cambrian–Ordovician boundary. However, while the upper limit is very precise and reliable given the recent nature of the data, the lower limit is not so accurate and appears to be in the upper

Guzhangian (dotted line in Fig. 7) if we trust the results of Vanguestaine (1992) which may be out of date.

7. Thickness of the formation

The latest estimate of its thickness is 1500 m (Herbosch & Verniers, 2013). It is not possible to use the fieldwork as a basis for even an approximate estimate of the thickness of the MF, as the outcrops are too small and too scattered to have an idea of the fold pattern. A lower limit to the thickness of the formation is given by adding the thickness of the four boreholes that were drilled in probably stratigraphical distant locations (Fig. 2). This gives: 160 m (Court-St-Etienne) + 50 m (Tangissart) + 50 m (Noirhat) + 35 m (Bousval) which makes roughly a total of about 300 m.

An estimation based on the Chastres - Gembloux geological map (Delcambre et al., 2002) can be obtained with a few realistic assumptions. Indeed, between Gembloux and the Asquempont Detachment System (ADS), the northern flank of a syncline shows strata that are fairly constant in direction (near E-W) and dip (65–75° N) (Fig. 1 section B-B' and Fig. 10). A
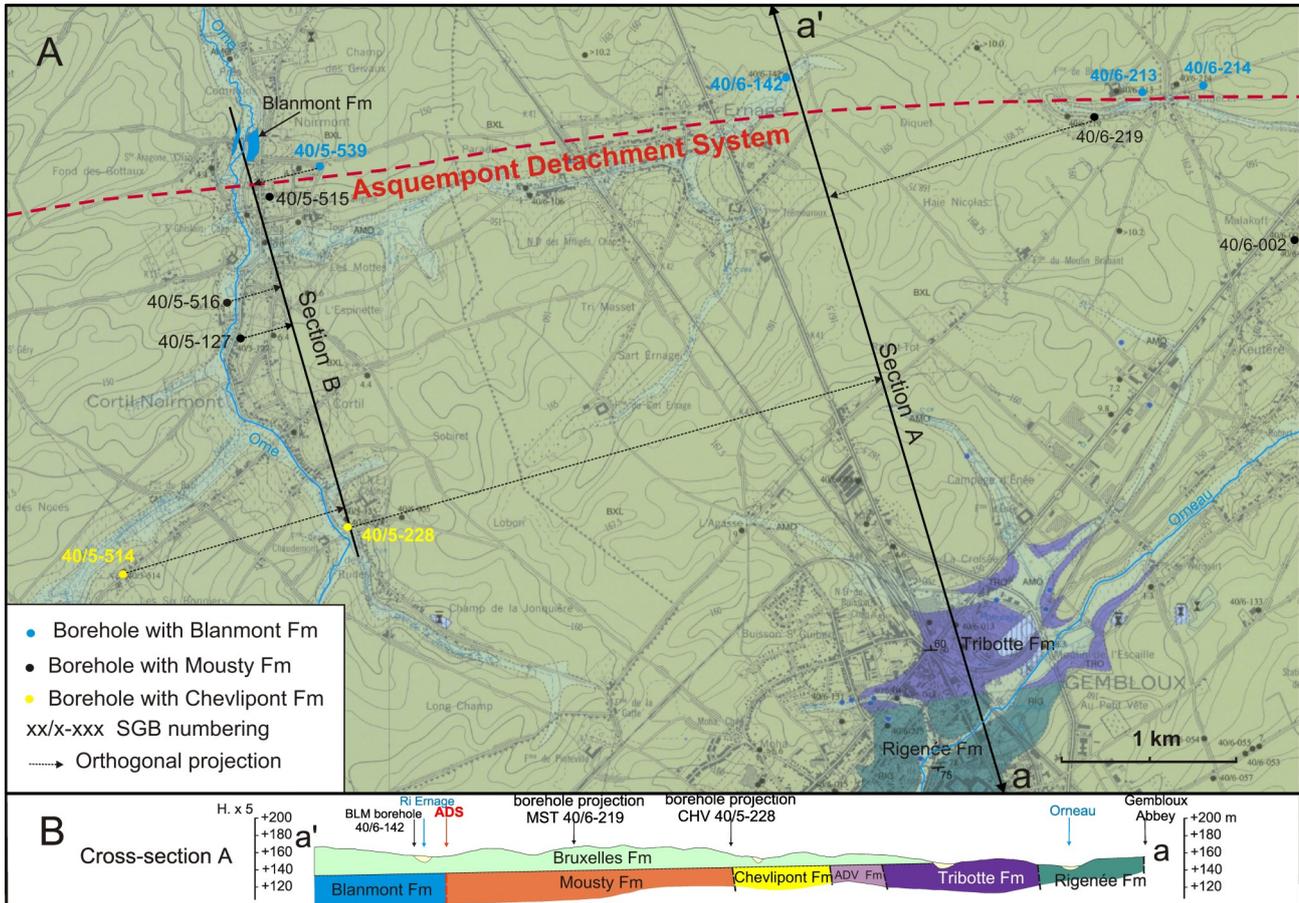
Figure 10. Estimation of the thickness of the Mousty Fm on two NNW-SSE sections in the northern flank of the Cambrian–Ordovician Gembloux syncline, which is interrupted to the N by the Asquempont Detachment System (ADS; Fig. 1 section BB'). **A.** Geological situation on the Chastre - Gembloux map (Delcambre et al., 2002). The Cenozoic cover (greenish) masks most of the basement. Several boreholes precisely constrain the ADS trace. The position of sections A and B perpendicular to the direction of the strata and the projection of the nearest boreholes are also shown. **B.** Cross-section aa' at the same scale. See text for explanation.

large part of the MF is most probably present in its northern part as five boreholes have identified it on a lithological basis, including borehole 40/5-539 located right next to the ADS (Fig. 10; see Chap. 6) dated with caution to the Cambrian. The Abbaye de Villers, Chevlipont, Mousty and partly Blanmont formations are known only from boreholes in the southern part of the same syncline, where they are hidden by the Cenozoic cover. The measurement of the apparent thicknesses along section A drawn perpendicularly to the direction of the strata gives an apparent thickness of ~1540 m (Fig. 10A). The section B, parallel to the previous one, located in the same syncline 4 km to the W in the Orne valley (Fig. 10A), has the advantage of being closer to the drillings in the Blanmont, Mousty and Chevlipont formations. This section gives an apparent thickness of ~1880 m. The discrepancy between these two estimates is due to the poor positioning of the Chevlipont Fm (with no close drilling in section A) whereas the position of the ADS is well known both by boreholes and geophysics (Herbosch & Debacker, 2018, fig. 7). This is an estimate which is only correct if the syncline structure continues to the N and if the dip remains more or less constant in the area under cover. If we assume that the average dip in the hidden zone is 70°, the real thickness range is from about 1300 m to 1600 m. Furthermore, as we have no palaeontological control of the boreholes in the MF, we do not know what proportion of the formation is present. Furthermore, we do not know the dip of the Asquempont Detachment System Fault which limits the MF to

the N. The estimated thickness is therefore surely a minimum thickness.

In conclusion, the thickness of the MF can be estimated to be at least 300 m and is much more likely to be at a minimum in the range 1300–1600 m. This minimum high thickness seems to be reasonable in view of the subsidence curve, which shows that Megasequence 1 corresponds to a very subsiding rift with more than 9 km of sediment deposited during the Cambrian (Debacker, 2001; Verniers et al., 2001; Linnemann et al., 2012, fig. 6).

8. Sedimentology and depositional environment

8.1. Lithological description and sedimentology (except the Tangissart Mbr)

In § 4.2 we have seen that the main lithology found in the MF is black graphitic and/or pyritic slates with a frequent laminar structure. In the field classification of Lundegard & Samuels (1980), these mudrocks (>50% of grain less than 62 μm) usually show a silt content of less than 1/3 and are therefore clayslates if they have a laminar structure (Photos 11, 16, 19) or claystones if they do not. The silt content is sometimes higher (1/3<silt<2/3) and these mudrocks are then mudslates if laminated or mudstones if not. The bedding is quite often marked by silty laminae frequently enriched in pyrite (Photo 18). The lamination is marked by the variations of the grain size of the

quartz silt and clay minerals and by colour variation essentially due to the abundance of organic matter (Photos 11, 16, 19). It is also marked by the fabric, i.e. what results from the parallel orientation of platy mineral grains a few microns in size. In the latter case, as the rocks are folded rocks, the orientation of the clay minerals is that of the cleavage, which is hardly visible in the field but clearly visible in thin sections.

Another, less common type of lithology is the graded mudstone-siltstone, interpreted as low-density turbidites (Stow & Piper, 1984; Stow & Smillie, 2020). In this type of rock, we observe a rhythmic alternation of millimetric laminae of siltstone and sub-centimetric laminae of clayslate whose succession and internal structures are characteristic and follow the "silt-mud laminated turbidite" so-called Stow model (Fig. 11; Stow & Smillie, 2020). In the majority of real cases, the model is incomplete and, as can be seen in Figure 11, the sequences are incomplete either cut from above or from below. The easiest division to recognise is the base T0 division which is lenticular and composed of silt. T0 results from the flow of the low-density current, which loses its coarser particles, creating current ripples that produce the wavy bedding structure. Then comes T1 which is a lamina with convolute structure, T2 which is a wavy-lenticular lamina, T3 a series of thin regular laminae, etc. The Photo 15 shows an example of a top-cut sequence consisting of the reddish-brown coloured T0 division (altered pyrite), most often followed by a T1 division of variable thickness and poorly visible internal structures. A third division, thin and very black (graphite), corresponds to the final division T8, i.e. the final fallout of the turbiditic cloud enriched with light organic matter. Towards the top of the photo, there are three sequences without apparent basal lamina and a hardly visible T2,3 division with still the presence of the thin black T8 division. Photo 18 shows a similar example where pyrite is still present (borehole sample) in the basal division T0, in addition to T1, the lighter and very fine T2 and T3 divisions can be seen. These examples show that in the MF, these silt-mud turbidites are quite distal due to the very thin thickness of each of the sequences (<1 cm). Exceptionally, high-density turbidites are found (Bouma, 1962; Stow & Smillie, 2020) but they are small in size and of fine sandstone granulometry (Photos 5, 17).

The rather scarce lithology of lydite is dealt with in a separate paragraph given the interesting questions of its occurrence and origin (see § 8.4). Similarly, the particular lithology of the Tangissart Mbr is considered in § 8.2. All the lithologies described above (except in the Tangissart Mbr) are devoid of bioturbation as shown by the perfect preservation of the fine laminations (Photos 11, 15, 16, 18, 19) which testifies of the anoxic conditions of the depositional environment (references in § 8.6). This assumption is supported by other observations such as the complete absence of macrofossils such as trilobites, brachiopods, the abundance of organic matter (currently graphitized; see § 12.1), the presence of manganese (see § 8.3), pyrite and the radon anomalies (see § 10.4).

8.2. Lithological description and sedimentology of the Tangissart Member

The uppermost Tangissart Mbr marks a gradual transition from the black slate lithology of the MF to the wavy bedding siltstone lithology of the Chevlipont Fm. It is indeed characterized by the progressive and recurrent development of clearer (without graphite pigment) millimetre-sized silty laminae within the black slates. The wavy siltstone intervals become increasingly important as you move upwards and invade all the sediments in the Chevlipont Fm. These clear laminae show an undulating, sometimes discontinuous structure (Photo 14), and when thicker they show oblique laminations at their base. All observations of the microstructures are very typical of graded mudstone-siltstone interpreted as low-density turbidites (Fig. 11; Stow & Piper, 1984; Stow & Smillie, 2020). In contrast to the dominant black slate of the MF, the more or less argillaceous siltstones of the Tangissart Mbr are weakly bioturbated (b in Photo 14), mainly *Planolites*-type bioturbation. It should be remembered that it is in this member that graptolites as well as trilobite

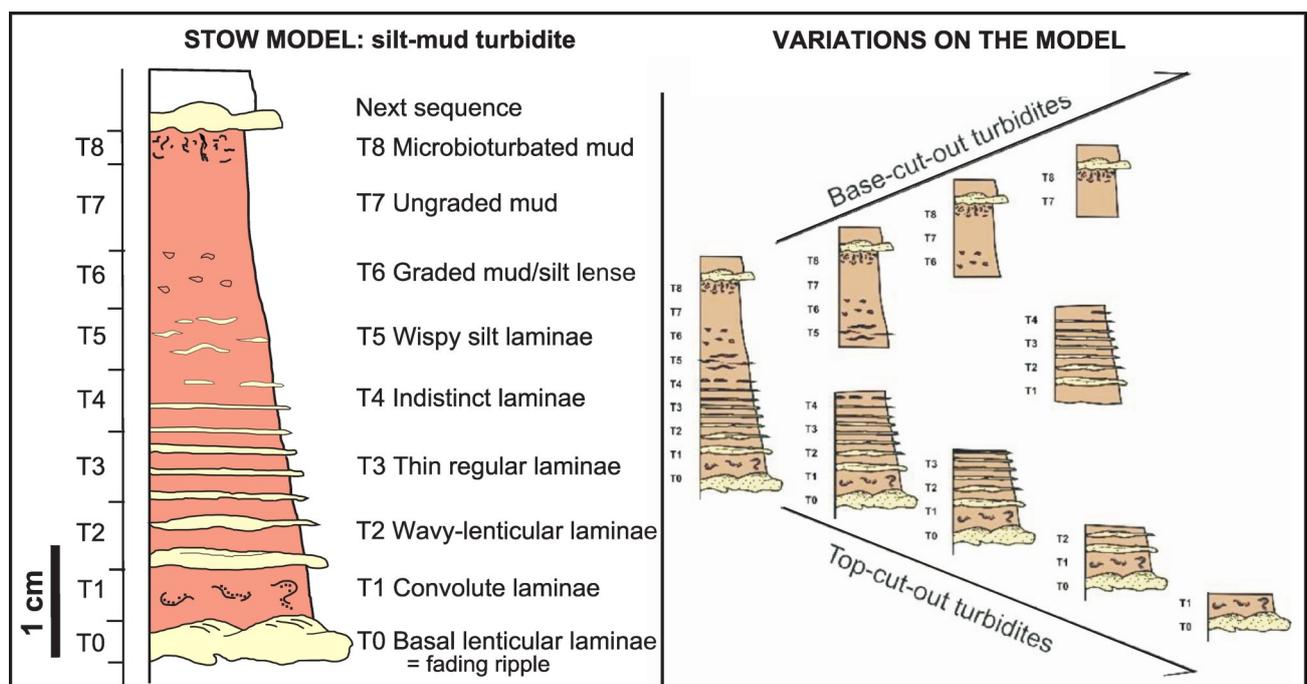**Figure 11.** Fine-grained turbidite model for silt-mud turbidites. The facies model showing the complete sequence of divisions T0 to T8 (Stow & Piper, 1984) and variations on the model found in the field are shown. The T8 division which corresponds to the deposition of pelagic sedimentation is not bioturbated in anoxic conditions which is our case. Modified after Stow & Smillie (2020, fig. 10).

remains have been found (see Chap. 6).

8.3. Nature of the protolith of the metamorphic manganese-bearing minerals

Manganese appears to be fairly common and randomly distributed in the MF where it is expressed by spessartine garnet and other metamorphic Mn-minerals (see Chapter 11). Given the reducing nature of the depositional environment of these slates and that many sedimentary Mn deposits have formed and are still forming in the present day in anoxic environments (e.g. Robb, 2005; Maynard, 1983, 2003, 2010; Johnson et al., 2016), it seems useful to examine what the Eh-pH diagrams of Mn and Fe predict as potential stable phases. Euxinic oceanic environments show towards the bottom Eh between -2 and -3 volts and pH around 7 (Krumbein & Garrels, 1952; Maynard, 2003). Mn behaviour is largely controlled by dissolved carbonate, in contrast to Fe, which is controlled more by the sulphide. The addition of carbonate creates a large region in which solid Mn species are stable under reducing condition (Maynard, 1983). Plotting these environmental conditions in the Eh-pH diagrams of Mn and Fe (Fig. 12) shows that rhodochrosite and pyrite are the stable phases with the following conditions: T = 25 °C, P = 1 bar, molarities of Fe^{2+}, Mn^{2+}, S, and HCO_3^{2-} respectively: 10^{-6}, 10^{-6}, 10^{-6} and 1 (Robb, 2005). It is therefore reasonable to assume that at the time of deposition or more likely during early diagenesis the rhodochrosite was the protolith of the spessartine. The same is probably true for pyrite, although its diagenetic history is, in detail, more complex, but it is indeed pyrite that is currently observed.

The diagenetic reaction that leads to the precipitation of carbonates containing Mn^{2+} from the reduction of Mn^{4+} oxides by organic carbon is presented as follows (Okita et al., 1988;

Johnson et al., 2016):

$$2 \ Mn^{4+}O_2 + CH_2O + 4H^+ = 2 \ Mn^{2+} + CO_2 + 3 \ H_2O$$
$$Mn^{2+} + CO_3^{2-} = MnCO_3.$$
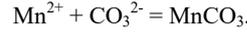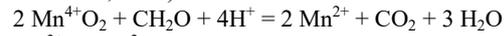
The validity of these reactions has been demonstrated on many rhodochrosite sedimentary deposits by measuring $\delta^{13}C$ which indicates a considerable contribution of $\delta^{13}C$-depleted carbon from decaying organic matter (e.g. Okita et al., 1988; Maynard, 2010).

8.4. Lithological description, sedimentology and origin of the lydites

We have previously seen that lydites are found at several stratigraphic levels in the MF, particularly in the Franquenies and Bois des Rêves Domain quarries (location Fig. 2; see § 5.3). These occur in two distinct lithological types: (1) in the Franquenies quarry, they occur either as oblong metric lenses elongated in the cleavage within the black slates (Photo 9) or as heaps with a conchoidal fracture and a botryoidal or reniform structure (Photo 10), (2) in the Bois des Rêves quarry, they occur as stratified decimetric jay-black banks, extremely hard with a conchoidal fracture (Photo 12). The thin section appearance of these two occurrences is entirely different, in case (1) an opaque black cryptocrystalline mass can be seen, probably made of quartz and finely dispersed graphite (see analysis § 10.2). Some very fine rutile, muscovite sticks and small mica-chlorite stack are visible in the opaque matrix. In case (2) numerous elongated clear submillimetric objects (mean$_{38}$ = 108 μm sd = 50 μm) filled with microquartz are embedded in an extremely fine and almost opaque matrix of quartz, graphite and rare sticks of muscovite and rutile (Photo 13). The clear structures are filled with microquartz and show a diffuse contour and are aligned along the layering and flattened
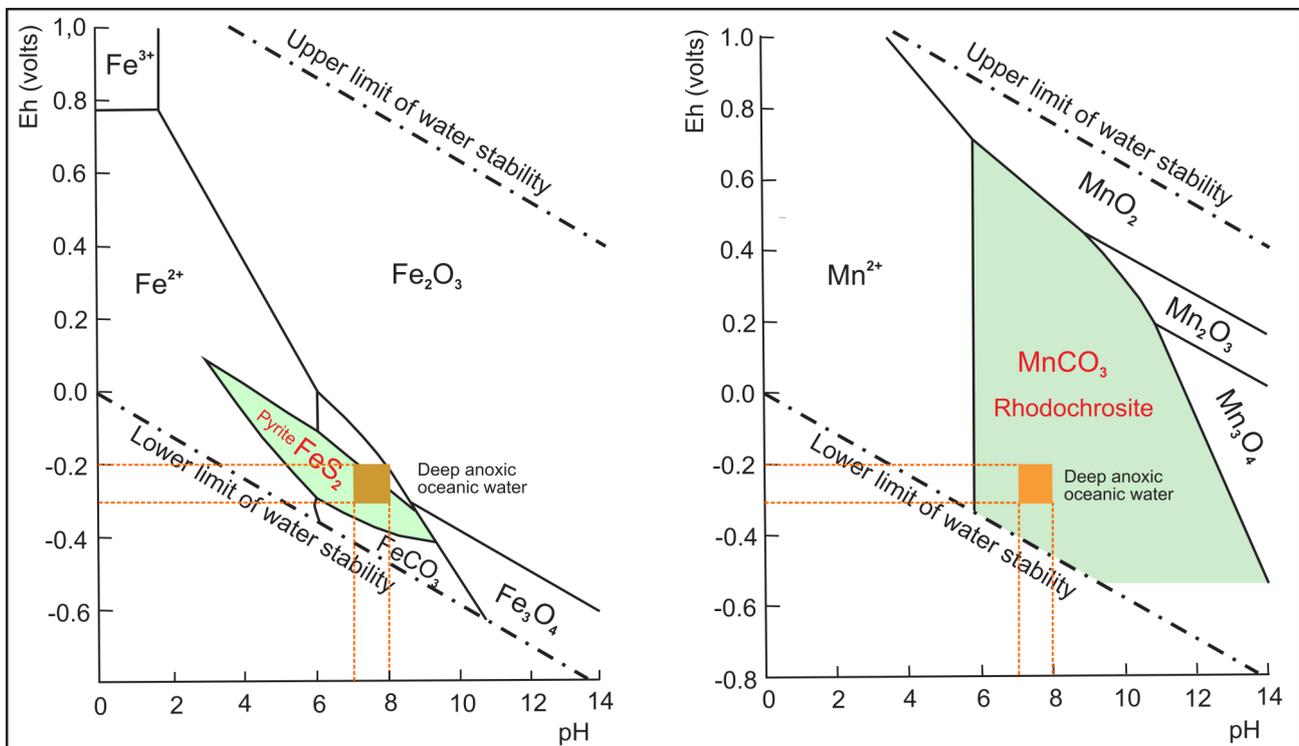
Figure 12. Eh-pH diagrams for Fe and Mn with the following conditions: T = 25 °C, P = 1 bar, molarities of Fe, Mn, S and CO_3 respectively: 10^{-6}, 10^{-6}, 10^{-6} and 1. The two orange rectangles correspond to the Eh (-0.2 to -0.3) and pH (7 to 8) range of deep anoxic ocean waters (Krumbein & Garrels, 1952; Maynard, 2003). The green-coloured areas correspond to the stability fields of pyrite and rhodochrosite respectively. Modified from Robb (2005, fig. 5.17).

in the perpendicular direction, suggesting their compaction. We have already suggested (Herbosch & Verniers, 2013) that these clear objects correspond to radiolarite phantoms. Their identity could not be confirmed by M. Caridroit (comm. pers., 2000) due to diagenesis and metamorphic overprint. However, there are several arguments in favour of this hypothesis:

- radiolarians are known to have existed since the lower Cambrian (Tolmacheva et al., 2001) and are already well diversified in the Furongian (Pouille, 2012);
- the size of the assumed radiolarians phantoms, 50 to 150 μm, corresponds roughly to that of the upper Cambrian radiolarians (De Wever et al., 2001);
- at the highest magnification in thin sections, some kind of spines seem to be visible at the periphery of some rare phantoms (observations of B. Mamet, 2000);
- radiolarians are often associated with organic-rich sediments, particularly those found in upwelling (De Wever et al., 2001, chap. 2);
- if today radiolarians are a major source of organic matter, in the Palaeozoic they were probably more important since planktonic foraminifera, nannofossils and diatoms were not yet present;
- in the Furongian, the sea level was high (Marcilly et al., 2022, fig. 5) which enhances the nutrient supply from the continent and increases the bioproductivity.

It can be concluded from these observations, firstly, that the difference in macroscopic and microscopic structures between these two occurrences of lydite can reasonably be attributed to diagenetic recrystallisation during the Brabantian orogeny. This recrystallisation could not take place in the thicker and more rigid bedded lydites from the Bois des Rêves. Secondly, even if we cannot prove that these "phantom objects" are indeed radiolarians, there is a cluster of evidence to support that they are radiolarians and that these rocks are true lydites.

8.5. Depositional environment of the Mousty Formation

Now that we have been able to decipher the way in which the different lithologies of the MF were formed, we can put all the pieces of the puzzle together. These results are consistent and converge towards an anoxic oceanic depositional environment, presumably deep. Indeed, if the depositional environment of the black slate fits clearly with the pelagic deposits of the abyssal plain, the low-density turbidites, which seem to be quite frequent, are deposited at a lesser distance from the coasts. As the turbidites are clearly distal given their very small thickness, they can be considered as hemipelagic sediments deposited either on nearby basin plains or on the distal part of turbidite fans (e.g. Cojean & Renard, 2013; Stow & Smillie, 2020).

All the lithologies observed contain abundant organic matter (presently in graphite) which requires an anoxic environment for its preservation. This environment is also essential for the formation of rhodochrosite and pyrite (see § 8.3). This also means that only the lower part of the ocean was anoxic because in order to have high organic productivity, an oxygenated upper part was necessarily required. Given this high productivity and the presence of radiolarites, which adds a new constraint, we propose that this ocean was at a continental margin with an upwelling bringing abundant nutrients. Such coastal upwelling shows an expanded mid-water oxygen-minimum zone (OMZ) and thus the organic material is not or hardly oxidized in the water column (e.g. Peru upwelling). It is also important to emphasize that the late Cambrian corresponds to greenhouse conditions, a very high sea level (Marcilly et al., 2022, figs 5, 6) and an overall oxygen deficiency in the oceans (see § 8.6). All these conditions favour high biological productivity in the surface layers and anoxia in the deep layers of the ocean.

Let us consider the palaeogeographic situation corresponding to the deposition of the MF during the Furongian (Fig. 13). The future Avalonia E microplate is still part of the Gondwana continent and lies on the NW margin of the West African craton (Herbosch et al., 2020, fig. 20) at a latitude of about 60°S (Fig. 13; Domeier, 2016, fig. 7a, b). The MF was deposited in an aborted rift that had formed as early as the lower Cambrian (e.g. Verniers et al., 2002; Herbosch et al., 2020) and whose very strong subsidence began to slow during the Furongian, announcing the rifting with Gondwana at the dawn of the Ordovician (see subsidence curve in Herbosch et al., 2020, fig. 4). This palaeogeographic situation is consistent with an upwelling in the sea that occupied the rift along the N margin of Gondwana (Fig. 14). The pronounced slowing of subsidence at the approach of the Ordovician also explains the sedimentological changes observed in the uppermost Tangissart Mbr. Indeed, the rapid increase in the frequency of low-density turbidites indicates a clear decrease in the depositional depth which continues in the Chevlipont Fm entirely invaded by turbidites, including high-density turbidites (e.g. Marcq area: Longueville, 1997; Debacker, 1999; Thyle valley: Beckers, 2004; Herbosch & Verniers, 2013). This is consistent with an uplift preceding the rifting of Avalonia from Gondwana.

8.6. Synthesis, discussion and comparison with contemporaneous anoxic series

All the observations and considerations presented in this chapter are consistent with the conclusion that the black slate and other MF lithologies were deposited in an anoxic sea as pelagic to hemipelagic sediments situated on the rifted northern margin of the Gondwana continent from the uppermost Miaolingian to the lowermost Tremadocian (Fig. 14). They were deposited alternately on proximal abyssal plains and on the distal part of a turbidite fan, depending on sea level variations and continental events that occurred during its ~13 m.y. lifetime. Another palaeogeographic reconstruction, more speculative and motivated by the occasional presence of radiolarites, is that of an anoxic deep sea but located in an upwelling on the same rifted margin of Gondwana. Both hypotheses allow us to explain all the observations such as the high content of organic matter (graphite), the occurrence of Mn, the different lithological facies, ... However, the second hypothesis gives a better account of the high preservation of organic matter and the presence of radiolarites, probably more frequent than that observed given the limited number of outcrops. Figure 14 is a schematic representation of the depositional environment of the MF during the Furongian as discussed above under the assumption of an upwelling.

There is considerable evidence to suggest that large parts of the lower Palaeozoic oceans were consistently or frequently in oxygen deficit (Gill et al., 2011, 2021; Dahl et al., 2014; Saltzman et al., 2015; Edwards, 2019). This observation is reflected in a clear decrease in atmospheric content in the late Cambrian (Large et al., 2022). One such interval is the SPICE (Steptoidal Positive Isotope Carbon Excursion), which occurs in the early Furongian (Paibian Stage) and records a shift from -1 to $4.5^0/_{00}$ δ^{13}C during 2 to 4 m.y. This is the largest positive excursion in δ^{13}C, followed by recurrent, less positive and frequent excursions along the Furongian and Tremadocian (Fig. 15). It can be seen that the SPICE excursion starts exactly at the beginning of the MF (uppermost Guzhangian, see Figs 7, 9), and up to its summit (lowermost Tremadocian) the δ^{13}C values are positive.
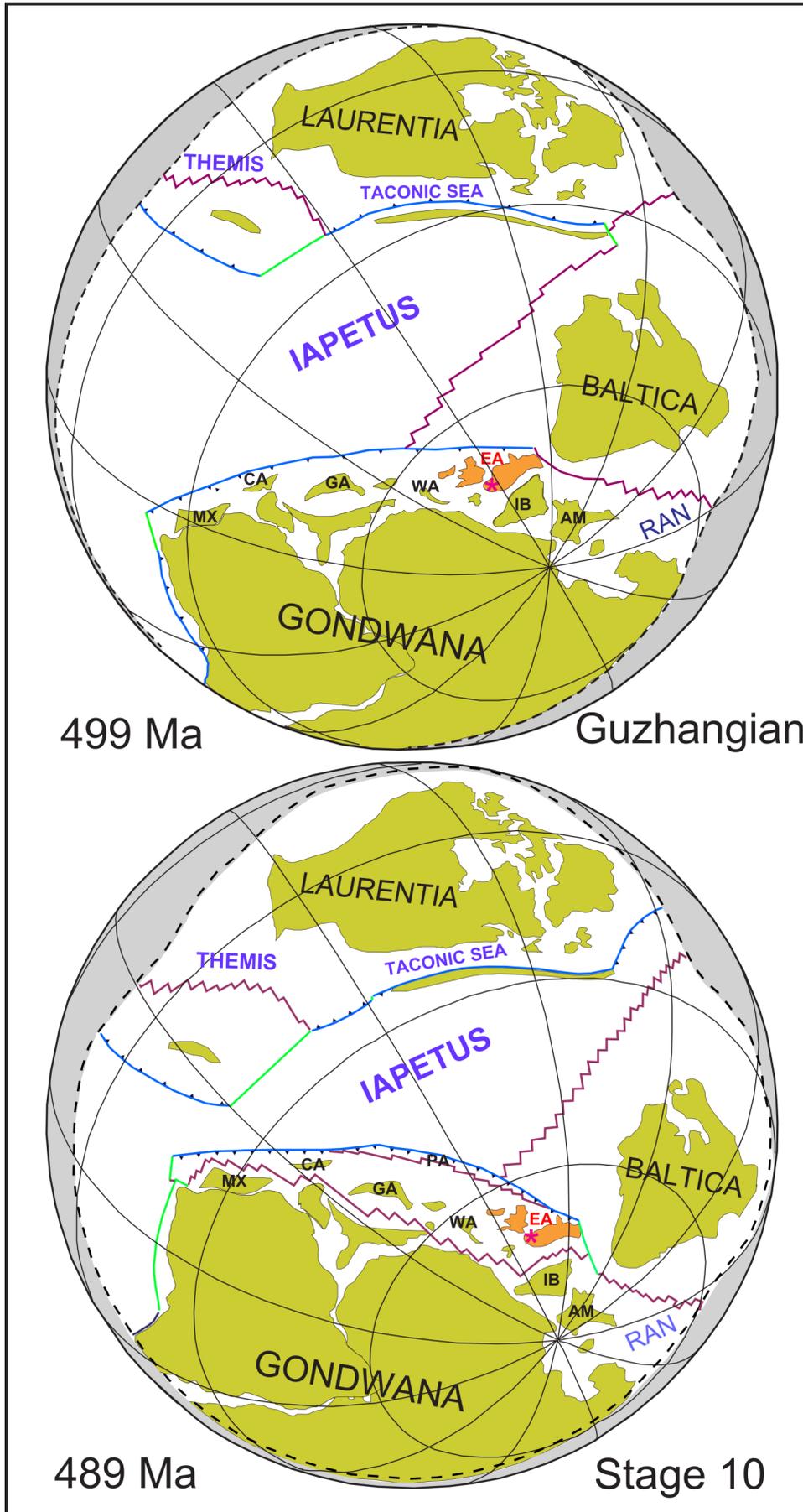
Figure 13. Palaeogeographic reconstruction following the model of Domeier (2016) for 499 Ma and 489 Ma which correspond roughly to the depositional age of the Mousty Fm (see Fig. 7). The schematic plate boundaries are shown (blue = subduction, green = transform, red = spreading ridge) and labels of some major features. The dashed external boundary is an arbitrary perimeter marking the outer limit of the domain considered in the model. Only the peri-Gondwanian terranes are named: AM = Armorican Massif, CA = Carolinia, EA = East Avalonia (in orange, a red star shows the location of the Brabant Massif), GA = Ganderia, IB = Iberia, MX = Mixteca-Oaxaca block, PA = Penobscot arc, WA = West Avalonia. Note that at 489 Ma, the Rheic Ocean is not yet truly open and that, in this model, the Avalonia E and W, Carolinia and Ganderia microplates form a single plate that will break away from Gondwana at the onset of the Ordovician (~488 Ma). Modified and simplified from Domeier (2016, fig. 7).
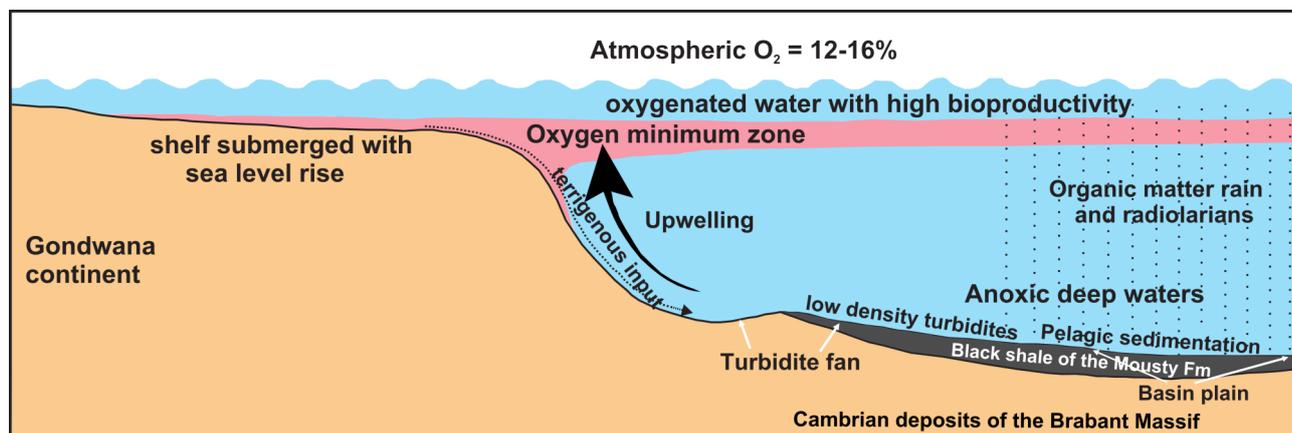
Figure 14. Sketch (not to scale) of the proposed depositional environment of the Mousty Fm during the late Cambrian (except the Tangissart Mbr). Atmospheric oxygen contents according Large et al. (2022, fig. 10) and sea-level variations according to Marcilly et al. (2022, fig. 5).
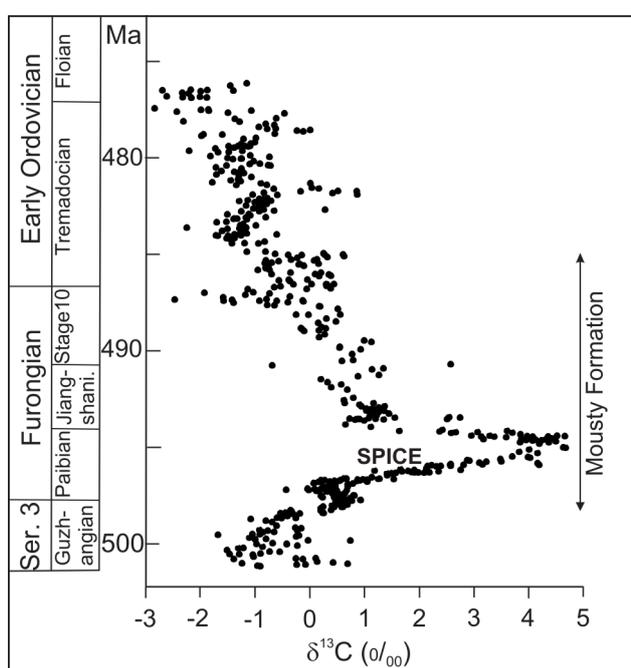
Figure 15. Composite $\delta^{13}C$ with Cambrian data from the Great Basin and Ordovician from Argentina. The Steptoidal Positive Isotope Carbon Excursion (SPICE) starts exactly at the beginning of the sedimentation of the Mousty Fm. Time scale from Gradstein et al. (2020) and ages of the Mousty Fm from Fig. 7. Modified from Saltzman et al. (2015, fig. 1).

8.6.1. Comparison with the Alum Shale of the Baltic Basin

Several anoxic series of the same age as the MF are known from Avalonia and Baltica. The most famous is the Alum Shale Formation which was deposited from the middle Cambrian (Miaolingian) to the Early Ordovician (Tremadocian) in the Baltic Basin where they occupy a large area. Due to its huge total organic carbon content (mean 2 to 15%), widespread occurrence and low maturity, it is a well-known conventional source rock for hydrocarbons and gaz. It is also enriched in S, Mo, V, Ni and U, the last element having been exploited until 1989 (Schovsbo, 2002; Schulz et al., 2021, figs 1, 2; Gill et al., 2021). This formation was deposited in a large shallow epicontinental sea that covered a substantial part of the Baltica plate; at the maximum sea-level stand, near the depocenter, the

thickness does not exceed 100 m (Andersson et al., 1985), demonstrating the very low sedimentation rate. The Alum Shale Fm corresponds not only to the MF but also to the Jodoigne Fm (Fig. 4; see Chap. 9) and is a good example of the oxygen deficiency generally observed in the lower Palaeozoic oceans. However, this formation is not a good example for comparison because, apart from its age, organic matter richness and anoxia which are comparable, all its other characteristics are very different from the MF: the shallow depositional environment, the absence of metamorphism, the very low thickness, to name only the major differences.

8.6.2. Comparison with the Harlech Dome of N Wales

Now compare with contemporary sediments most likely deposited in the same aborted rift as the MF but located in North Wales, specifically the Harlech Dome where sedimentation is the most complete (Fig. 16). Two major sedimentation cycles have been identified: Harlech Grits Group and the overlying Mawddach Group, the latter corresponding in age to the MF (Brenchley et al., 2006; Pothier et al., 2015, fig. 3). These deposits, about 6 km thick, were probably accumulated in a deep-sea rift basin (Waldron et al., 2011; Linnemann et al., 2012) from the Stage 2 (Terreneuvian) to the upper Tremadocian (Megasequence 1 sensu Woodcock 1990, 1991). The Mawddach Group was defined by the appearance of strata containing layers of black pyritic mudstone and by the presence of mature sandstone beds. Its base shows dark laminated slates with benthic fauna of later mid-Cambrian age. The main thickness of the group is made up of an alternation of fine sandstone and silty mudstone showing turbidites and is interpreted as a deep basinal setting (Maentwrog Fm). The succeeding Flestiniog Flags Fm, about 1000 m thick, is composed predominantly of silty mudstone alternating with flaggy sandstone that shows hummocky cross-stratification and ripples. The formation was deposited in shallow water, above the wave-base, with a rapid subsidence (Prigmore et al., 1997). It progressively passes into the black pyritic and thinly laminated carbonaceous mudstone of the Dolgellau Fm interpreted as hemipelagic deposits formed in quiet conditions in poorly oxygenated waters. This is a condensed series characteristic of the "olenid biofacies". The upper part of the formation is dated at 489 ± 0.6 Ma on tuffitic material (*Acerocarina* Biozone, see Fig. 7; Landing et al., 2000). Lastly, the silty mudstones of the Dol-cyn-afon Fm show shelly fauna accompanied by the planktonic graptoloid *Rhabdinopora* ("Dictyonema shale"). The mudstone shows fine lamination
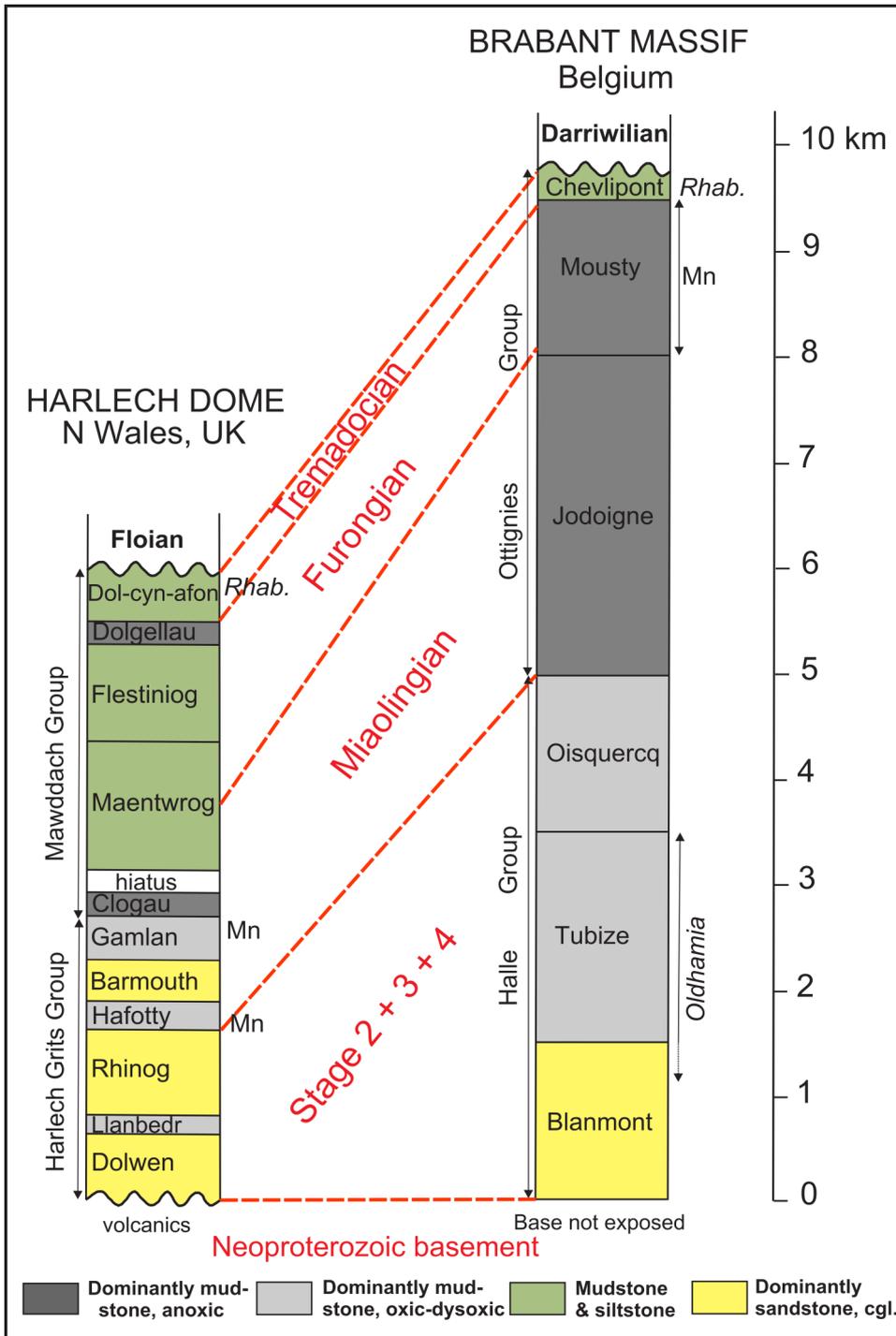
Figure 16. Comparison of the sedimentary registration between the Harlech Dome and the Brabant Massif. The names in the two logs correspond to the different formations and groups. This record extends from Stage 2 (pro parte) to the Tremadocian. The Neoproterozoic basement of both regions is the metacratonic margin of the West African Craton (Herbosch et al., 2020, figs 19, 20). Stratigraphy, thickness, sedimentology from Brenchley et al. (2006, fig. 3.10), age from Pothier et al. (2015, fig. 3) for the Harlech Dome and from Herbosch & Verniers (2013) for the Brabant Massif. Time scale from Gradstein et al. (2020). Cgl. = conglomerate, *Rhab. = Rhabdinopora*.

frequently disrupted by bioturbation, and the sandstone may be graded and shows ripples and cross-bedding. An unconformity caps the silty slates dated from the upper Tremadocian (trilobite *Angelina sedwickii* Biozone).

Although the sedimentation of the Mawddach Group of the Harlech Dome is more diverse than that of the MF where it is always deep and anoxic, there are strong similarities (Fig. 16) These include strong subsidence reflected in its great thickness (>3 km), often deep depositional environments with low- and high-density turbidites, condensed black slate series rich in organic matter and pyrite. The top of both series is marked by an unconformity which is followed respectively by Lower Ordovician (Floian) and Middle Ordovician (Darriwilian) sediments. It is also worth pointing out the presence of "Dictyonema shale" at the same stratigraphic level and with the

same lithology as the MF. The presence of a larger benthic fauna than in the MF is explained by more diverse and shallower environments. Overall, the similarity is remarkable even if there are some minor differences. Due to these similarities and following the suggestion of Waldron et al. (2011), we proposed that the Harlech Dome (N Wales), the Meguma Terrane (Nova Scotia) and the Brabant Massif were part of a single large aborted rift (an aulacogen?) which extended along the margin of the Gondwana continent (Linnemann et al., 2012, fig. 23). This hypothesis is endorsed by Pothier et al. (2015, fig. 10) who propose a new tectonic model that appears to be consistent with the palaeogeographic position of the Brabant Massif.

9. Stratigraphic relation between Mousty and Jodoigne formations

It is quite recently that a series of arguments, too long to be outlined here (see Herbosch et al., 2008), have made it possible to place the Jodoigne Fm stratigraphically under the MF (Figs 4, 7). Nevertheless, in their conclusions, these authors note: "We cannot rule out the possibility that the Jodoigne Fm partly overlaps in time with the upper Cambrian Mousty Fm, and that for instance (the younger) parts of the Jodoigne Fm represent more proximal, more energetic facies of (the older) parts of the Mousty Fm". This assertion remains valid and is even premonitory because we have seen (see § 5.2) that it is highly likely that a part of the lower part of the Court-St-Etienne borehole, as well as part of the corresponding outcrops at Court-St-Etienne along the Ravel (Fig. 6), belong to the Jodoigne Unit which constitutes the upper part of the Jodoigne Fm. It should also be added, as can be seen in Figure 9, that the Jodoigne Fm has only been dated by one borehole (Leuven 89E1). In fact, despite numerous attempts, all the field samples of the Jodoigne Fm are acritarch barren, as is also the case for the MF.

The Jodoigne Fm also shows organic-rich black slates distributed throughout its high thickness (<3 km) but also, which differentiates it from the MF, frequent low- and high-density turbidites (Debacker & Herbosch, 2011).

10. Geochemistry

A geochemical study of the MF seems to be necessary given the presence not only of manganese anomalies but also the presence of different varieties of lydite and high levels of radon in the houses (see § 10.4).

10.1. Major elements of black slate and lydite

Analyses of the major elements of the MF black slate (Table 1) are few and often old (Van Tassel, 1986; Stryckmans, 1989) except for some more recent analyses taken from André (1991) and Linnemann et al. (2012). The analyses of the major elements of the Jodoigne and Chevlipont fms that frame the MF are presented in Table 2. Analyses of some different varieties of lydite (Table 3) are from Van Tassel (1986) and Bonjean et al. (2015a, 2015b). Average shale: North American Shale Composite (NASC, Gromet et al., 1984), Mean Russian Platform Shale (MRPS, Ronov & Migdisov, 1996), mean Lithogenous Pelagic Clay (LPC, Chester, 1990), two Black shale composites (Vine & Tourtelot, 1970; Quinby-Hunt et al., 1989), mean Dictyonema shale (Tremadocian) and mean Alum shale (Cambrian) from the Baltic Basin (Gautneb & Saether, 2009) are used for comparison. The description, position and references for all these analysed samples are reported in Tables 4 and 5. The complete data set with major and trace elements recalculated to 100% is provided in the Supplementary data. For comparison purposes we have also added the analyses of Thuringian slate (n = 12, Cambrian to Permian, Römer & Hahne, 2010), Brabant Massif slate (n = 17, Cambrian to Silurian, Linnemann et al., 2012), Stavelot Inlier slate (n = 85) and coticule from Ottré Fm (n = 58) both from Herbosch et al. (2020, fig. 14).

10.1.1. Lithological-geochemical classification of the slates

In the terrigenous shale and sandstone classification graph SiO_2/Al_2O_3 versus Fe_2O_3t/K_2O by Herron (1988), most MF slates are well grouped and most are within the Shale compositional field, with only a few in the Wacke and Fe-shale (Fig. 17A). In detail, the 8 slates with garnets are considerably to highly enriched in total iron (mean$_8$ Fe_2O_3t = 9.7% sd = 5.3%) compared to the 22 other slates without garnets (mean$_{22}$ Fe_2O_3t = 5.1% sd = 1,9%).

The slates with garnet (red circles) are consequently located in the upper part of the Shale field and three of them are even in the Fe-shale field (Fig. 17A). This suggests that a high iron content favours the formation of garnet but also that it is not the only condition when the iron is only moderately enriched. Rhodochrosite, which is most probably the protolith of garnet (see § 8.3), could also have incorporated Fe^{2+} into its lattice if iron was in great abundance. The majority of these slates, with or without garnet, show a fairly constant SiO_2/Al_2O_3 ratio which varies between 2 and 4 (Fig. 17A). This is also the case for all other comparative shales, including the Stavelot, Thuringia and Brabant slate, Jodoigne and Chevlipont fms slate and siltstone. The two average shales from Baltic Basin are located in the same zone but in the right part of the Shale field close to the international reference shales (NASC, MRPS, LPC).

The more or less argillaceous siltstones of the overlying Chevlipont Fm (green triangles), whose depositional environment is shallower and closer to the continental slope than the hemipelagic slates of the MF (see § 8.5), plot in the Shale field and are geochemically indistinguishable from the MF slates (Fig. 17A). On the contrary, the black slates of the underlying Jodoigne Fm (blue squares) are richer in K_2O and poorer in Fe_2O_3t resulting in a lower ratio: mean$_3$ Fe_2O_3t/K_2O = 0.44 vs mean$_{30}$ = 2.1% for the MF. The Stavelot Inlier slates (white triangles) are in the same range of SiO_2/Al_2O_3 ratio but are generally richer in iron which can be related to their oxidizing depositional environment (see next §).

10.1.2. Geochemical bivariate comparison

In the $SiO_2 + Al_2O_3$ versus Fe_2O_3t graph (Fig. 17B) which is a proxy for the detrital component of terrigenous rocks, all the studied and reference rocks, except the coticule and some Stavelot slates show a strong negative correlation. Sedimentologically, this means that the major terrigenous influx of clays and quartz (mean$_{30}$ $SiO_2 + Al_2O_3$ = 79.8%) from the MF has strongly diluted the iron input which, consequently, appears very variable (mean$_{30}$ Fe_2O_3t = 6.4% sd = 3.8%). By contrast, coticule does not follow this negative correlation: its iron content is less variable and globally independent from the detrital component. This can be attributed to the rapid deposition of the coticule protolith as turbidite (Herbosch et al., 2016), the incorporation of iron being the result of the remobilization of the surrounding mudstones very rich in this element. The slates of the Stavelot Inlier are indeed significantly richer in Fe than the other slates, which is a characteristic of this basin that was located close to the mid-ocean ridge (Herbosch et al., 2016, 2020). Note that the NASC and MRPS reference shales are slightly distant from the main shale cloud (Fig. 17B), i.e. less terrigenous component and less iron, which is explained by their depositional environment closer to the continent (MRPS = platform shale). In contrast to the mean Lithogenous Pelagic Clay (LPC) whose deep oceanic depositional environment is closer to that of most shales represented.

Most reference and studied slates have 1 to 9% Fe_2O_3 and <0.3% MnO (Fig. 18A). An important exception is the Stavelot slate which contains 10–23% Fe_2O_3 and 0.3 to 6% MnO, which has been related to the proximity of the nascent Rheic oceanic ridge. The coticules are low in Fe_2O_3 and high in MnO: they represent distal limy turbidites where Ca has been replaced by Mn from the surrounding Fe- and Mn-rich sediments during diagenesis (Herbosch et al., 2016). If most of the MF slate has MnO contents less than 1% (mean$_{26}$ = 0.18% sd = 0.20%), five samples have 0.5 to 1% MnO and three samples have very high contents in MnO (1.5 to 15 %) (Fig. 18A). The other Brabant Massif slates have normal values in MnO, Jodoigne Fm slates (0.0, 0.02, 0.12% MnO), Chevlipont Fm clayey siltstones

Table 1. Major element elements of the black slate and lydite from Mousty Formation. Lin. = Linneman et al.; Sch. lydite = Van Tassel, 1986; Black Pigment of Sclayn = Bonjean et al., 2015b, table 4. Sch. lydite = schistose lydite; n.a. = not analysed; LOI = loss on ignition.

SAMPLE FROM MOUSTY FORMATION

Ref.		Slate Lin. 2012		Slate André, 1991			Slate without garnet Van Tassel, 1986							Slate with garnet Van Tassel, 1986					
Formation		MST	MST	MST	MST	MST	MST	MST	MST	MST	MST	MST	MST	MST	MST	MST	MST	MST	MST
Sample		Brab-6	Brab-13	sed1/14	sed2/1	sed2/4	sed2/5	W7 206	W7 213	W3 212	W7 210	W5 211	C13	C18	G73	W6	C29	C45	G74
SiO2	%	57.25	59.06	57.61	58.25	61.04	61.67	57.90	59.50	62.38	60.45	60.54	59.50	58.85	58.42	53.07	43.52	61.75	60.98
Al2O3	%	22.67	20.92	19.62	21.87	20.05	16.79	23.61	24.56	22.28	23.80	18.86	22.13	22.11	23.71	20.55	19.21	12.11	21.08
Fe2O3	%	4.57*	6.87*	4.72	2.50	2.05	4.54	3.02	3.21*	3.68*	2.49*	5.49	2.61	0.35	3.52	4.35	7.22	5.61	1.36
FeO	%	n.a.	n.a.	1.71	3.75	3.70	0.11	n.a.	n.a.	n.a.	n.a.	1.13	2.98	5.02	2.75	6.80	12.85	2.77	3.56
MnO	%	0.13	0.38	5.18	0.55	0.13	0.02	0.11	0.05	0.08	0.07	0.16	0.12	0.10	0.18	3.87	1.31	14.32	0.39
MgO	%	1.67	1.97	1.14	2.01	1.80	0.49	1.61	0.42	0.37	1.15	1.54	1.81	1.84	1.24	2.25	4.81	0.35	1.76
CaO	%	0.16	0.07	0.79	0.13	0.16	0.18	0.00	0.26	0.18	0.00	0.52	0.40	0.00	0.13	0.88	0.92	1.70	0.30
Na2O	%	0.62	0.15	0.08	0.38	0.32	0.19	0.73	0.63	0.40	1.01	0.43	0.54	0.45	0.40	0.71	0.08	0.10	0.27
K2O	%	4.21	4.75	3.32	4.33	4.42	3.30	4.28	4.04	4.25	3.31	3.62	4.12	3.62	4.01	2.53	0.96	0.50	4.18
TiO2	%	1.02	0.95	0.95	1.03	1.04	0.93	0.50	1.09	1.00	0.72	0.92	1.00	0.86	0.83	0.92	0.78	0.62	0.88
P2O5	%	0.11	0.08	0.01	0.01	0.02	0.04	n.a.	n.a.	n.a.	n.a.	n.a.	n.a.	n.a.	n.a.	n.a.	n.a.	n.a.	n.a.
LOI	%	7.26	4.79	4.87	4.84	4.44	4.22	8.19	6.93	5.82	6.80	7.79	5.05	4.57	5.45	4.46	5.64	0.92	4.51
Total	%	99.67	100.00	100.00	99.65	99.16	99.48	99.94	100.69	100.44	99.80	101.00	100.26	97.77	101.10	100.39	97.30	100.75	99.27

Ref.		Slate (garnet?) Van Tassel, 1986				Slate (garnet?) Stryckmans, 1989							
Formation		MST	MST	MST	MST	MST	MST	MST	MST	MST	MST	MST	MST
Sample		W19	G2	C14	C8 217	Mo1	Mo2	Mo4	Mo5	Mo6	No4	No6	No3
SiO2	%	63.47	61.99	40.36	59.88	66.88	58.14	63.60	58.26	63.19	59.51	75.27	60.39
Al2O3	%	21.62	19.97	33.84	21.79	15.14	21.52	16.44	19.15	17.44	20.35	10.41	17.62
Fe2O3	%	2.95	1.30	1.41	2.38	3.20*	3.72*	1.17*	7.15*	2.66*	3.63*	4.33*	7.90*
FeO	%	1.64	4.51	4.70	4.50	n.a.	n.a.	n.a.	n.a.	n.a.	n.a.	n.a.	n.a.
MnO	%	0.09	0.38	0.45	0.15	0.03	0.06	0.06	0.07	0.01	0.01	0.01	0.78
MgO	%	1.35	1.90	2.45	2.18	0.39	1.21	0.71	0.66	0.65	1.72	1.09	0.92
CaO	%	0.00	0.00	0.28	0.00	0.76	0.65	0.81	1.10	1.10	1.15	0.96	0.95
Na2O	%	0.41	0.29	0.60	0.42	0.84	0.98	0.88	1.80	0.91	0.63	0.46	1.47
K2O	%	4.44	4.34	7.64	4.05	3.00	4.04	3.34	3.60	3.42	5.69	1.55	4.96
TiO2	%	1.03	0.92	1.53	0.96	0.71	1.01	0.95	0.91	0.90	1.01	0.67	0.99
P2O5	%	n.a.	n.a.	n.a.	n.a.	0.16	0.16	0.15	0.17	0.17	0.18	0.08	0.46
LOI	%	3.53	3.59	5.88	4.04	5.30	6.70	10.00	8.50	7.60	4.20	3.56	4.80
Total	%	100.53	99.22	100.16	100.45	98.40	98.19	98.11	101.37	98.05	98.08	98.48	101.24

Ref.		Sch. lydite	Black Pigment of Sclayn		
Formation		MST	MST?	MST?	MST?
Sample			Sc-1	Sc-2	Sc-3
SiO2	%	89.06	95.85	98.19	97.28
Al2O3	%	6.77	0.40	0.26	0.38
Fe2O3	%	1.61*	1.74*	0.14*	0.32*
FeO	%	n.a.	n.a.	n.a.	n.a.
MnO	%	n.a.	n.a.	n.a.	n.a.
MgO	%	0.30	0.03	0.02	0.02
CaO	%	0.128	0.18	0.12	0.18
Na2O	%	0.05	0.03	0.02	0.03
K2O	%	0.40	0.07	0.05	0.09
TiO2	%	1.50	1.51	1.08	1.64
P2O5	%	n.a.	n.a.	n.a.	n.a.
LOI	%	n.a.	n.a.	n.a.	n.a.
Total	%	99.87	99.81	99.88	99.94

*only Fe2O3t

Table 2. Comparative major elements data for the underlying Jodoigne and overlying Chevlipont formations. Data source: Brab-4, Brab-5, Brab-23 from Linnemann et al., 2012; J01, Re8, DY2 from Stryckmans, 1989; LE13 to LE17 from Herbosch, unpublished. L.D. = Lower Detection limit; LOI = loss on ignition.

Formation		Jodoigne Formation			Chevlipont Formation							
Formation		JOD	JOD	JOD	CHV	CHV	CHV	CHV	CHV	CHV	CHV	CHV
Sample		Brab-4	Brab-5	J01	Re8	DY2	Brab-23	LE13	LE14	LE15	LE16	LE17
SiO_2	%	64.25	50.47	65.82	56.56	61.84	49.78	60.04	67.09	59.92	60.70	59.67
Al_2O_3	%	21.88	30.54	16.26	21.15	18.15	26.46	20.23	15.03	21.07	19.58	20.14
Fe_2O_3t	%	1.07	2.57	4.02	8.81	7.97	7.00	6.68	6.91	5.83	6.51	7.73
MnO	%	0.00	0.02	0.12	0.26	0.12	0.11	0.10	0.11	0.08	0.12	0.13
MgO	%	0.55	0.73	0.36	2.75	1.95	1.86	1.67	1.63	1.47	1.77	1.87
CaO	%	0.04	0.10	0.48	1.34	0.96	0.17	0.28	0.46	0.27	0.34	0.22
Na_2O	%	0.24	0.99	0.23	0.92	1.30	0.63	1.08	1.23	0.86	1.18	1.11
K_2O	%	5.84	6.88	4.49	3.14	3.25	7.31	4.68	2.83	5.09	4.37	4.35
TiO_2	%	1.06	1.33	0.95	0.88	1.01	1.13	1.08	0.81	1.02	0.94	0.98
P_2O_5	%	< L.D.	0.07	0.04	0.22	0.32	0.22	0.24	0.22	0.27	0.20	0.25
LOI	%	5.43	5.99	4.20	4.30	4.01	4.96	3.96	3.78	3.89	3.91	3.84
Total	%	100.36	99.67	96.97	100.33	100.87	99.63	100.02	100.10	99.70	99.62	100.29

Location		Northern wall Franquenies quarry W7					Bois des Rêves small quarry W11				
Lithology		Schistose lydite					Conchoi.	Stratified with conchoidal break			
Sample		1906	1908	1912	1907	Mean n=4	1909	1910	1914	1915	Mean n=3
SiO_2	%	88.69	89.80	86.57	90.59	88.91	90.14	91.57	89.93	93.79	91.05
Al_2O_3	%	3.81	4.57	5.90	3.52	4.45	3.09	3.40	4.05	2.43	3.47
Fe_2O_3t	%	1.45	0.44	1.11	0.25	0.81	0.63	0.80	0.44	0.71	0.65
LOI	%	5.26	3.88	5.12	4.92	4.79	4.64	4.01	4.93	2.75	4.11
Total	%	99.21	98.69	98.70	99.28	98.97	98.50	99.35	99.35	99.68	99.60

Table 3. Major elements of the different varieties of lydite from the Franquenies and Bois des Rêves quarries from Van Tassel (1986). Conchoi. = conchoidal; LOI = loss on ignition.

(mean$_8$= 0.13% sd = 0.05%) (Fig. 18A, Table 2). The Fe_2O_3 content of the MF is highly variable, averaging between 3 and 8%, but ranging up to 23% (mean$_{30}$ = 6% sd = 3.6%). The Fe_2O_3 content of the Chevlipont Fm is of the same order of magnitude but without strong variations (mean$_8$ = 7.2% sd = 0.9%) while that of the Jodoigne Fm is clearly lower (mean$_3$ = 2.5%). The enrichment of Mn and Fe in the MF is consistent with its deep-sea environment (see § 8.5). The input of Mn by rivers is probably sufficient unless it is the first manifestation of the forming Rheic oceanic ridge. The two mean black shales from the Baltic Basin, with very high organic matter content (losses on fire 6.9% and 14.9%) revealing an anoxic environment, have almost no MnO content (Table 6), this can be related to their shelf depositional environment.

Opposing Fe^{2+} and Fe^{3+} allows to see that the MF black slates are only slightly richer in FeO (mean$_{16}$ = 4.0% sd = 2.8%) than in Fe_2O_3 (mean$_{16}$ = 3.3% sd = 1.8%) and that they show a negative correlation (Fig. 18B). The Stavelot slate main group that has higher Fe_2O_3 and much lower FeO, shows a distinct behaviour. However, a minority of Stavelot slates plots on the same negative trend, which also corresponds to that of the Brabant and Thuringia slates. Two MF garnet black slates are very enriched in FeO. The negative trend can be explained by a mixing between muscovite, a Fe^{3+} carrier mineral (Tschermak substitution of Al by Fe^{3+}), major constituent of the black slate, and Fe^{2+} bearing minerals such as pyrite, chlorite, spessartine and ilmenite. The high Fe_2O_3 content of the Stavelot Inlier slate stems from their oxidizing depositional environment as explained above (Herbosch et al., 2016, 2020).

10.1.3. Comparison of the mean major elements of the Mousty Fm slate with average shale standards

Table 6 compares the average contents of the 30 MF samples with the average shale standards already referenced. The element-by-element comparison is as follows: the SiO_2 content (range 53–66%) is similar to the four existing values that are in the MF range. The average Al_2O_3 content (range 16–24%) is quite high compared to the two Black shale composites and Alum shale (~15%) and close to, but still lower than, the Dictyonema shale and LPC (~18%). The latter two areas are sedimentologically closer to the MF. The very variable Fe_2O_3t content (range 2.4–9.6%) is close to the other standard except for the higher LPC (8.2%) but within the range of its variation. The MnO content (1% sd = 2.8%), which is extremely variable, is significantly higher than most standards except for LPC (0.48%) and one of the Black shale standards (1.1%). The MgO content (range 0.6–2.3%) is quite similar to both Black shale and Baltic shale and significantly lower than NASC (2.8%) and LPC (3.4%) which are outside the range of variation of the MF. The CaO content (range 0–0.9%) is significantly lower than most standards, however, it is within the range of MF variation for LPC (0.9%) and Dictyonema shale (0.66%). Na_2O content (range 0.2–1%) is within the MF range of variation for all the standards except NASC and LPC (>1%). K_2O content (range 2.5–5.1%) is highly variable and within the range of standards but is lower than Baltic shales (>5.0%), reflecting their extremely low sedimentation rates (see § 8.6.1).

It can be concluded that the mean major element composition of the MF black slate is very similar to the shale and black shale standards except for manganese which is abnormally high (mean$_{30}$ = 0.97% sd= 2.77%) and calcium which is very low (mean$_{30}$ = 0.48% sd = 0.46%). These low Ca

Table 4. Description and location of the Mousty Formation samples used for geochemical investigations.

Sample	Lithology	Lithostratigraphy	Chronostratigraphy	Location	Coordinate	Reference
Brab-6	Black slate (garnet ?)	Middle ? part of the Fm	Furongian	Noirha borehole p=33 m, Dyle valley	N 50°37'48''/ E 4°32'11''	Linnemann et al., 2012
Brab-13	Black slate (garnet ?)	Upper part of the Fm	Furongian, Stage 10	Tangissart borehole p=15 m Thyle valley	N 50°36'22''/ E 4°32'15''	Linnemann et al., 2012
Sed 1/14	Black slate (garnet ?)	Middle ? part of the Fm	Furongian	Near Faux, Thyle valley	N 50°37'18''/ E 4°32'55''	André, 1991
Sed 2/1	Black slate (garnet ?)	Middle ? part of the Fm	Furongian	N-E of Court -St-Etienne, Thyle valley	N 50°38'13''/ E 4°34'18''	Ibid.
Sed 2/4	Black slate (garnet ?)	Middle ? part of the Fm	Furongian	SE of Court, Orne valley	N 50°38'75''/ E 4°34'17''	Ibid.
Sed 2/5	Black slate (garnet ?)	Middle ? part of the Fm	Furongian	NE of Court, Orne valley	N 50°39'39''/ E 4°34'25''	Ibid.
W7 206	Black slate without garnet	Lower ? part of the Fm	Furongian, Paibian ?	Franquenies, Ri Angon valley	N 50°39'52''/ E 4°34'27''	Van Tassel, 1986, Table 2
W7 210	Black slate without garnet	Lower ? part of the Fm	Furongian, Paibian ?	Franquenies, Ri Angon valley	N 50°39'52''/ E 4°34'27''	Ibid.
W7 213	Black slate without garnet	Lower ? part of the Fm	Furongian, Paibian ?	Franquenies, Ri Angon valley	N 50°39'52''/ E 4°34'27''	Ibid.
W3 212	Black slate without garnet	Middle ? part of the Fm	Furongian	Mousty, 400 m SW Church Court, Dyle v.	imprecise location	Ibid.
W5 211	Black slate without garnet	Middle ? part of the Fm	Furongian	Mousty, 600 m SW Church Court, Dyle v.	imprecise location	Ibid.
C13 221	Black slate without garnet	Middle ? part of the Fm	Furongian	Court, 400 S of the Orne valley	N 50°38'25''/ E 4°34'37''	Ibid.
C18 238	Black slate without garnet	Middle ? part of the Fm	Furongian	Court, km 31 railway trench, Thyle valley	N 50°38'14''/ E 4°33'57''	Ibid.
G73 240	Black slate without garnet	Middle ? part of the Fm	Furongian	Château de La Motte, Ri Cala valley	N 50°38'29''/ E 4°31'42''	Ibid.
W6 214	Black slate with garnet	Lower ? part of the Fm	Furongian, Paibian ?	Franquenies, Ri Angon valley	N 50°39'52''/ E 4°34'27''	Van Tassel, 1986, Table 5
C29 333	Black slate with garnet	Middle ? part of the Fm	Furongian	Faux, railway trench, Thyle valley	N 50°37'09''/ E 4°32'49''	Ibid.
C45 235	Siltstone with garnet	Upper Tangissart Mbr	Lowermost Tremad.	La Roche, St Gertrude brook	N 50°36'41''/ E 4°39'60''	Ibid.
G74 241	Black slate with garnet	Middle ? part of the Fm	Furongian	La Motte, Ri Cala valley	N 50°38'19''/ E 4°31'37''	Ibid.
W19 215	Grey slate with ilmenite	Middle ? part of the Fm	Furongian	E of Court-St-Etienne, Orne valley	imprecise location	Van Tassel, 1986, Table 4
G2 237	Grey slate (garnet ?)	Middle ? part of the Fm	Furongian	Railway trench km 29, Noirha, Dyle valley	imprecise location	Ibid.
C14 236	Greenish slate, ilmenite	Lower ? part of the Fm	Furongian, Paibian ?	Railway trench S of Court, Thyle valley	N 50°38'11''/ E 4°33'54''	Ibid.
C8 217	Greenish slate, ilmenite	Lower ? part of the Fm	Furongian	Path to the E of Court-St-Etienne	imprecise location	Ibid.
Mo 1	Silicified black slate	Lower ? part of the Fm	Furongian, Paibian ?	NE Franquenies quarry, Ri Angon valley	N 50°39'52''/ E 4°34'27''	Stryckmans, 1989
Mo 2	Inconsistent black slate	Lower ? part of the Fm	Furongian, Paibian ?	NE Franquenies quarry, Ri Angon valley	N 50°39'52''/ E 4°34'27''	Ibid.
Mo 4	Laminated black slate	Lower ? part of the Fm	Furongian, Paibian ?	Franquenies quarry, Ri Angon valley	N 50°39'52''/ E 4°34'27''	Ibid.
Mo 5	Homogeneous black slate	Lower ? part of the Fm	Furongian, Paibian ?	Franquenies quarry, Ri Angon valley	N 50°39'52''/ E 4°34'27''	Ibid.
Mo 6	Homogeneous black slate	Lower ? part of the Fm	Furongian, Paibian ?	Franquenies quarry, Ri Angon valley	N 50°39'52''/ E 4°34'27''	Ibid.
No 4	Black slate (garnet ?)	Middle ? part of the Fm	Furongian	Noirha, entry W highways bridge, Dyle v.	N 50°37'20''/ E 4°31'38''	Ibid.
No 6	Black slate (garnet ?)	Middle ? part of the Fm	Furongian	Noirha, entry E highways bridge, Dyle v.	N 50°37'20''/ E 4°31'38''	Ibid.
No 3	Laminated slate (garnet ?)	Middle ? part of the Fm	Furongian	Noirha, entry W highways bridge, Dyle v.	N 50°37'20''/ E 4°31'38''	Ibid.
	Schistose lydite	Lower ? part of the Fm	Furongian, Paibian ?	Franquenies quarry, Ri Angon valley	N 50°39'52''/ E 4°34'27''	Bonjean et al., 2015b
Sc-1	Black of Sclayn	Lower ? part of the Fm	Assumed Furongian	Scladina cave (Andenne, Belgique)	N 50°29'09''/ E 5°01'33''	Ibid.
Sc-2	Black of Sclayn	Lower ? part of the Fm	Assumed Furongian	Scladina cave (Andenne, Belgique)	N 50°29'09''/ E 5°01'33''	Ibid.
Sc-3	Black of Sclayn	Lower? part of the Fm	Assumed Furongian	Scladina cave (Andenne, Belgique)	N 50°29'09''/ E 5°01'33''	Ibid.

Table 5. Description and location of the samples from the Chevlipont and Jodoigne formations used for comparisons.

Sample	Formation	Lithology	Chronostratigraphy	Location	Reference
Brab-4	Lower part of Jodoigne	Black slate	Wuliuan	Orbais, temporary excavation	Linnemann et al., 2012
Brab-5	Upper part of Jodoigne	Black slate	Guzhangian	Jodoigne, Old Grand-Moulin Street	Linnemann et al., 2012
JO1	Upper part of Jodoigne	Black slate	Guzhangian	N of Jodoigne	Stryckmans, 1989 Annexe
Re 8	Chevlipont	Fine laminated siltstone	Lower half Tremadocian	Tangissart, Renoussart sunken path	Stryckmans, 1989 Annexe
DY 2	Chevlipont	Black argillaceous siltite	Lower half Tremadocian	S of Tangissart level crossing	Stryckmans, 1989 Annexe
Brab-23	Chevlipont	Grey wavy siltstone	Lower half Tremadocian	Lessines borehole, 357 m	Linnemann et al., 2012
LE 13	Chevlipont	Argillaceous siltstone	Lower half Tremadocian	Lessines borehole, 302 m	Unpublished
LE 14	Chevlipont	Grey wavy siltstone	Lower half Tremadocian	Lessines borehole, 302 m	Unpublished
LE 15	Chevlipont	Argillaceous siltstone	Lower half Tremadocian	Lessines borehole, 303 m	Unpublished
LE 16	Chevlipont	Grey wavy siltstone	Lower half Tremadocian	Lessines borehole, 329 m	Unpublished
LE 17	Chevlipont	Grey wavy siltstone	Lower half Tremadocian	Lessines borehole, 357 m	Unpublished

Table 6. Mean major elements from Mousty Formation compared with average shale. St. dev. = standard deviation; NASC = North American Shale Composite; LPC = Lithogenous Pelagic Clay; LOI = loss on ignition; n.a. = not analysed.

%	MOUSTY Formation		NASC	LPC	Black shale	Black shale	Alum shale	Dictyonema shale
	Mean	St. dev.	Gromet et al., 1984	Chester, 1990	Vine & Tourtelot, 1970	Quinby-H. et al., 1989	Gautneb & Saether, 2009	
							Cambrian	Tremadocian
	n = 30	n = 30	n = 40		n = 779	n = 247	n = 107	n = 22
SiO_2	59.40	6.24	64.80	55.59	n.a.	n.a.	54.26	59.92
Al_2O_3	20.37	4.15	16.90	17.56	15.12	15.5	15.58	18.12
Fe_2O_3t	5.99	3.63	6.33	8.21	6.07	5.26	5.23	5.46
MnO	0.97	2.77	0.06	0.48	1.10	0.5	0.01	0.02
MgO	1.45	0.89	2.85	3.43	1.16	1.72	1.25	1.39
CaO	0.48	0.46	3.56	0.94	3.09	2.4	1.24	0.66
Na_2O	0.57	0.39	1.15	1.54	0.94	0.71	0.66	0.55
K_2O	3.79	1.32	3.99	3.27	3.20	2.88	4.95	5.45
TiO_2	0.93	0.18	0.78	0.85	0.77	0.72	n.a.	n.a.
P_2O_5	0.13	0.12	0.11	0.14	n.a.	n.a.	0.14	0.20
LOI	5.47	1.84		8.00	n.a.	n.a.	14.85	6.89
Total	99.55			100.01			98.17	98.66

contents are also observed in the Jodoigne Fm and Chevlipont Fm (mean$_{11}$ = 0.42% sd = 0.37%; Table 2). More generally, these low values are observed in all the Cambrian and Ordovician rocks of the Brabant Massif (mean$_{31}$ = 0.32% sd = 0.36%; Stryckmans, 1989). A likely explanation for the very low calcium values is that in the Cambrian there is no plankton with a calcareous skeleton.

We have just seen that the MF slates are enriched in Mn, strongly for three of them (Fig. 18A). Such Mn enrichment is characteristic of the Ottré Fm from the Stavelot slates (early Floian, c. 478 Ma), whose origin is related to the nearby oceanic ridge of the nascent Rheic Ocean (Herbosch et al., 2016, 2020). The MF is a little older (Furongian, 497–485 Ma) and could therefore have been connected, especially in its younger part, to

the very first stammering of the still infantile Rheic Ocean. Such a still narrow ocean would share several features with the Phanerozoic intracratonic euxinic basins whose water mass structure constitutes a large reservoir from which Mn is mobilized with a very steep redox gradient (Maynard, 2010). Such a palaeogeographic and palaeotectonic situation corresponds to the basin where the MF was deposited. We have seen previously (§ 8.5) that from the early Cambrian, an extremely subsiding aborted rift opened on the northern margin of the Gondwana continent (Verniers et al., 2002; Herbosch et al., 2020) and became anoxic between the Miaolingian (Jodoigne Fm), the Furongian (MF) and the lower half of the Tremadocian (Chevlipont Fm) before the rift-drift of Avalonia from Gondwana. The MF would thus bring information on the
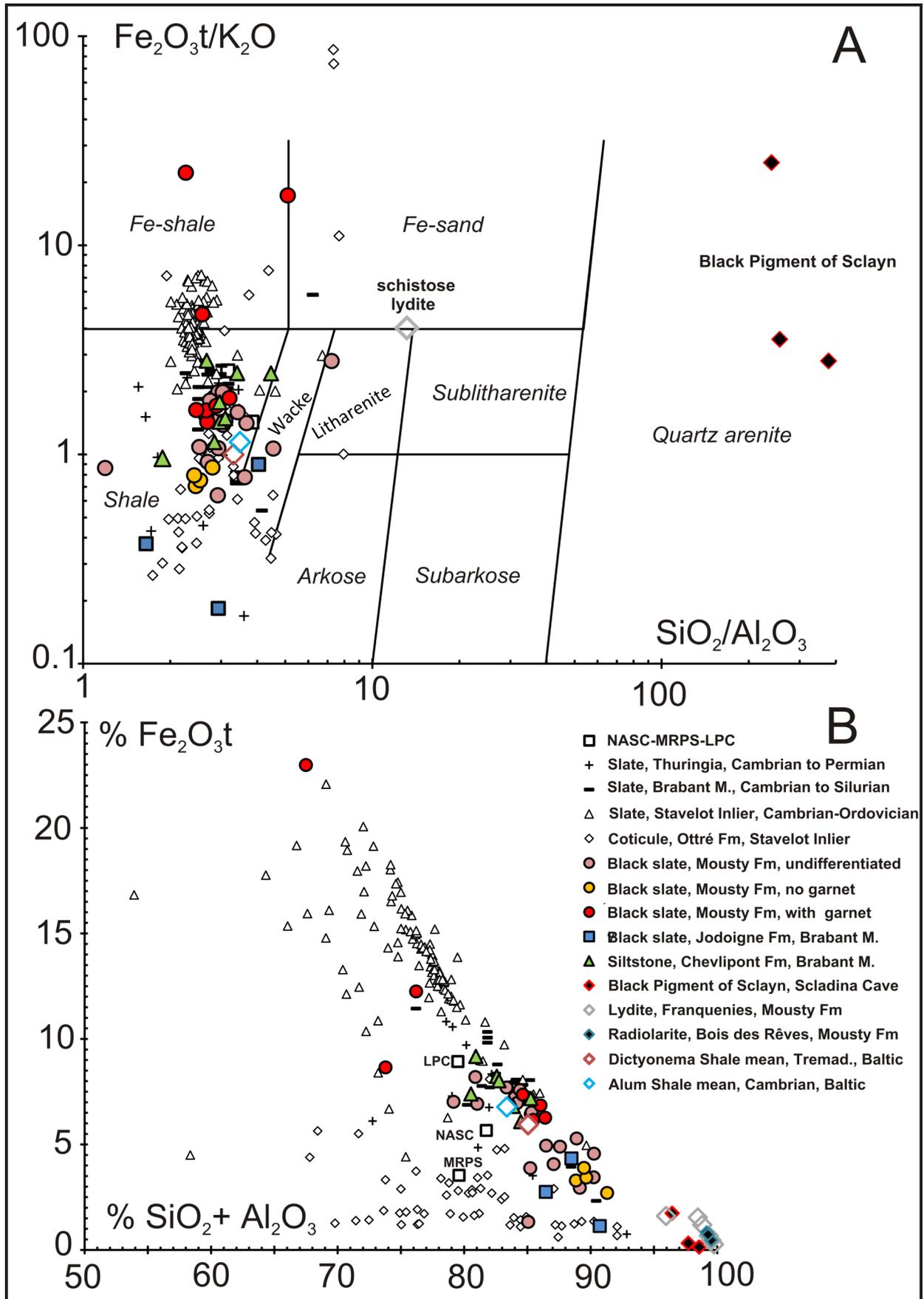
Figure 17. A. Lithological-geochemical classification Fe_2O_3t/K_2O versus SiO_2/Al_2O_3 (Herron, 1988). For Mousty, Chevlipont and Jodoigne formations, the location, description, references and data are given in Tables 1 to 6. NASC = North American Shale Composite (Gromet et al., 1984); MRPS = Mean Russian Platform Shale (Ronov & Migdisov, 1996); LPC = mean of 12 Lithogenous Pelagic Clays (Chester, 1990); Thuringian slates (n = 12, Cambrian to Permian) from Römer & Hahne (2010); Alum and Dictyonema shales from Gautneb & Saether (2009); Brabant slates (n = 26, Cambrian to Silurian) from Linnemann et al. (2012); SVM slates and coticules from Herbosch et al. (2016). **B.** Bivariate plot % Fe_2O_3t versus % SiO_2 + Al_2O_3. Same data as Fig. 17A. See text for explanation.
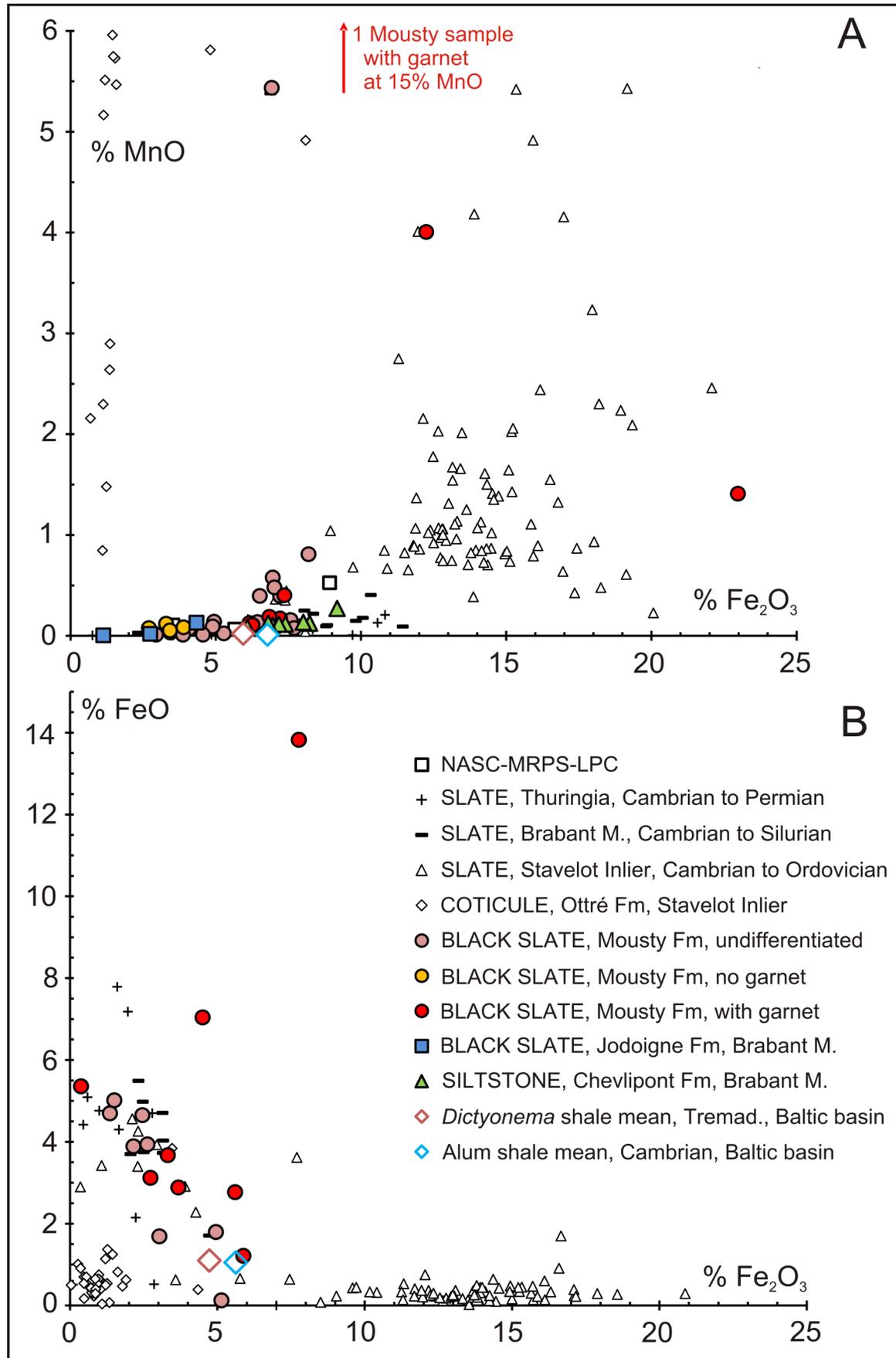
Figure 18. A. Bivariate plot % MnO versus % Fe$_2$O$_3$. **B.** Bivariate plot % FeO versus % Fe$_2$O$_3$. Symbols and references as in Fig. 17. See text for explanation.

first jolts of the opening of the Rheic Ocean which would have begun during the Furongian, the period during which the coticule was deposited (early Floian) corresponding to an ocean already well formed, even if still narrow. This audacious hypothesis would be worth testing by systematically analysing the Mn content of the slates in relation to their stratigraphic position.

10.2. Major elements in the different varieties of lydite (phtanite)

Van Tassel (1986) analysed the major elements of the lydite from the Franquenies quarry where he made the distinction between the schistose lydite from the Franquenies quarry and the stratified lydite with conchoidal fracture of the Bois des Rêves quarry. Despite the small number of samples analysed, it can be seen in Table 3 that the schistose lydite shows lower SiO_2 ($mean_4 = 88.9\%$) and higher Al_2O_3 ($mean_4 = 4.5\%$) contents than the stratified lydite ($mean_3$ $SiO_2 = 91.1\%$ and $mean_3$ $Al_2O_3 = 3.5\%$). This supports the hypothesis previously put forward (see § 5.3, 8.4) according to which the lydites observed in the Franquenies quarry are the result of recrystallisation and their reorientation in the cleavage during the Brabantian orogeny. Thin sections and geochemistry show that these lydites are essentially composed of quartz, highly dispersed graphite and very low amounts of muscovite which explains the relatively high fire losses of between 2.8 and 5.3%. The sum of the four elements analysed is close to 100%, especially for the stratified lydites ($mean_3 = 99.60\%$).

In the graph SiO_2/Al_2O_3 versus Fe_2O_3t/K_2O (Fig. 17A) the schistose lydite is found in the upper right corner of the Litharenite field (grey diamond) far away from the MF slate which reflects its very high SiO_2 and its notable Al_2O_3 contents. The three samples of the Black Pigment of Sclayn (red diamonds) are found in an even more SiO_2-rich field, i.e. Quartz arenite. More convincingly, in the graph $SiO_2 + Al_2O_3$ versus Fe_2O_3t (Fig. 17B) all lydite varieties and the Black Pigment of Sclayn are clustered towards the end of the x-axis in agreement with the existence of a geochemical relation between the lydites and the Black Pigment of Sclayn (Bonjean et al., 2015a, 2015b).

10.3. Trace elements in the black slate

Table 7 gives an indication of the trace element composition as these data are largely incomplete. Only three analyses of the MF, two black slates and one lydite are complete. This makes any meaningful discussion difficult. However, we will consider uranium first because of the presence of strong radon anomalies in the MF outcrop area (see § 10.4). Only four analyses (two on borehole and two on field samples) give an average of 4.3 ppm, which is quite low compared to the average of 15.2 ppm for the Black shale composite (Quinby-Hunt et al., 1989), 40 and 14 ppm for the Alum and Dictyonema shales respectively (Gautneb & Saether, 2009). If we consider all the U analyses of the sedimentary rocks from the Brabant Massif (Linnemann et al., 2012, tables 1, 3) the calculation of the averages (1) for the black slates gives: $mean_7 = 4.14$ ppm sd = 1.63 ppm, (2) for the organic-poor silt-clay rocks: $mean_7 = 2.19$ ppm sd = 0.66 ppm. The value of 2.19 ppm is close to the average value for sedimentary rocks of 1–2 ppm (Rogers & Adams, 1969). It can be tentatively concluded that either the U contents of the black shales of the Brabant Massif rocks are about twice the average for sedimentary rocks or, given the very frequent presence of pyrite, that this mineral alters under weathering conditions, leading to the formation of sulphuric acid which leaches out the U contained in the field samples (Ichikuni, 1959; Roth, 2007).

Calculated averages for the elements generally considered to be enriched in anoxic environments, i.e. As, Cr, Cu, Mo, Ni, Pb, U, V, Zn are compared with average black shales, Alum and Dictyonema shales (Vine & Tourtelot, 1970; Quinby-Hunt et al., 1989; Gautneb & Saether, 2009). Generally speaking and taking into account the very low number of data, the comparison of the means for the MF with the two Black slate composites (Table 7) shows that they are of the same order for As, Cr, a little lower for Co, V, and much lower for Mo, U, Zn. The comparison with the Alum and Dictyonema shales is even more telling: in addition to the Zn and Cr contents, which are of the same order of magnitude, the contents of Mo, Ni, U and V are 5 to 10 times higher than those of the MF. The explanation is probably the same as that seen previously for U, i.e. the strong weathering of the field samples.

10.4. The radon risk

10.4.1. The facts

For more than 30 years, F. Tondeur and his team at the Institut Supérieur Industriel de Bruxelles (ISIB) have been accumulating radon measurements in buildings in Wallonia. The geographical distribution of these data (Tondeur, 1998) shows that in Walloon Brabant, the municipalities of Villers-la-Ville and Court-Saint-Etienne are high to very high radon risk areas. In Court-Saint-Etienne, this author noted 13 abnormal cases out of 75 measurements with extremely high anomalies (>5000 Bq/m^3) on the ground floor, whereas the standards recommended not to exceed 400 Bq/m^3. The comparison of these results with the geological maps of the upper Dyle basin shows a strong correlation with the MF outcrops (Tondeur et al., 2001).

Since these preliminary works, new measurements have been made by ISIB and new geological maps of the region have been published (see Chap. 3). We have reported the radon measurements (F. Tondeur, pers. comm., 2020) on these maps where the Brabant basement is exposed in the Dyle, Thyle valleys and their tributaries (Fig. 19). In the considered area, the Mousty and Tubize fms occupy large areas and show respectively 127 and 72 radon measurements. The Blanmont Fm and the Ordovician fms occupy less surface area and only 20 measurements are reported. It is important to note that outside the valleys the old Palaeozoic basement is covered by thick layers of Cenozoic sand (e.g. Brussels Fm) with very low radioactivity. In the same way, the middle of the valleys is occupied by modern alluvium with a low permeability that blocks radon migration.

The statistical parameters of radon measurements for the MF are:
- average: $x_{127} = 457$ Bq/m^3 sd = 945
- geometric mean: $x_{127} = 130$ Bq/m^3
- median: M = 97 Bq/m^3
- number of values >300 Bq/m^3 = 31 (24%)

For the Tubize Fm:
- average: $x_{72} = 194$ Bq/m^3 sd = 694
- geometric mean: $x_{72} = 68$ Bq/m^3
- median: M = 55 Bq/m^3
- number of values >300 Bq/m^3 = 8 (11%).

Comparison of means and standard deviation shows that radon levels are higher in the MF but the distribution of values is highly skewed, with many low values and some very high values. Given a log-normal distribution of radon contents (Cinelli & Tondeur, 2015), the geometric mean or even better the median is much more representative of the central tendency. This shows that the central values are much higher (about 2 times) in the MF than in the Tubize Fm. Examination of Figure 19 shows indeed many more red (>801 Bq/m^3), purple (401–800 Bq/m^3) and orange (201–400 Bq/m^3) dots distributed fairly

Table 7. Trace elements of the Mousty Formation compared to black shale average. Lin. = Linneman et al.; V & T = Vine & Tourtelot; Q-Hunt = Quinby-Hunt et al. L.D. = Lower Detection limit.

Ref.		Lin., 2012		André, 1991		Stryckmans, 1989 slate (garnet?)									Lydite		AVERAGE BLACK SHALE			
																	Black shale V & T, 1970	Black shale Q-Hunt 1989	Alum shale (Gautneb & Saether, 2009)	Dictyonema shale (Gautneb & Saether, 2009)
Formation / Sample		MST Brab-6	MST Brab-13	MST sed1/14	MST sed2/1	MST sed2/4	MST Mo1	MST Mo2	MST Mo4	MST Mo5	MST Mo6	MST No4	MST No6	MST No3	MST	Mean MST	n = 779	n = 333	Cambrian n = 107	Tremadocian n = 22
As	ppm	< L.D.	36.84												12	**21**	300	28.8		
Ba	ppm	850.9	684.8	1531	737	613									144				2655	1226
Co	ppm	8.24	13	9	6	9									0.8	**8**	10	16.9		
Cr	ppm	117	98.79	119	101	104									37	**96**	100	111	212	173
Mo	ppm	16.32	< L.D.												6.2	**11**	10	65	209	88
Ni	ppm	16.61	27.26	33	27	27	8	14	5		16	7	10	11	10	**16**	50		154	137
Pb	ppm	17.32	9.53												73	**33**			n.d.	
Rb	ppm	188.8	212.7	133	211	197	130	178	154		156	277	130	165	18					
Sr	ppm	193.7	53.12	44	84	41	109	154	111		111	71	40	59	168					
Th	ppm	13.5	12.85		15.7		<3	<3	<3		<3	<3	7	<3	17				9	15
U	ppm	5.59	2.49		3.9										5.3	**4.3**		15.2	40	14
V	ppm	171.6	140.9	153	138	127									102	**139**	150	500	1151	929
Zn	ppm	131.5	102.5													**117**	300	310	85	166
Zr	ppm	172	164.9	180	183	197	92	144	145		131	161	312	165			70			

evenly in the MF. In contrast, in the Tubize Fm, these dots are significantly fewer (8 of 72 measurements). In addition, high values are absent from the northern outcrop zone (Limelette area) and are confined in a narrow band N of Mont-St-Guibert.

We refer the reader to Paragraph 10.3 concerning the surprisingly low U content of the MF black shale. The radon anomalies of the Tubize Fm are difficult to explain because its lithology ranges from sandstones to green clayey siltstones, i.e. an oxidizing depositional environment without organic matter and therefore with very low U content (1.8 ppm in Linnemann et al., 2012). However, Roth (2007) points out that the availability of radon in the ground and its transfer to the house depend largely on the release of radon from the weathering products, and much less on the radon release of rocks. Although radium on the weathering products is mainly bound to pedogenic clay minerals, it is rather the amount of radium bound in the Fe and Mn oxides/hydroxides that is the cause for enhanced radon emanation (Roth, 2007). The Tubize Fm is locally very rich in magnetite and pyrite which can also be altered to Fe-oxide.

10.4.2. Synthesis

Over the last 10 years, the Belgian Federal Agency for Nuclear Control (AFCN) has carried out new measurements in the Brabant Massif (Tondeur et al., 2014, 2015). These authors define a "high radon area" with more than 1% of houses above the reference level. In the Brabant Massif four geological units are strongly affected by radon (Tondeur et al., 2015, table 2):
- the Silurian of the Mehaigne basin: median =114 Bq/m^3 for 30 measurements,
- the Ordovician of the Dyle basin: median = 100 Bq/m^3 for 101 measurements,
- the MF: median = 90 Bq/m^3 for 292 measurements,
- the Tubize Fm (Limelette and Mont-St-Guibert areas, Fig. 19): median = 72 Bq/m^3 for 79 measurements, values that are not significantly different from those quoted at the beginning of this paragraph.

In conclusion, if the MF, exposed on a small surface (about 10 km^2) in the Dyle basin, is clearly a "high radon area", it is neither the only nor the most affected area in the Brabant Massif. It is interesting to note that these "high radon areas", except for the Tubize Fm, are lithologically characterized by shales rich in organic matter that were deposited in deep seas with a slow sedimentation environment.

11. Metamorphic mineralogy

Of all the formations in the Brabant Massif, the MF contains the largest number of metamorphic minerals: muscovite, chlorite-mica stack, chlorite, garnet, ilmenite, rutile, biotite and andalusite in decreasing order of abundance. The presence of graphite will be discussed separately in § 12.1.

11.1. Chlorite-mica stack and muscovite

The chlorite-mica stacks (Jodard, 1986; Alomène, 1987; Geerkens & Laduron, 1996; Larangé, 2002; Herbosch & Verniers, 2013) are very common in these black slates. In thin sections, these stacks are characterized by the simple or repeated joining of sheets of chlorite and white mica, the whole taking the form of an elongated spindle with a fairly regular contour of variable size between 20 μm and a maximum of 200 μm (Photo 21). Their size is much larger than the other components of the rock, which makes them true porphyroblasts. They are arranged parallel to the stratification and are essentially formed of chlorite, the mica being reduced to a few thin sheets (Photo 23).
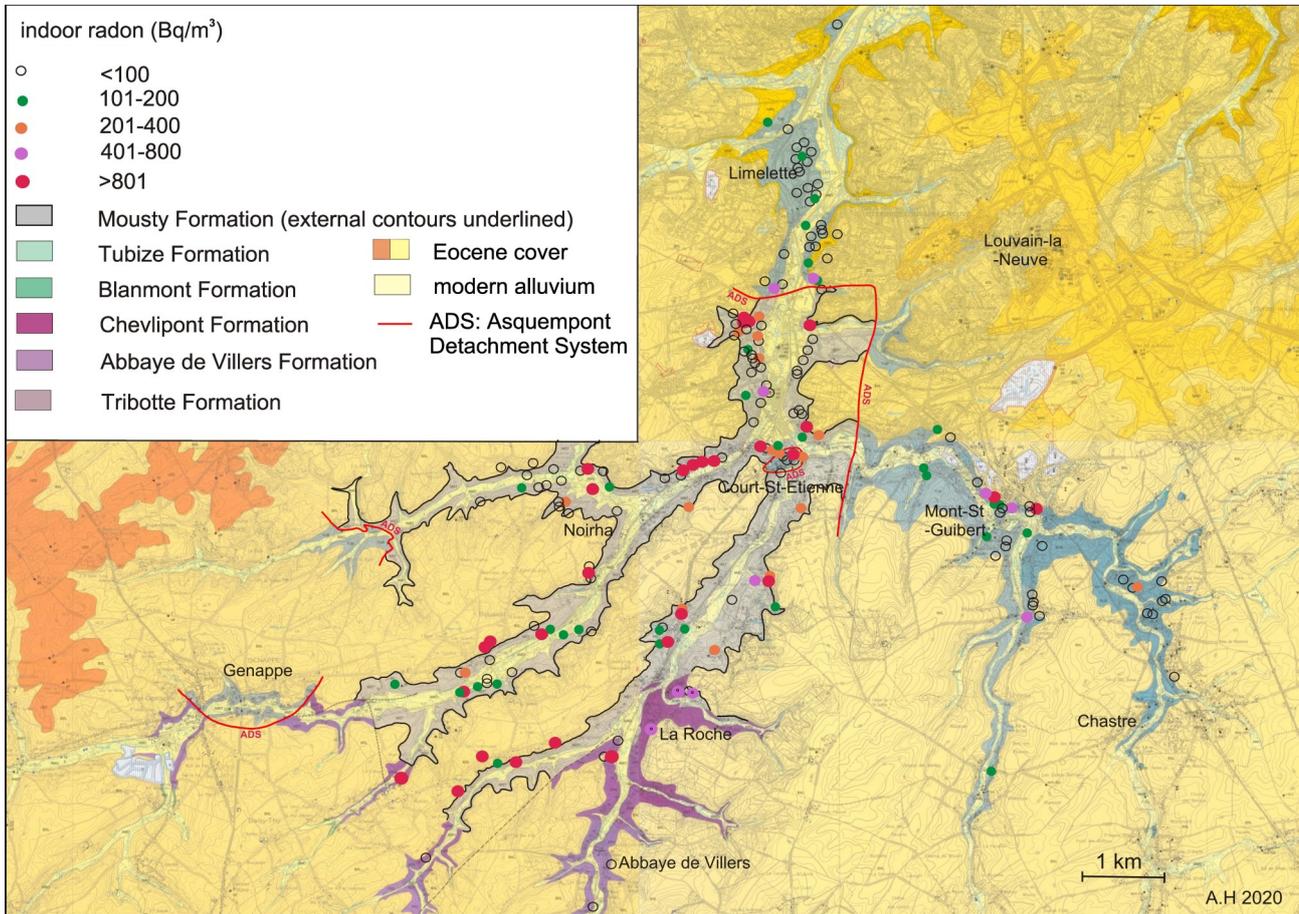
Figure 19. Geological map of the Dyle basin (Herbosch & Lemonne, 2000; Delcambre et al., 2002; Herbosch & Blockmans, 2012) with the distribution of radon measurements in buildings. Radon data from F. Tondeur, written comm., 2020.

The alternation of the chlorite and mica lamellae is roughly parallel to the elongation of the grains and the contact is always very sharp. Chlorite shows a distinct pleochroism colourless to faintly green and interference colours range from first-order grey to abnormal blue. The stacks develop less well in the MF than in the higher Chevlipont and Abbaye de Villers fms which are richer in terrigenous material.

Microprobe analysis of the chlorite from the chlorite-mica stacks (Jodart, 1986; Alomène, 1987) shows that they are enriched in manganese (0.81, 1.84, 2.09%; Table 8) compared to the overlying Chevlipont and Abbaye de Villers fms where their content is lower (mean$_5$ = 0.53% sd = 0.18). These chlorites belong to the ripidolite variety in the Hey classification (1954) and they are trioctahedral type I or Fe-chlorites in more recent classifications (e.g. Zane & Weiss, 1998; Yavuz et al., 2015). Except for their slightly higher Mn contents in the MF, all the chlorites in the stacks have similar compositions (Table 8; Fig. 20) despite the considerable differences in the lithology of the Chevlipont (siltstone) and Abbaye de Villers (clay siltstone) formations. Considering the errors inherent in the microprobe analysis, the composition of the chlorites in the stacks can be considered to be identical for the same rock and therefore neoformed in equilibrium with the rock geochemistry. The spot analysis of the micas in the stacks shows that they are always muscovites (Table 9). They do not contain Mn, which demonstrates that micas and chlorite have distinct origins. However, we observe a strong dispersion of their chemical composition with substitution of Al^{VI} by Fe^{3+} of the order of 5 to 10% and to a lesser extent by Mg^{2+} (Tschermark substitution). These variations are not only from one rock to another but also within the same rock, which suggests that the metamorphism

was not sufficiently intense to bring all the detrital muscovites to equilibrium.

Without going into the details of the controversy concerning the origin of chlorite-mica stacks (e.g. Dandois, 1985; Milodowski & Zalasiewicz, 1991; Li et al., 1994; Larangé, 2002), it can be concluded that in the present case, the white mica has a detrital origin whereas the chlorite is neoformed. The following observations support this statement: (a) the variable composition of the mica and the homogeneous composition of the chlorite, (b) the similarity in shape and size between the micas of the stacks and those of the rock matrix, (c) a positive correlation between the granulometry of the quartz and the size of the micas of the stacks (Jodard, 1986), (d) their disposition parallel to stratification.

11.2. Chlorite

In addition to the stacks described above, chlorite also exists in very small crystals that form a significant part of the fine matrix of the rock ("matrix" in Table 8). In some levels, they show also xenomorphic crystals of larger size (15–25 μm, "grain" in Table 8). Their Mn content is highly variable but on average higher (mean$_8$ = 1.12%) than in the Chevlipont and Abbaye de Villers fms (mean$_{10}$ = 0.45%). As seen previously all these chlorites, whether they belong to the stacks, matrix or as grain, are trioctahedral Fe-chlorites and show a very similar chemical composition proving that they are in equilibrium with the metamorphic conditions.
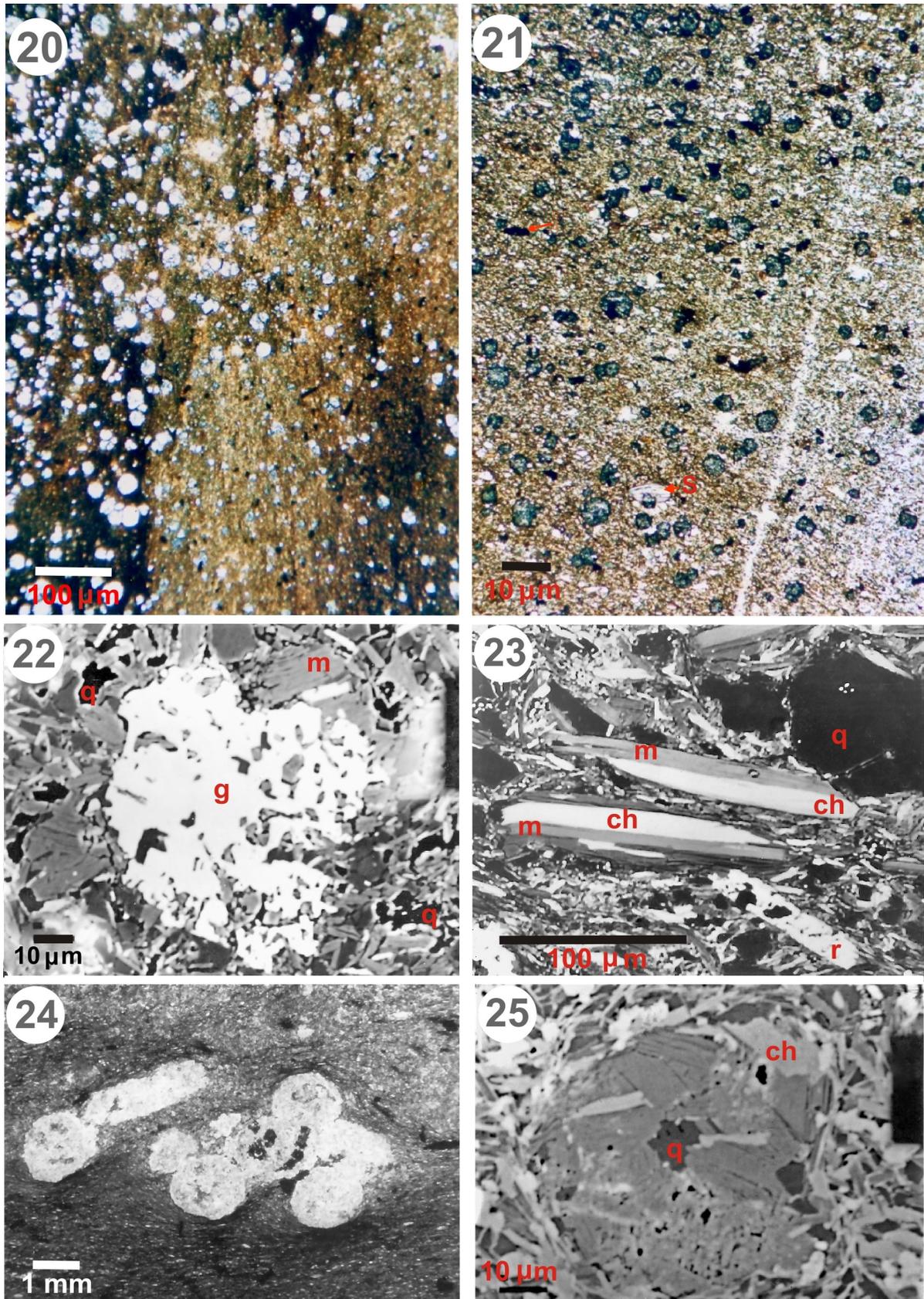
Plate 4. Photo 20. Garnet porphyroblasts in black slate rich in organic matter laminae. The smaller opaque needles are Mn-ilmenite. Thin section, normal light. Bois Ste-Gertrude near La Roche, upper part of the formation (location Fig. 2). Photo A. Herbosch, 2000. **Photo 21.** Slate with tiny single crystals of garnet. There are also some ilmenite sticks (I) and illite-chlorite stacks (S). Same location as Photo 20. Thin section, normal light. Photo A. Herbosch, 2000. **Photo 22.** Microprobe BSE image of poeciloblastic spessartine crystal (g) which includes various matrix minerals like quartz (black). Quartz (q) and micas (m) with their cleavage can be seen all around. Photo from Jodard (1986). **Photo 23.** Microprobe BSE image from two illite-chlorite stacks (ch = chlorite, m = mica). The quartz crystals (q) are black, the rutile porphyroblast (r) includes several quartz crystals. Photo from Jodard (1986). **Photo 24.** Retromorphosed andalusite porphyroblasts that form lenticular to subspherical aggregates. The core of the right clusters shows small lamellae of chlorite associated with a blackish submicroscopic substance (chiastolite remnant?) and quartz. Thin section, normal light. Photo from Jodard (1986). **Photo 25.** BSE microprobe image of a retromorphosed andalusite porphyroblast consisting of embedded muscovite flakes. Quartz (q) and chlorite (ch) inclusions. Photo from Jodard (1986).

Table 8. Microprobe analysis of different types of chlorite in three Ordovician formations. Three types of chlorite are distinguished: in chlorite-mica stacks, in matrix and in xenomorphic crystal. From Jodard (1986). Analyst J. Wauthier, CAMST, Université Catholique de Louvain, Belgium.

Formation	Abbaye de Villers Formation					Chevlipont Formation						Mousty Formation						
Sample	4	4	4	9	9	11	11	14	14	14	18	23	23	23	25	25	25	25
Type	stack	matrix	stack	matrix	stack	stack	matrix	stack	grain	matrix	matrix	stack	matrix	stack	matrix	grain	grain	stack
%																		
SiO_2	22.93	26.52	23.04	23.65	23.34	23.74	22.68	22.34	22.69	24.82	22.87	22.10	22.87	22.68	28.24	23.40	25.72	22.63
TiO_2	0.06	0.29	0.17	0.22	0.02	0.03	0.05	0.05	0.09	0.08	0.04	0.05	0.05	0.07	0.01	0.08	0.11	0.09
Al_2O_3	23.69	23.98	24.04	23.48	22.9	24.42	24.12	24.14	23.50	25.04	22.47	23.89	23.73	24.16	27.46	24.03	27.19	24.17
FeO	31.71	29.9	31.61	30.33	32.64	30.35	30.29	30.89	30.12	28.81	29.37	30.46	29.02	28.73	22.74	29.18	27.57	30.07
MnO	0.61	0.49	0.71	0.26	0.35	0.31	0.27	0.65	0.46	0.44	0.23	2.09	1.53	1.84	0.66	1.02	0.81	0.81
MgO	7.20	6.18	6.97	7.62	7.24	7.90	7.80	8.10	8.62	7.13	8.81	7.70	7.68	7.41	5.58	7.87	6.71	8.03
CaO	0.03	0.08	0.00	0.03	0.00	0.00	0.01	0.03	0.07	0.04	0.51	0.00	0.06	0.00	0.30	0.02	0.02	0.01
Na_2O	0.0	0.05	0.09	0.06	0.02	0.08	0.00	0.09	0.04	0.08	0.04	0.11	0.15	0.04	0.47	0.02	0.23	0.02
K_2O	0.11	0.47	0.13	0.35	0.05	0.32	0.05	0.07	0.06	0.38	0.08	0.05	0.27	0.16	1.48	0.10	0.96	0.05
Number of cations on the basis of 28 oxygens																		
Si	5.107	5.6712	5.102	5.239	5.202	5.177	5.068	4.962	5.056	5.367	5.162	4.936	5.116	5.082	5.872	5.179	5.364	5.029
Ti	0.010	0.047	0.028	0.037	0.003	0.005	0.008	0.008	0.015	0.013	0.007	0.009	0.008	0.012	0.002	0.013	0.017	0.015
Al	6.220	6.044	6.275	6.131	6.016	6.277	6.353	6.320	6.173	6.382	5.978	6.289	6.257	6.381	6.730	6.269	6.683	6.331
Fe	5.907	5.347	5.854	5.619	6.084	5.535	5.660	5.738	5.614	5.210	5.544	5.689	5.429	5.384	3.954	5.401	4.808	5.589
Mn	0.115	0.089	0.133	0.049	0.066	0.057	0.051	0.122	0.087	0.081	0.044	0.395	0.290	0.349	0.116	0.191	0.143	0.152
Mg	2.391	1.970	2.301	2.516	2.405	2.568	2.598	2.682	2.864	2.298	2.964	2.563	2.561	2.475	1.730	2.597	2.083	2.660
Ca	0.007	0.018	0.000	0.007	0.000	0.000	0.002	0.007	0.017	0.009	0.123	0.000	0.014	0.000	0.067	0.005	0.004	0.002
Na	0.000	0.021	0.039	0.026	0.009	0.034	0.000	0.039	0.017	0.034	0.018	0.048	0.065	0.017	0.189	0.009	0.093	0.009
K	0.031	0.128	0.037	0.099	0.014	0.089	0.014	0.020	0.017	0.105	0.023	0.014	0.077	0.046	0.393	0.028	0.255	0.014
OH	8.000	8.000	8.000	8.000	8.000	8.000	8.000	8.000	8.000	8.000	8.000	8.000	8.000	8.000	8.000	8.000	8.000	8.000
Total	27.788	27.335	27.770	27.722	27.799	27.741	27.751	27.899	27.859	27.498	27.863	27.943	27.818	27.747	27.053	27.692	27.452	27.802
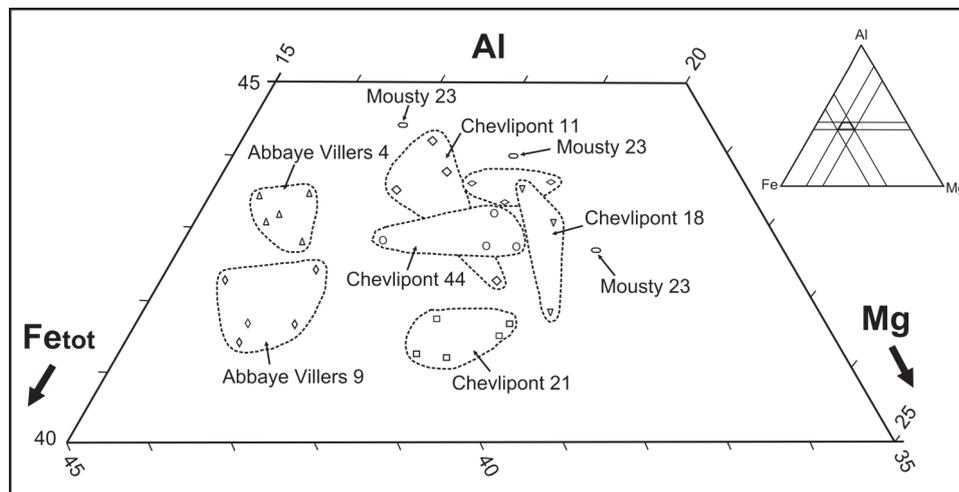
Figure 20. Projection of atomic percentages of Al - Fe_{tot} - Mg contents of the chlorite-mica stack in formations close to Mousty Fm. Data in Table 8. See text for explanation.

11.3. Spessartine garnet

Spessartine garnet has long been known in the MF (De Windt, 1897; Anthoine & Anthoine, 1943; de Magnée & Anciaux, 1945; Van Tassel, 1986), they are common but in highly variable abundance (0 to 30%). They most often occur in crystals ranging from a few microns to a few hundred microns dispersed in the silty-clay matrix (Photos 20, 21). They are sometimes observed in silty laminae or beds where they are very abundant. Garnets are most commonly found in the form of small rhombic dodecahedrons. When they are very small (<10 μm), only their strong refringence allows them to be recognised and then they have a subspherical shape (Photo 21). When they are larger (>50 μm) the crystals tend to stick together and form a kind of cluster (Photo 20). Seen with the microprobe, the garnets show a poeciloblastic structure that encloses the minerals of the matrix (Photo 22). Microprobe analysis (Jodard, 1986; Alomène, 1987) shows that the garnet is a mixture of 2/3 spessartine and 1/3 almandine of fairly constant composition Sp 59–70% ($mean_{13}$ = 65%) Al 23–30% ($mean_{13}$ = 26%) Gr 5–11% ($mean_{13}$ = 7%) Py 0.7–1.3% (Table 10). The grossular content is low, which is not surprising as the MF and in general, the rocks of the Brabant Massif are particularly low in calcium (Stryckmans, 1989; see § 10.1). Garnets are slightly zoned with Mn increasing from the edge of the crystals towards the centre (Sp 59 to 69.4%) while Fe decreases (Al 28 to 23.5%) and Ca decreases by half (Gr 11 to 5.5%) (Table 10).

The only other garnets observed in the Brabant Massif are those reported in the phosphatic conglomerate of the Thy sunken path (de Magnée & Lambeau, 1965). These small conglomeratic levels are interbedded in the Abbaye de Villers Fm (Herbosch & Lemonne, 2000) and are interpreted as debris flow deposits (Debacker et al., 2009a). The garnets have the same composition as those of the MF (Sp 68% Al 26% Gr 6% Py 0.7%; Table 10) which would tend to show that the elements with garnet of the conglomerate are derived from the MF.

It is interesting to point out that spessartines of the MF, with their specific signature, are found in great abundance in the heavy minerals of the Cenozoic cover from the Brabant Massif (Van der Sluys, 1990, 1991). In particular, the Heers and Landen fms (Palaeocene) where they form 100% of the heavy minerals, the Bruxelles Fm (Eocene) where they constitute 25% and finally the Diest Fm (Miocene) where they form about 55%. This further shows that the MF occupied large areas that were subject to erosion during the successive transgressions that eroded the Brabant Massif (Vandenberghe et al., 1999).

11.4. Ilmenite

Ilmenite is very common and occurs as elongated, automorphic to subautomorphic sticks whose size (80–200 μm) greatly exceeds that of the detrital particles forming the rock matrix (Photos 20, 21). Its poeciloblastic structure includes crystals of quartz and muscovite, proving its metamorphic origin. Ilmenite slates without garnets are common and vice-versa (de Magnée & Anciaux, 1945). Their chemical analysis (Table 11) shows highly variable manganese content, ranging from 0.05 to 10% MnO and a Ti/Fe ratio higher than the theoretical stoichiometry due to the replacement of Fe by Mn (Van Tassel, 1986; Jodard, 1986; Alomène, 1987).

11.5. Biotite

Chlorite transformed into greenish or brown biotite was described by de Magnée & Anciaux (1945) and more reliably by Walraevens (1982) and Van Tassel (1986, fig. 4) who observed biotite in thin sections. This identification has never been confirmed by microprobe analysis, but it is almost certain since it has been identified in the Abbaye de Villers Fm (Jodard, 1986), in the Jodoigne Fm (André et al., 1981; Giese et al., 1997), and in the Tubize Fm (Herbosch, unpublished).

11.6. Rutile

Rutile also occurs as elongated automorphic sticks of variable abundance but less than 1%. Inclusions of quartz or muscovite are frequent. Porphyroblasts are not oriented and are observed alone or sometimes in association with garnet (Photo 23 bottom left). Analysis shows that it is almost pure TiO_2 ($mean_{5\ TiO2}$ = 99.7% sd = 1.0, $mean_{5\ FeO}$ = 0.32% sd = 0.13). The microprobe reveals the mixed nature of some Ti porphyroblasts formed of rutile and ilmenite. It could be that ilmenite was stabilized at a lower temperature by Mn and that it would be the result of a prograde conversion of rutile.

11.7. Retromorphosed andalusite

Andalusites are millimetre-sized aggregates whose outer shape is spherical to lenticular and whose direction of elongation is more or less parallel to the stratification (Photo 24). They are observed in the upper part of the MF, especially in the Tangissart Mbr. They were initially described by Michot (1977), who suggested an epigenesis of cordierite. Taking up his study, Jodard (1986) shows that it is most probably the retromorphosis

Table 9. Microprobe analysis of different types of muscovite from the Mousty Formation and from the retromorphosed andalusite. From Jodard (1986). Analyst J. Wauthier, CAMST, Université Catholique de Louvain.

Mineral Type	Muscovite from Mousty Fm									Muscovite retromorphosed from andalusite								
Type	stack	matrix	stack	matrix	stack	matrix	stack	stack	stack									
Sample	18	18	18	18	23	23	44	44	44	23	23	46	46	46	25	25	25	25
%																		
SiO_2	44.73	45.04	46.60	45.68	46.54	44.99	45.85	45.17	44.66	44.83	46.85	45.27	45.75	45.36	46.35	45.94	45.78	45.57
TiO_2	0.43	0.39	0.36	0.31	0.44	0.14	0.48	0.93	1.04	0.21	0.05	0.11	0.25	0.18	0.08	0.07	0.09	0.09
Al_2O_3	36.18	36.35	29.56	36.77	34.52	38.12	34.03	33.14	33.79	37.61	37.01	36.02	35.84	36.78	37.50	38.35	37.99	37.84
FeO	1.71	1.27	3.66	1.08	2.22	0.74	2.80	3.90	3.36	0.68	1.06	1.03	1.05	1.04	0.57	0.40	0.79	0.50
MnO	0.05	0.02	0.04	0.00	0.00	0.00	0.02	0.05	0.01	0.00	0.07	0.00	0.00	0.00	0.00	0.04	0.00	0.00
MgO	0.69	0.41	2.42	0.38	0.97	0.16	0.91	0.98	0.89	0.14	0.26	0.59	0.58	0.45	0.17	0.16	0.17	0.21
CaO	0.00	0.00	0.00	0.00	0.00	0.00	0.06	0.00	0.00	0.00	0.00	0.00	0.02	0.00	0.02	0.00	0.02	0.00
Na_2O	0.54	0.65	0.20	0.63	0.73	1.08	0.29	0.72	0.35	1.11	1.03	0.49	0.39	0.42	1.31	1.23	1.34	1.27
K_2O	10.44	9.70	9.65	9.80	9.06	8.50	10.28	9.96	10.46	8.98	8.48	9.76	10.25	9.89	8.22	8.82	8.93	9.01
H_2O	3.68	3.68	3.69	3.72	3.75	3.70	3.71	3.69	3.67	3.68	3.78	3.67	3.70	3.70	3.75	3.75	3.74	3.72
Total	98.46	97.59	96.28	98.44	98.26	97.44	98.44	98.62	98.23	97.26	98.59	96.94	97.82	97.82	97.97	98.77	98.91	98.22
NUMBER OF CATIONS ON THE BASIS OF 22 OXYGENS																		
Si	6.009	6.060	6.440	6.081	6.221	6.001	6.181	6.125	6.073	6.011	6.174	6.116	6.140	6.075	6.128	6.044	6.035	6.043
Ti	0.044	0.040	0.037	0.031	0.044	0.014	0.049	0.095	0.106	0.022	0.005	0.011	0.025	0.018	0.008	0.007	0.009	0.008
Al	5.727	5.763	4.814	5.769	5.437	5.993	5.406	5.296	5.416	5.943	5.747	5.736	5.669	5.805	5.844	5.946	5.904	5.913
Fe	0.193	0.143	0.423	0.120	0.248	0.082	0.315	0.442	0.382	0.077	0.117	0.116	0.118	0.116	0.063	0.044	0.087	0.055
Mn	0.005	0.002	0.005	0.000	0.00	0.000	0.003	0.006	0.001	0.000	0.008	0.000	0.000	0.000	0.000	0.004	0.000	0.000
Mg	0.139	0.083	0.499	0.075	0.193	0.033	0.183	0.198	0.179	0.028	0.051	0.119	0.117	0.089	0.034	0.031	0.034	0.041
Ca	0.000	0.000	0.000	0.000	0.000	0.000	0.008	0.000	0.000	0.000	0.000	0.000	0.002	0.000	0.002	0.000	0.003	0.000
Na	0.140	0.169	0.054	0.161	0.190	0.280	0.077	0.190	0.092	0.289	0.263	0.129	0.100	0.108	0.335	0.314	0.343	0.328
K	1.790	1.665	1.701	1.664	1.545	1.447	1.767	1.722	1.814	1.537	1.426	1.682	1.754	1.690	1.387	1.480	1.502	1.524
OH	4.000	4.000	4.000	4.000	4.000	4.000	4.000	4.000	4.000	4.000	4.000	4.000	4.000	4.000	4.000	4.000	4.000	4.000
Al/Fe+Mg	17.2	25.5	4.9	29.6	12.3	52.1	10.8	8.3	9.7	56.6	34.2	24.4	24.1	28.3	60.2	79.2	48.8	61.6

Table 10. Microprobe analysis of garnets from Mousty Fm (MST) and Thy conglomerate from Abbaye de Villers Fm (ABV). SP = spessartine, AL = almandine, GR = grossular, PY = pyrope. From Jodard (1986) and Alomène (1987). Analyst J. Wauthier, CAMST, Université Catholique de Louvain.

Sample	MST 46	MST 46	MST 46	MST 46	MST 46	ABV Thy	MST L45	MST L45	MST L45	MST L45a	MST L45b	MST L45c	MST F55	MST F55	MST F55	MST L58
Position								center	edge	edge	interm.	center				
%																
SiO_2	36.68	37.27	37.04	37.14	37.49	37.23	36.03	35.42	35.81	36.42	36.21	35.73	37.13	37.12	37.06	36.56
TiO_2	0.10	0.09	0.08	0.09	0.18	0.11	0.08	0.15	0.13	0.13	0.11	0.12	0.07	0.08	0.17	0.10
Al_2O_3	21.97	21.54	21.49	21.68	21.71	22.28	21.48	20.99	21.01	21.27	21.31	21.58	21.76	21.92	21.77	21.25
FeO	10.35	10.90	10.77	11.15	10.74	10.97	11.33	10.31	11.73	12.04	10.54	9.91	12.79	11.50	10.91	12.40
MnO	28.51	28.40	28.40	28.45	28.44	28.63	26.69	27.74	25.12	24.77	28.64	28.94	26.62	28.20	28.21	25.06
MgO	0.26	0.17	0.23	0.24	0.16	0.16	0.28	0.25	0.30	0.30	0.23	0.32	0.28	0.19	0.28	0.32
CaO	1.83	2.03	1.90	1.87	1.84	2.10	3.09	2.55	3.81	3.85	2.50	1.94	2.34	2.63	2.35	2.94
Na_2O	0.00	0.00	0.03	0.03	0.10	0.04	0.02	0.03	0.03	0.07	0.03	0.07	0.02	0.03	0.05	0.00
K_2O	0.00	0.06	0.05	0.00	0.01	0.02	0.03	0.01	0.00	0.02	0.00	0.01	0.03	0.00	0.00	0.01
Total	99.73	100.48	100.05	100.65	100.71	101.57	99.07	97.45	97.93	98.94	99.57	98.62	101.06	101.68	100.83	98.73
End-Members																
SP	68.8	67.6	67.9	67.4	68.4	67.6	63.2	66.8	59.8	59.0	67.3	69.4	62.4	65.3	66.6	60.3
AL	24.7	25.6	25.4	26.1	25.5	25.6	26.5	24.5	27.6	28.3	24.4	23.5	29.6	26.3	25.4	29.5
GR	5.1	5.8	5.3	5.3	4.9	5.8	8.8	7.3	11.1	11.0	7.1	5.5	6.7	6.1	6.1	8.3
PY	1.1	0.7	1.0	1.0	0.7	0.7	1.2	1.1	1.2	1.2	1.0	1.3	1.2	1.2	1.2	1.1

of andalusite porphyroblast. The core of these clusters is frequently occupied by small lamellae of chlorite associated with a blackish submicroscopic substance (chiastolite remnant?, Photo 24) and quartz. The micas of the aggregates are not oriented which shows that their formation pre-dates the cleavage (Photo 25).

Microprobe analysis shows that these aggregates are formed from a multitude of muscovite flakes (Table 9). Their chemical homogeneity, their very aluminous character (mean$_{Al2O3stack}$ = 5.515 at% and mean$_{Al2O3andalusite}$ = 5.756 at%) and the size of the aggregates eliminates a detrital origin for the mica. The Al/Fe+Mg ratio of the muscovite aggregates (mean$_9$ = 42) is significantly higher than that of the mica in the stacks and the matrix (mean$_{10}$ = 18), suggesting a retromorphosis of an Al-rich mineral such as andalusite (Jodard, 1986). On the other hand, the Na/Na+K ratio of muscovite aggregates (mean = 0.16 at%) is higher than that of other muscovites (mean = 0.08 at%) which favours the hypothesis of the reaction Na-muscovite + quartz = andalusite + albite + K-muscovite + H_2O common in slates (Guidotti, 1984). Micaceous pseudomorphoses of very similar andalusite porphyroblasts have been described in the Cambrian slates of the Givonne Inlier (Beugnies, 1976). Theunissen (1970) also described the different stages of retromorphosis of andalusite into muscovite of the coticule and purplish slates of the Ottré Fm in the Stavelot-Venn Inlier. However, contrary to the Brabant Massif, these two Cambrian–Ordovician inliers were probably affected by two metamorphic events during the Caledonian and Variscan orogens.

11.8. Discussion

The metamorphism in the MF is expressed by the abundance of porphyroblastic minerals as we have just seen. Their chemical analysis shows that they are in equilibrium with the local metamorphic conditions. Most of these minerals are also found in other formations of the Brabant Massif but in lesser abundance and often alone, for example biotite in the Blanmont Fm (André et al., 1981; Giese et al., 1997) and magnetite with sometimes biotite and exceptionally chloritoid in the Tubize Fm (Herbosch, unpublished). The chlorite-mica stacks are common not only in almost all the Brabant Massif formations but also in the Devonian silto-argillaceous rocks of the Ardenne (Dandois, 1985; Larangé, 2002). Garnets are found exclusively in the MF as well as magnetite in the Tubize Fm (de Magnée & Raynaud, 1944; Vander Auwera & André, 1985) and grey monazite in the Silurian formations (Herbosch, unpublished).

Garnets are abundant in the Stavelot-Venn Inlier and also reported in the Rocroi Inlier. The garnets of the Ottré Fm from the southernmost area of Stavelot-Venn Inlier and in particular those of the coticule, are much purer spessartine Sp 94 Al 1 Gr 2.5 Py 2.5 (Kramm, 1973; Schreyer et al., 1992). This area belongs to the epizone (P-T conditions 400–450 °C and 2–3 kbar; Kramm, 1982; Fransolet & Kramm, 1983; Fielitz & Mansy, 1999). The slates of this area were deposited in a deep-sea oxidizing environment extremely rich in iron and manganese (Herbosch et al., 2016) which was geochemically very different from the black slate of the MF. In the less metamorphic zone of the Chevron Syncline where P-T conditions are about 300 °C and 1–2 kbar (Theye et al., 1996), the garnets are virtually pure spessartine and the paragenesis includes rhodochrosite and garnet. This strongly suggests that in the MF the spessartines were formed out of a rhodochrosite precursor, which itself was formed in the anoxic environment of deposition (see Chap. 8). Due to the strong sedimentological and geochemical difference between the slates of these two regions, it is not possible to transpose the P-T conditions as they stand. However, given the absence of rhodochrosite relics in the

Table 11. Microprobe analysis of ilmenites from the Mousty Fm. From Jodard (1986, sample 23) and Alomène (1987, sample 258). Analyst J. Wauthier, CAMST, Université Catholique de Louvain.

Mineral	Ilmenite				
Sample	23	23	23	23	258
%					
SiO_2	1.69	0.08	0.04	1.43	0.17
TiO_2	55.18	56.08	56.12	53.51	53.25
Al_2O_3	4.42	0.07	0.07	0.05	0.11
FeO	36.19	38.46	38.67	41.14	34.40
MnO	0.05	1.91	1.88	2.13	10.54
MgO	0.00	0.02	0.02	0.00	0.00
CaO	0.03	0.01	0.00	0.02	0.03
Na_2O	0.01	0.09	0.01	0.04	0.00
K_2O	0.07	0.05	0.07	0.04	0.07
Total	97.66	96.77	96.88	98.36	98.57

MF, metamorphic conditions can be estimated to be in the epizone as in the southernmost part of the Stavelot-Venn Inlier. The garnets described in the black slate of the Petite Commune Fm (Furongian; Herbosch, 2021) of Rocroi Inlier (Potdevin et al., 1993) have a rather similar composition as the MF (Sp 52 Al 41 Gr 6 Py 2) and an estimated formation temperature of 400–450 °C.

The observation of retromorphosed andalusite porphyroblasts suggests the presence of two episodes of metamorphism, the second being of lower intensity. A similar observation was made in the Blanmont Fm at Opprebais quarry (NE of the Brabant Massif, Fig. 1; André et al., 1981) where a first pre-cleavage phase shows the development of poecilitic porphyroblasts of biotite and a second phase allows the recrystallisation of the biotite in the crenulation cleavage.

12. The metamorphism of the Mousty Fm, and by extension of the southern outcropping area and the entire Brabant Massif

In this chapter, we will mainly consider the intensity of the metamorphism reached by the MF. However, it will be difficult not to overlap with the southern outcrop of the Brabant Massif and even with its part hidden by the cover (borehole samples).

12.1. Coalification of the organic matter

One of the main characteristics of the MF is its dark colour due to the finely dispersed organic matter in an argillaceous matrix. Although reported by many authors, organic matter has been little studied, especially concerning its "thermal alteration" (e.g. reflectivity, Rockeval). Only old analyses are reported: 0.21 to 2.69% carbon ($mean_{11} = 1.0\%$ sd= 0.7) for Anthoine & Anthoine (1943) and 0.07 to 1.25% carbon ($mean_{15} = 0.55\%$ sd = 0.38) for Van Tassel (1986, table 8). These low and highly variable contents seem normal, especially for metamorphic shale. Indeed, in non-metamorphic black shale, the total organic carbon mean content varies between 0.5 and 5% and is strongly dependent on the sedimentation rate (e.g. Baudin et al., 2007). It can be much higher as in the alum shale of the Baltic basin (see Table 6). The colouring power of this graphite is clearly due to its strong dispersion which has been increased by diagenesis and metamorphism.

Vitrinite reflection value of Rmax around 6% in the Cambrian–Ordovician of the Brabant Massif (Giese et al., 1997,

fig. 6) shows that these formations, including the MF, have reached or passed the boundary high anchizone-epizone (the boundary is around Rmax = 5%) which corresponds to the graphite stage.

The degree of thermal maturation of organic matter was determined in about ten samples of lydite (phtanite) from the Franquenies quarry (see § 5.3) using Raman microspectrometry. This determination gave a peak metamorphic temperature of 442 °C sd = 16 °C (E. Goemaere, pers. comm., 2020). This analysis was carried out following the discovery of a black pigment in small blocks (Black Pigment of Sclayn) found by archaeologists in the cave of Scladina (Sclayn, Andenne). The Raman spectrum was identical for both materials. This temperature and other geochemical analyses (see Bonjean et al., 2015a, 2015b) proved that these black pigments came from the Franquenies quarry and its surroundings, the only sites where these lydites are currently outcropping. This shows that the Neanderthals used the lydite and/or the host black slates not only to make adze (e.g. Malaise, 1909; Dupréel, 1937; Michel & Haesaerts, 1975) but also as pigments. These adzes are found in the old Neolithic, in the Meuse and Sambre basins (Caspar, 1984).

In conclusion, the analysis of the organic matter of the MF shows that these black slates have undergone metamorphism well within the epizone (greenschist facies). However, Raman microspectrometry of graphite was only carried out in the small area of the Franquenies quarry.

12.2. White mica crystallinity as a palaeothermometer

The most widely used method of determining grade in metapelitic sequences is the XRD-based illite crystallinity (IC) technique (Kubler, 1964). The IC index is given in Δ°2Ø and has the advantage of being sensitive over a wide range of metapelite conditions, from the late diagenetic zone (IC ≈ 0.42) to the beginning of the epizone (IC ≈ 0.15) through the anchizone (0.25 < IC < 0.42). The value of 0.15 marks approximately the upper limit of T-sensitivity of the IC index which corresponds to about 350–400 °C (Merriman & Frey, 1999).

The illite crystallinity method has been applied throughout the Brabant Massif, i.e. mainly in boreholes from its hidden part and some outcrops (178 samples including 46 from outcrops; Geerkens & Laduron, 1996; Van Grootel et al.,1997; Larangé, 2002). Unfortunately, many borehole and outcrop samples are identified on the basis of old biostratigraphic results or solely on the basis of their lithofacies, and as a result many do not have a reliable stratigraphic position. Van Grootel et al. (1997, figs 4, 5) have reported uncritically the results of Geerkens & Laduron (1996), which makes their deductions very tentative. In fact, since then the stratigraphic scale used (De Vos et al., 1993) has changed considerably (Verniers et al., 2001; Herbosch & Verniers, 2013, 2014; Herbosch & Debacker, 2018, fig. 4). By comparing all the outcrop samples from Larangé (2002, pp.186–191) with the new maps of the Brabant Massif, new palaeontological data (Vanguestaine et al., 1989a, b; Vanguestaine, 1992) and our extensive knowledge of the field, we are able to accurately identify 46 field samples and 11 boreholes from the southern outcropping area of the Brabant Massif. All these samples are currently reliably identified at the formation level and cover the entire Cambrian to Silurian stratigraphic record, as well as geographically from the Senne basin in the W to the Mehaigne basin in the E (Table 12). The only area not covered by measurements is the Gette basin (NE part of Fig. 1).

In a first step, we selected 23 samples from Larangé (2002) in the Dyle basin, 16 from outcrops and 7 from two boreholes

(Table 12 A), 10 of these samples certainly belong to the MF and 6 are uncertain belonging to Mousty or Tubize fms. As shown in Figure 21 the samples are fairly well distributed in the area surrounding the outcrops of the MF and belong mostly to the Peripheral Brabant Domain. Most of the IC index are lower than 0.25, the value that marks the base of the epizone, as proved by the mean $IC_{23} = 0.218$ sd $= 0.061$. It is however surprising to see that the four IC values from the Court-St-Etienne borehole (BGS 40/5-540) are significantly higher (mean $IC_4 = 0.31$) than those of the samples taken in the immediate vicinity of the Court-St-Etienne anticlinal uplift (see Fig. 5 and § 14.6). An explanation linked to meteoric alteration of the outcrop samples could be rejected as it would cause a decrease in crystallinity. The most plausible explanation would be a calibration problem since only these four measurements come from Larangé (2002) and all the others from Geerkens & Laduron (1996). If we exclude the samples from the Court-St-Etienne boreholes (Bb96 to Bb99) from the calculation, we obtain: $IC_{19} = 0.20$ sd $= 0.045$ (Table 12 A), which shows that the whole Dyle basin area has reached the epizone. It may also be concluded, given the homogeneity of the crystallinity index on both sides of the Asquempont Detachment System (Fig. 21), that the metamorphism occurred after the formation of the detachment which confirms its anteriority. In fact, geological arguments show that the detachment must have occurred after the deposition of the Ittre Fm (lower Katian, c. 453 Ma) and before the intrusion of the Quenast pipe (430 Ma; T.N. Debacker, comm. pers., 2009; Debacker et al., 2011). These IC values are confirmed by the study of Giese et al. (1997, fig. 6) who showed that all field samples belonging to the Cambrian have an IC well below 0.20 (mean$_8$ = 0.14 sd = 0.03). The conclusion of these authors is: "...the outcrop area of the Brabant Massif has experienced an epizonal Caledonian metamorphism".

Given this last conclusion and although it is not the goal of this work, we feel the need to calculate the mean IC on the 57 well-identified samples from the southern outcropping area of the Brabant Massif (Table 12 B). The result ($IC_{57} = 0.229$ sd $= 0.054$) shows that this average is a little higher than that of the Dyle basin ($IC_{19} = 0.20$ sd $=0.048$). Taking into account the IC range of 0.18–0.28 for one standard deviation, it can be seen that while the large majority of the samples are in the epizone, 13 from 57 are however in the high anchizone. This suggests a variation of crystallinity with the age of the rocks, which was a conclusion of Giese et al. (1997) and was better argued by Larangé (2002, figs 7.7, 7.10). However, the latter author's results show only significant differences for Cambrian–Ordovician samples located in the epizone-anchizone (mean$_{94}$ = 0.26) compared to Silurian located in the anchizone-diagenesis (mean$_{31}$ = 0.33). But as noted above, these conclusions are questionable given the poor stratigraphic attribution of a large part of the samples used. Therefore, we find it necessary to calculate the mean IC as a function of age for the 57 well-identified samples (Fig. 22):
- for the Cambrian: $IC_{24} = 0.215$ sd $= 0.065$
                (range for 1 sd: 0.15–0.28)
- for the Ordovician: $IC_{21} = 0.251$ sd $= 0.047$
                (range for 1 sd: 0.20–0.30)
- for the Silurian: $IC_{12} = 0.227$ sd $= 0.043$
                (range for 1 sd: 0.18–0.27).

These results are unexpected, the mean value and range of the Cambrian are identical to those of the Cambrian of the Dyle Basin and lower than those of the outcrops of the S margin of the Brabant Massif. For these three areas, the mean values are all located in the epizone, the standard deviations are fairly close and only the range of the outcrops of the S margin of Brabant Massif overlaps with the high anchizone (Fig. 22).

More surprisingly, the Ordovician mean located at the epizone to high anchizone boundary is less metamorphic than the Cambrian and Silurian samples. Finally, the Silurian mean is found in the epizone and its range covers mainly the epizone and weakly the high anchizone. These results do not seem to confirm the initial assumption of a simple relationship between rock age and metamorphism, the relation is probably more complex. However, it should be noted that the number of samples for the Silurian is small (n = 12).

Referring to the illustrated model of the Cambrian to Devonian evolution of the Brabant Massif (Debacker et al., 2005a, fig. 9) these new results can be interpreted more easily. Let us briefly describe this evolution in four temporal stages (Fig. 23):
- Hirnantian: the very subsiding aborted rift basin was filled with Cambrian to lowermost Ordovician sediments (>9 km), overlain by less subsiding Middle and Upper Ordovician sediments (~1.2 km).
- upper Llandovery: ongoing inversion of the basin, first affecting the core of the Brabant Massif, which caused a rise of the core and the steepening of the deposits. Silurian foreland basin development (>3.5 km in the southern basin) is the result of the weight of the raising core.
- Lochkovian: continuation of the deformation and emergence of the core of the Brabant Massif, with erosion of the upper Silurian deposits. The N and S foreland basins became separated.
- Pragian to Givetian: continued shortening caused a further spreading of the deformation from the core towards the rim and resulted in the final inversion of the Silurian basin during the late Pragian/Emsian. Givetian deposits are transgressive on the Brabant Massif.

This model allows us to conclude that there is a clear correlation between the degree of metamorphism and the age of the strata for the whole set of Cambrian rocks. The degree of metamorphism of the Silurian, which is higher than that of the Middle and Upper Ordovician, is in contradiction with this same model. Indeed, the latter are located at the base of the foreland basin (Fig. 23) and should be more metamorphic due to the important thickness of overlying Silurian sediments. However, the Ordovician results are most likely biased because the calculation should have been made by separating the Lower Ordovician and Cambrian from the Middle and Upper Ordovician. This calculation gives:
- for Middle + Upper Ordovician: IC mean$_6$ = 0.22 sd = 0.04;
- for Cambrian + Lower Ordovician: IC mean$_{37}$ = 0.22 sd = 0.06 (range 0.17–0.29).

Unfortunately, the result for the Middle and Upper Ordovician is not significant as there are only six samples. Recalculation for the Cambrian plus Lower Ordovician set gives an IC that is almost identical to the entire Brabant Massif values (Fig. 22). Given the latter calculations, it seems very likely that the Middle and Upper Ordovician and Silurian strata as a whole also show a metamorphic-age correlation with a metamorphic grade that does not seem to be significantly lower despite a much lower sediment thickness. Only a more complete study including well-identified borehole samples, would allow to solve this question which is outside the scope of this paper.

Let us return to the subject of this article which is the MF and accessorily the Cambrian of the Brabant Massif core. The good correlation between age and degree of metamorphism in Cambrian and Lower Ordovician rocks is typical of burial metamorphism (Coombs, 1961), i.e. developed in situ and resulting from a depth-controlled low-grade metamorphic reaction caused by basin subsidence. Such a burial pattern is found in basins where the geothermal gradient is high, typically >35 °C/km (Roberts et al., 1996; Merriman & Frey, 1999).

Indeed, to reach a temperature of about 425–450 °C, which is the peak temperature measured on organic matter, and with a thickness of Cambrian and Lower Ordovician sediments of about 9 km, a geothermal gradient of about 47–50 °C/km is necessary.

12.3. K-white mica b0 cell dimension as a palaeobarometer

The measurement of the $b0$ cell dimension of K-white mica using the XRD line (006) is a rapid and inexpensive method that provides information on the relative pressure of the formation of metapelite rich in muscovite (Guidotti & Sassi, 1976, 1986). This technique can be used as a semi-quantitative geobarometer for levels of metamorphism from high anchizone to epizone and also gives information concerning the palaeogeothermal gradient (Merriman & Frey, 1999).

The terrigenous rocks of the Brabant Massif are ideally suited to this technique, which has been applied to a large part of the samples used for illite crystallinity (Larangé, 2002). The average value of all 121 measures from the entire Brabant Massif is: $b0_{121} = 8.995$ Å sd = 0.011 Å. The latter value was recalculated by eliminating three Devonian and two volcanic rocks from the data of Larangé (2002, pp. 188–191). The variations of the $b0$ values with the age of the samples are within the range of standard deviation:
- Cambrian mean $b0_{45} = 8.997$ Å sd = 0.011 Å
  range 8.986–9.008
- Ordovician mean $b0_{45} = 8.989$ Å sd = 0.009 Å
  range 8.980–8.998
- Silurian mean $b0_{31} = 8.998$ Å sd = 0.011 Å
  range 8.987–9.009.

By comparing the average values of the Brabant basement with the empirical scale of $b0$ average values of Sassi & Scolari (1974) we can choose between different types of metamorphism:
- scale 1: *for an average of* b0 ≈ 8.990Å: *low-pressure metamorphism (andalusite + cordierite) without chlorite zone;*
- scale 2: *for an average of* b0 ≈ 8.995Å: *low-pressure metamorphism (andalusite + cordierite) with chlorite zone;*
- scale 3: *for an average of* b0 ≈ 9.010Å: *low-intermediate pressure metamorphism with the chlorite-biotite-almandin paragenesis in the greenschist facies;*
- scale 4: *for an average of* b0 ≈ 9.020Å *to* 9.025Å: *typical Barrovian metamorphism; etc.*

Table 12 A. Illite crystallinity (IC) and b cell dimension of 23 samples outcropping mainly in the upper Dyle basin. IC, b cell dimension and clay composition from Larangé (2002). Stratigraphic attribution (formation, system) of all samples reviewed by Herbosch (see text). B = borehole. C = chlorite, K = kaolinite, I = illite, Pa = paragonite, Sm = Smectite.

Formation	n° Larangé	Localisation	Kubler index	Cell dimension	Clay composition	Metam. zone	Sample type	System
		Belgian Lambert	IC	b (Å)				
MOUSTY AND SURROUNDING FORMATIONS FROM THE DYLE BASIN								
Mousty	Bb 2	162100/144750	0.15	8.982	I, C, K +mixC/Sm	epizone	outcrop	Cambrian
Mousty	Bb 7	162200/144800	0.23	8.980	I, C, K, Sm	epizone	outcrop	Cambrian
Chevlipont	Bb 6	161800/143750	0.20	8.980	I, C, K	epizone	outcrop	Ordovician
Mousty	Bb 96	163776/148002	0.29	8.990		high anchizone	B 40/5-540	Cambrian
Mousty	Bb 97	163776/148002	0.26	8.990		high anchizone	B 40/5-540	Cambrian
Mousty	Bb 98	163776/148002	0.30	8.989		low ancizone	B 40/5-540	Cambrian
Mousty	Bb 99	163776/148002	0.37	8.991		low ancizone	B 40/5-540	Cambrian
Mousty	Bb 117	159440/147060	0.25	9.003	I, C, K, Sm	epizone	B 129E 197	Cambrian
Mousty	MB 130	159440/147060	0.24		I, C, K, Sm	epizone	B 129E 197	Cambrian
Mousty	MB 131	159440/147060	0.23		I, C, K, Sm	epizone	B 129E 197	Cambrian
Mousty or Tubize	Bb 174	Court St Etienne	0.15			epizone	outcrop	Cambrian
Mousty or Tubize	Bb 175	Court St Etienne	0.14			epizone	outcrop	Cambrian
Mousty or Tubize	Bb 176	Court St Etienne	0.15			epizone	outcrop	Cambrian
Mousty or Tubize	Bb 177	Court St Etienne	0.14			epizone	outcrop	Cambrian
Mousty or Tubize	Bb 178	Court St Etienne	0.16			epizone	outcrop	Cambrian
Mousty	Bb 157	162300/144850	0.20			epizone	outcrop	Cambrian
Tubize	Bb 95	167200/145800	0.21	9.016	I, K +mix C/Sm	epizone	outcrop	Cambrian
Abbaye de Villers	Bb 156	161600/142400	0.25		I, C, K, Sm	epizone	outcrop	Ordovician
Tubize	Bb 158	156250/144300	0.20		I, K	epizone	outcrop	Cambrian
Tubize	Bb 159	156250/144350	0.29		I, C, K, Pa, + mixC/Sm	epizone	outcrop	Cambrian
Mousty or Tubize	Bb 172	Court-St-Etienne	0.21			epizone	outcrop	Cambrian
Tubize	Bb 171	Mont-St-Guibert	0.25			epizone	outcrop	Cambrian
Tubize	Bb 173	Beaurieu	0.15			epizone	outcrop	Cambrian
Mean without Court borehole n = 18			**0.200**	**sd = 0.045**				

Table 12 B. Illite crystallinity (IC) and *b* cell dimension of 38 samples from the southern outcropping area of the Brabant Massif. IC, *b* cell dimension and clay composition from Larangé (2002). Stratigraphic attribution (formation, system) of all samples reviewed by Herbosch (see text). B = borehole. C = chlorite, K = kaolinite, I = illite, Pa = paragonite, Sm = Smectite.

Formation	n° Larangé	Localisation	Kubler index	Cell dimension	Clay composition	Metam. zone	Sample type	System
		Belgian Lambert	IC	*b* (Å)				
OTHER FORMATIONS FROM THE OUTCROPPING AREA OF SOUTHERN BRABANT MASSIF								
Ittre or Bornival	Bb1	131750/149750	0.21	8.991	I, C, K,Sm	epizone	outcrop	Ordovician
Steenkerque	Bb3	127900/146500	0.21	9.006	I, C, K	epizone	outcrop	Silurian
Abbaye Villers	Bb4	140700/148700	0.32	8.994	I, C, K, Pa	low anchizone	outcrop	Ordovician
Abbaye Villers	Bb5	140850/147450	0.33	8.994	I, (Sm)	low anchizone	outcrop	Ordovician
Chevlipont	Bb46	113858/156002	0.28	8.990	I, C	high anchizone	B 113E1015	Ordovician
Oisquercq	Bb47	idem	0.42	8.992	I, C, Sm	low anchizone	B 113E1015	Cambrian
Chevlipont	Bb57	124850/154430	0.21	8.986	no data	epizone	B 114E92	Ordovician
Chevlipont	Bb58	idem	0.20	8.985	no data	epizone	idem 44 m	Ordovician
Fauquez	Bb67	113858/156002	0.31	8.993	I, C	low anchizone	B 113E1015	Ordovician
Chevlipont	Bb72	124850/154430	0.30	8.986	no data	high anchizone	B 114E92	Ordovicien
Chevlipont	Bb73	idem	0.30	8.976	no data	high anchizone	idem 147 m	Ordovician
Chevlipont	Bb74	idem	0.29	8.977	no data	high anchizone	idem 175 m	Ordovician
Froide Fontaine	Bb89	126250/144400	0.29	8.989	I, C, K, mix I/Sm	high anchizone	outcrop	Silurian
Ittre or Rigenée	Bb90	136900/149250	0.20	9.003	I, C, K	epizone	outcrop	Ordovician
Tubize/Oisquer.	Bb91	136750/151900	0.24	8.990	I, C, K, Sm	epizone	outcrop	Cambrian
Ronquière	Bb92	140350/143800	0.28	9.010	I, C, K	high anchizone	outcrop	Silurian
Fallais	Bb93	209050/143800	0.20	8.992	I, C, K, Sm	epizone	outcrop	Silurian
Ronquière	Bb94	200500/134550	0.20	9.020	I, C, K, Sm	epizone	outcrop	Silurian
Tubize	Bb95	167300/145600	0.21	9.016	I, K +mix C/Sm	epizone	outcrop	Cambrian
Chevlipont	Bb130	125400/154150	0.26		I, C, K	high anchizone	outcrop	Ordovician
Froide Fontaine	Bb131	127600/145750	0.20		I, C, K	epizone	outcrop	Silurian
Petit Roeulx	Bb132	132400/145250	0.24		I, K , Sm +mixC/Sm	epizone	outcrop	Silurian
Abbaye Villers	Bb133	137200/150500	0.24		I, C, K +mixC/Sm	epizone	outcrop	Ordovician
Ittre or Bornival	Bb134	134750/150950	0.19		I, C, K, Sm	epizone	outcrop	Ordovician
Oisquercq	Bb135	133500/150100	0.20	**Mean28 =**	I, C, K, (Sm)	epizone	outcrop	Cambrian
Abbaye Villers	Bb136	135950/151350	0.20	**8.993**	I, C, K, (Sm)	epizone	outcrop	Ordovician
Tubize	Bb137	139100/153000	0.18	**sd = 0.011**	I, C, K, Sm	epizone	outcrop	Cambrian
Tubize	Bb138	140450/152000	0.22		I, C, K, Sm +mixC/Sm	epizone	outcrop	Cambrian
Oisquercq	Bb141	140700/148600	0.22		I, C, K, (Sm)	epizone	outcrop	Cambrian
Abbaye Villers	Bb142	140600/147400	0.29		I, (K), (Sm)	high anchizone	outcrop	Ordovician
Ittre	Bb143	140400/146350	0.20		I, C, K, Sm	epizone	outcrop	Ordovician
Madot	Bb144	140250/145800	0.24		I, K, Sm	epizone	outcrop	Ordovician
Fallais	Bb147	205700/145500	0.22		I, K, Sm	epizone	outcrop	Silurian
Fallais	Bb148	207100/144750	0.18		I, K, Sm	epizone	outcrop	Silurian
Fumal	Bb150	205500/140750	0.20		I, C, K	epizone	outcrop	Silurian
Fallais	Bb152	201850/141950	0.19		I, C, K	epizone	outcrop	Silurian
Bois Grand Père	Bb154	172600/137900	0.31		I, C, K	low anchizone	outcrop	Silurian
Abbaye Villers	Bb156	161600/142400	0.25		I, C, K, Sm	epizone	outcrop	Ordovician
Mean all samples except Court borehole n = 57 0.229 sd = 0.054								
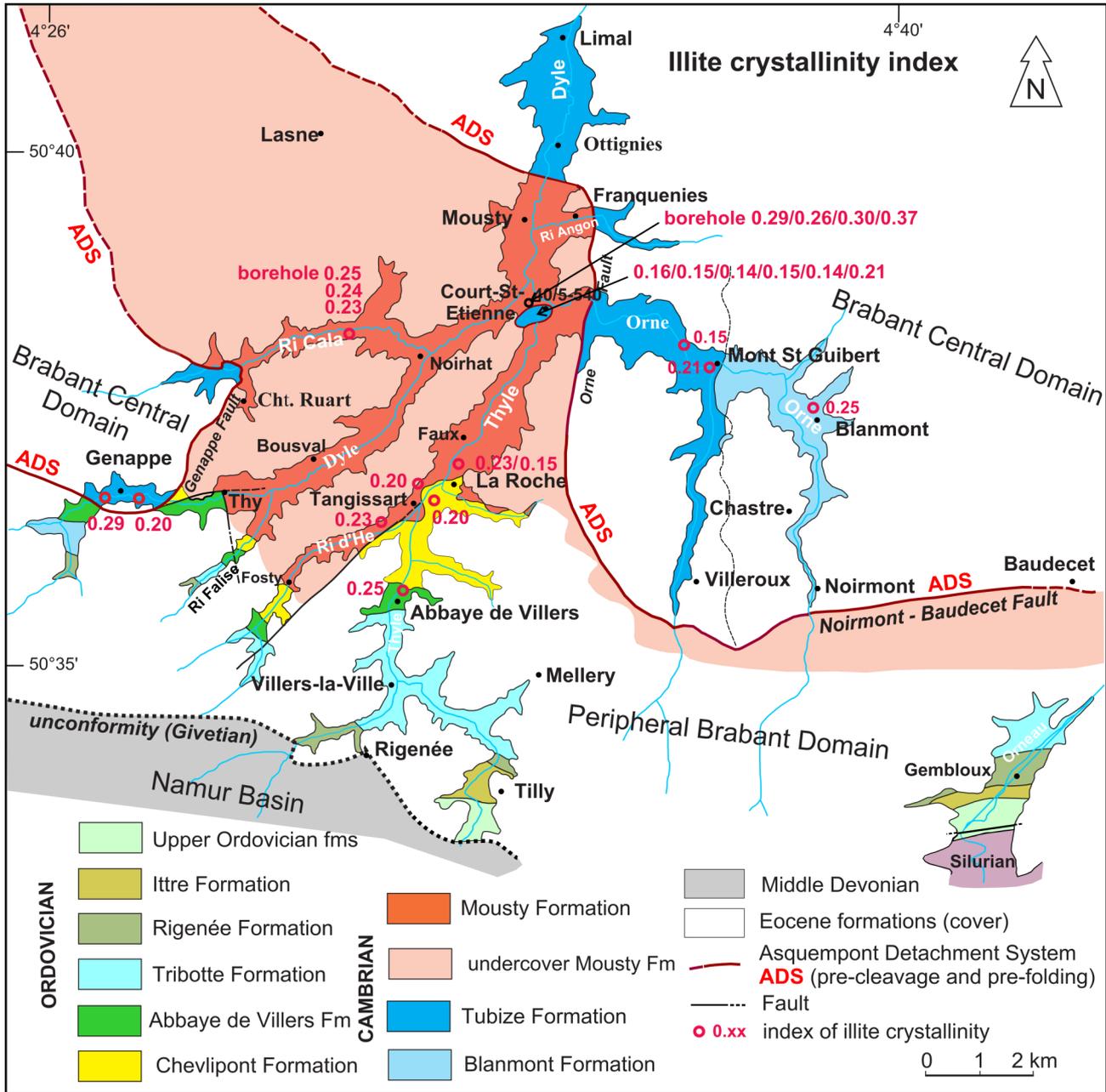
Figure 21. Geographic distribution of illite crystallinity (IC) index on the simplified geological map of the Dyle basin. Data in Table 12A.
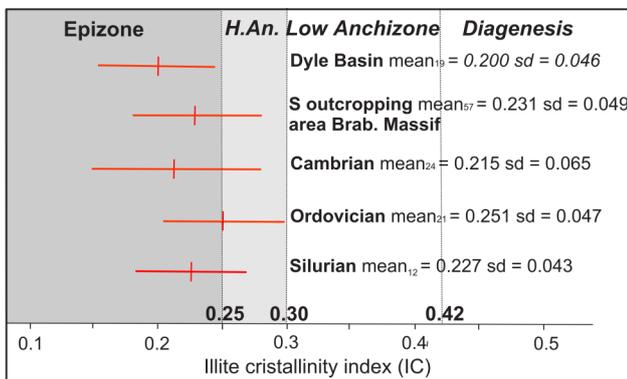
Figure 22. Diagram showing the mean, standard deviation and range of illite crystallinity (IC) respectively for the Cambrian and Ordovician formations from the Dyle basin (n = 19), all samples from the southern outcrop area of the Brabant Massif (n = 57) then separated by system: Cambrian (n = 24), Ordovician (n = 21) and Silurian (n = 12). H. An. = High Anchizone. Data from Larangé (2002), revised for their stratigraphic attribution for this paper (see Table 12A).

In this scale of average $b0$ values, the Brabant Massif seems at first sight to belong to the low-pressure metamorphic zone (scale 2), which is surprising considering the mineral paragenesis of the Cambrian which includes in particular chlorite, garnet and biotite (see Chap. 11). Moreover, the illite crystallinity shows that the Cambrian rocks are quite entirely in the epizone as well as an important part of the Ordovician and Silurian rocks (Fig. 22; see § 12.2). Consequently, we believe that despite the observed average value of $b0_{121}$, which is a bit low but in the upper bracket of the standard deviation range (9.006 Å), the metamorphism is rather indicative of a low-intermediate pressure (scale 3) certainly for the Cambrian–Lower Ordovician rocks, the question not being resolved for the Middle–Upper Ordovician and Silurian rocks.

Approximate burial pressure for the Cambrian–Lower Ordovician rocks can be derived from the P-T-$b0$ grid of Guidotti & Sassi (1986, fig. 1): assuming a minimum temperature of about 400–450 °C (see § 12.1, 12.2) and an average $b0$ value of 8.995 Å, a pressure of 2.5 kb for 400 °C to

Figure 23. Schematic model from the Ordovician to Devonian sedimentary and tectonic evolution of the Brabant Massif. See text for explanation. Modified from Debacker et al. (2005a, fig. 9).

Figure 24. P-T-$b0$ graph of Guidotti & Sassi (1986) used to estimate the palaeobarometry corresponding to white mica cell dimension $b0$ = 8.995Å and temperatures of 400 and 450°C in the Brabant Massif. The dotted curve corresponding to $b0$ = 8.995Å was interpolated. Modified from Guidotti & Sassi (1986, fig. 1).

Linnemann et al., 2012, fig. 23).

12.4.1. Synthesis

The presence of numerous metamorphic minerals in the MF does not allow formal conclusions to be drawn regarding the temperature conditions reached, given the presence of manganese, which is well known to catalyse their formation at lower temperatures (e.g. Bucher & Grapes, 2011). However, we have seen that the chlorite-muscovite stacks, chlorite, garnet and ilmenite are in thermodynamic equilibrium with the metamorphic conditions. This study also shows that spessartine was developed from rhodochrosite precursors that formed during the deposition of these black shales in an anoxic environment (see § 8.3).

The Raman microspectrometry analysis of the organic matter from the Franquenies quarry (Black Pigment of Sclayn) shows that the black slates of the MF underwent metamorphism well within the epizone, with a peak mean temperature of 442 °C sd = 16 °C.

The analysis of the illite crystallinity (IC) allows the following conclusions:
- the MF and the whole area of the Dyle basin that surrounds it (Figs 21, 22, Table 12) is entirely located in the epizone with an IC_{19} = 0.200 sd = 0.045, which means a temperature of a minimum of about 350 to 400 °C.
- Extending the analysis to the entire outcrop area of the Brabant Massif southern margin (with samples well identified stratigraphically) we find IC_{57} = 0.229 sd = 0.054, which shows that the majority of these Cambrian to Silurian rocks belong to the epizone.
- Analysis of the illite crystallinity as a function of rock age (Fig. 22) placed in a recent model of Brabant Massif evolution (Fig. 23; Debacker et al., 2005a), shows that the metamorphic grade increases with rock age for the Cambrian and Lower Ordovician core of the Brabant Massif. This is typical of a burial metamorphism. This type of burial is

3.3 kb for 450 °C is derived (Fig. 24). This value is significantly higher than the value of 1.7 kb obtained by Larangé (2002) with T ≈ 300 °C and $b0$ = 9.00 Å. In terms of geotectonic settings of very low grade metamorphism, the $b0$ values in the range 8.99–9.01 Å are characteristic of an extensional basin (Merriman & Frey, 1999) which is indeed the case of the Cambrian of the Brabant Massif. In fact, it exhibits more than 9 km of cumulated sediments which were deposited in an aborted rift, i.e. with a continental crust type substratum (e.g. Debacker 2001; Verniers et al., 2002; Debacker et al., 2005a; Linnemann et al., 2012).

*12.4. **Summary and discussion on the degree of metamorphism reached by the Mousty Fm, then the southern outcrop area and the entire Brabant Massif***

We will first examine the intensity and type of metamorphism affecting the MF and its surrounding Cambrian and Ordovician area (Fig. 2), then the outcropping area of the Brabant Massif southern margin (Peripheral Brabant Domain Fig. 1), and finally the whole Brabant Massif. We will conclude with a discussion and comparison with the Welsh Basin, which shows great similarities with the Brabant Massif (Verniers et al., 2002;

found in basins where the geothermal gradient is higher than 35 °C/km. In order to reach a temperature of about 425–450 °C with a thickness of Cambrian sediments of about 9 km, a geothermal gradient of about 50 °C/km is necessary.

The measurement of the $b0$ cell dimension of the K-white mica allows, taking into account the metamorphic minerals observed and the resulting temperatures, to specify the pressure and the palaeogeothermal gradient experienced by the Brabant Massif. The average value of the 121 measurements on all Brabant Massif samples shows a mean of $b0_{121}$ = 8.995 Å sd = 0.011 Å which shows that the metamorphism is of "low-intermediate pressure with the chlorite-biotite-almandine paragenesis in greenschist facies". Finally, from these values, we can derive the approximate burial pressure which ranges from 2.5 kb for 400 °C to 3.3 kb for 450 °C (Fig. 24). Given the temperature of 442 °C obtained by Raman microspectrometry (see §12.1) we can estimate that the T-P reached in the Cambrian and Lower Ordovician of the Brabant Massif is most probably in the range 400–450 °C and 2.5–3.3 kb.

All the above results show that the Brabant Massif underwent, at least from the Cambrian to the Lower Ordovician, a very low-grade metamorphism on a passive margin in extension of the diastathermal metamorphism type (sensu Robinson, 1987; Robinson & Bevin, 1989). In this type of metamorphism, an enhanced thermal flux develops early in the tectonic cycle in response to an extensional setting.

12.4.2. Discussion

The values obtained for the metamorphic temperature and for the geothermal gradient are significantly higher than those estimated by most authors (see references above), which can be easily explained given recent advances in the stratigraphy, cartography and tectonics of the Brabant Massif. Notable exceptions are Giese et al. (1997, fig. 6) who, despite a limited number of samples, showed that the metamorphism of the entire Brabant Massif is epizonal and pre- to early synkinematic. Also, Larangé (2002, figs 7.9, 7.10) who, in spite of the stratigraphic imprecision affecting many samples, drew up a metamorphic map of the Brabant Massif based on the illite crystallinity. Using the K-white mica $b0$ cell dimension, this last author obtained for the first time a value of the palaeobarometry (1.7 kb for 300 °C) which, even if underestimated (estimated metamorphic T° to low), showed that it is a burial-type metamorphism with a high geothermal gradient (>35 °C/km), confirming its pre-kinematic nature. Debacker et al. (2005b, p. 24) confirmed, by microscopic observations and X-ray analysis of chlorite and micas orientation, that the metamorphic conditions were reached during burial, before compression, and continued during deformation. Using the weak data of Geerkens & Laduron (1996), the previous authors found abnormally high crystallinity values for the Silurian foreland that cannot be explained by simple burial metamorphism, which is consistent with our results. They invoked an additional sedimentary load on the rims from the early Silurian which was much lower or absent above the more central part of the Brabant Massif (Fig. 23).

This last question is beyond the scope of this work. Nevertheless, it would be very useful to identify more precisely the exact stratigraphic position of the numerous Ordovician and Silurian borehole samples analysed by Larangé (2002). This should clarify the relations between age and metamorphism and their geographical variations in the Middle–Upper Ordovician and Silurian of the foreland basin.

12.4.3. Comparison with the Welsh Basin (N Wales)

The map of the degree of metamorphism in Wales was derived from illite crystallinity data (Merriman, 2002; Woodcock & Soper, 2006, fig. 6.11). Broadly speaking, this map shows an increase in the degree of metamorphism from the margin to the centre of the Welsh Basin, with the Harlech Dome almost entirely within the epizone surrounded by a high anchizone area. The significance of this metamorphic pattern has been the subject of much debate. However, given the great thickness of the deposited sediments (Fig. 16), one of the main hypotheses is that the increase in heat flow developed early in the tectonic cycle in response to the extensional setting, i.e. a diastathermal metamorphism (Robinson, 1987; Bevin & Robinson, 1988; Warr et al., 1991; Robinson et al., 1999). We again find the model we have advocated for the Brabant Massif core, which further increases the similarity between these two geological units and justifies the hypothesis that they belong to a same aborted rift (Waldron et al., 2011; Linnemann et al., 2012, fig. 23; Pothier et al., 2015; Nance et al., 2015).

13. Magnetic susceptibility

Magnetic susceptibility and its relationships with the mineral fabric of the Brabant Massif formations, including the MF, have been the subject of detailed studies to which the reader is referred (Debacker et al., 2004b, 2005b, 2009b, 2010). One conclusion is that the magnetic susceptibility does not allow a straightforward distinction between lithostratigraphic units, except for the high-susceptibility levels of the magnetite-bearing Tubize Fm. Another general conclusion is: "the discrepancy between the phyllosilicate preferred orientation and the result of magnetic fabric analysis may be attributed to the presence of relatively large, Fe-rich, bedding parallel chlorite. The relatively few but large bedding parallel chlorite strongly control Low-field AMS and High-field AMS but only exert a minor influence on the chlorite X-ray pole figure, which is dominated by a larger number of very small cleavage-parallel chlorite" (Debacker et al., 2009b, p. 45). The present study about the distribution and composition of chlorites (see § 11.1, 11.2) confirms that chlorite does exist under different habits and that they are Fe-chlorites in Mousty, Chevlipont and Abbaye de Villers fms (Table 8).

Finally, the variations in magnetic susceptibility with temperature (in the 0–40 °C "room temperature interval") are, contrary to the other formations, significantly higher (+4 to +16%) for the Mousty and Jodoigne fms (Debacker et al., 2010). It was this similar behaviour that was used by Herbosch et al. (2008) as one of the arguments for modifying the stratigraphic position of the Jodoigne Fm to just below the MF (Fig. 4; see also Chap. 9). The cause of this large T-dependant susceptibility change still remains unknown (diamagnetic behaviour?). It suggests a comparable magnetic mineralogy for both formations (Debacker et al., 2010), which is not surprising given the great similarity of their lithologies (see Chap. 9).

14. Mousty Formation and tectonics

14.1. Tectonic hypotheses concerning the origin of the abnormal contact between the Mousty Fm and the Tubize or Blanmont formations

As we have already seen (Chap. 3, 5; Figs 1, 2) the MF is everywhere limited at its base by an abnormal contact that has given rise to much controversy since the doubts expressed by Fourmarier (1920, pp. 10–12) "It also seems that the black rocks of the Mousty assise rest in concordance on the green rocks of the Tubize assise without, however, we have absolute proof of

this. In the Dyle Massif, where these two formations are in the vicinity of each other, we can only determine their reciprocal relations very imperfectly..." (translated from French). Later, Anthoine & Anthoine (1943) highlighted the Orne Fault which they linked to the Genappe Fault via the "Anse d'Ottignies" and the Court-St-Etienne klippe (Figs 2, 5). They considered this fault as a thrust fault, which was confirmed by a magnetic survey by de Magnée & Raynaud (1944). Finally, Delcambre et al. (2002) identified the Noirmont-Baudecet Fault, which they consider to be the eastern extension of the Orne Fault and as the trace of a large-scale thrust fault.

Recent investigations done for the new geological maps, confirm that in the Dyle basin, the Genappe Fault to the SW, the Orne and Noirmont-Baudecet faults to the N, NE and SE bring the MF into contact everywhere with the Tubize Fm, and more to the SE with the Blanmont Fm (Figs 1, 2). The aeromagnetic survey (De Vos et al., 1993; Everaerts, 2000; Debacker et al., 2004a; Herbosch & Debacker, 2018, fig. 7B) has allowed extrapolating the extension of these faults under the cover towards the NW and NE where the magnetic contrast is high (Lasne area; Figs 2, 3). Whatever the interpretation of this contact, it causes the Oisquercq, Jodoigne and Mousty fms to disappear near Genappe and the Oisquercq and Jodoigne fms to disappear towards Ottignies, which, according to the most recent estimates (Herbosch & Verniers, 2013, 2014), results in the disappearance of a cumulative thickness of the order of 4500 to 6000 m (see fig. 14 in Herbosch & Debacker, 2018).

A first hypothesis concerning the origin of these faults is a flat thrusting of the lower Cambrian over the MF and the whole Ordovician and Silurian. This hypothesis, supported by many authors (Anthoine & Anthoine, 1943; Mortelmans, 1955; André, 1983; Mansy et al., 1999), was adopted for some of the new 1/25 000 scale geological maps (Herbosch & Lemonne, 2000; Delcambre et al., 2002; Herbosch & Blockmans, 2012). Consequently, on these maps, the contact between the Mousty and Tubize fms was interpreted as a gentle N-dipping, high-amplitude thrust whose trace corresponds to the Genappe Fault to the W and the succession of the Orne - Noirmont-Baudecet faults to the E. The irregular contour of this trace as well as the existence of a klippe at Court-St-Etienne was explained by the gentle N-dipping of the thrust.

An alternative hypothesis was proposed and argued in depth in the Dyle basin by Debacker et al. (2004a) following his investigations in the Senne basin (Debacker, 2001). In this model, the Genappe Fault and the Orne - Noirmont-Baudecet Fault are considered as a low-angle extensional detachment called "Asquempont Detachment System" (ADS), predating the Brabantian cleavage and folding. A similar type of detachment has already been demonstrated in the Senne basin where the Asquempont Fault also predates cleavage and folding and separates the Cambrian core of the Brabant Massif from its rim (Debacker et al., 2003; Herbosch & Debacker, 2018). The same detachment system has more recently been observed in the Gette basin to the NE of the Brabant Massif (Fig. 1; Herbosch et al., 2008; Debacker & Herbosch, 2011; Herbosch & Debacker, 2018). As Debacker (2001) had already pointed out, the ADS is present all around the Brabant Massif where it separates the Blanmont, Tubize, and Oisquercq fms from the MF and/or younger formations. This structure is highlighted by large stratigraphic gaps between the formations on either side of the detachment (paraconformity-like or low-angle unconformity-like in Debacker et al., 2004a; see also fig. 14 in Herbosch & Debacker, 2018).

The very irregular and lobed trace of the Genappe - Orne - Noirmont-Baudecet relay faults (ADS Figs 1, 2) is explained, on the one hand, by the fact that they were folded during the Brabantian orogen (mid-Silurian to Lower Devonian, Debacker

et al., 2005a) and, on the other hand, by the very variable orientation of the folds associated with the transition zone between high and low plunging folds (see § 14.2; Debacker et al., 2004a, figs 13 and 14). Similarly, the supposed Court-St-Etienne klippe (Anthoine & Anthoine, 1943; Delcambre et al., 2002) is interpreted as a periclinal anticline culmination (Fig. 5; see § 14.6; Debacker et al., 2004a, fig. 7).

This second hypothesis provides many advantages over the oldest, it gives a better overall account of all field observations and applies to the situation observed in the Senne basin as well as to that of the Dyle, Orneau and Gette basins (e.g. Herbosch & Debacker, 2018). This is not the case for the first hypothesis, which moreover suffers from the absence of solid arguments concerning the gentle northern slope of the thrust (see Debacker et al., 2004a for a substantiated argumentation). The model of an early detachment fault (ADS in Figs 1, 2, 3) was used in the geological map at 1/200 000 of the Flemish part of the Brabant Massif (Piessens et al., 2005) and in the recent synthetic geological map of the southern part of the Brabant Massif (Fig. 1; Herbosch & Debacker, 2018).

14.2. Types of folds and cleavage

14.2.1. Types of folds

In a general and simplified form, two main fold types can be observed in the Brabant Massif (Fig. 25; for more detailed information see Debacker, 2012):
- type A folds: these are folds whose hinge line is subhorizontal or gently plunging (<30°) and whose axial surface is moderately to steeply inclined (dip between 30 and 80°). These folds generally have an asymmetry with a SW vergence and a wavelength of 2 to 4 km.
- type B folds: these are folds whose hinge line is steeply plunging (60 to 80°) and whose axial surface is steeply inclined (dip of 60 to 80°). The wavelength is of the order of 50 to 150 m. The cleavage is subvertical and fan-shaped with a change of direction along the long or short flanks.

The main difference between these two types of folds is the plunge of the fold hinge line. The cleavage-fold relationships show that both types of folds are cogenetic with cleavage. Type B folds were most often observed in the lower Cambrian core of the Brabant Massif or in the immediate vicinity of its margin, i.e. at the footwall of the Asquempont Detachment System. Type B folds have never been observed in units younger than the upper Cambrian MF (Debacker, 2001, 2012). In the Tubize and Blanmont fms of the Dyle basin, type B folds are often observed and more rarely type A folds, whereas in the MF type A folds are most often found except near ADS (Fig. 26; Debacker et al., 2004a).

14.2.2. Cleavage

The MF is affected by a cleavage, often not very visible due to alteration, with a strongly upright E-W direction with a dip >70° N (see for example Fig. 6A). This cleavage is characteristic of the whole of the Dyle basin basement, which belongs to the central part of the Brabant Massif (for more explanation see Sintubin, 1999).

14.3. The Genappe Fault belongs to the Asquempont Detachment System

The Genappe Fault (Fig. 27) is one of the few places where the faults that limit the MF could be objectively mapped in the field. Firstly, to the SW in Vieux-Genappe (Dyle valley), small outcrops bring the green magnetite siltstones and sandstones of
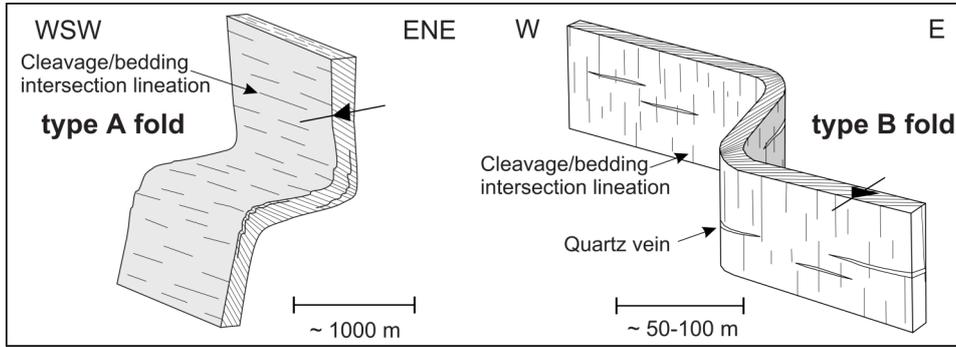
Figure 25. Two main syn-cleavage fold types observed in the Brabant Massif, type A fold and type B fold. Modified from Debacker & Herbosch (2011, fig. 6).
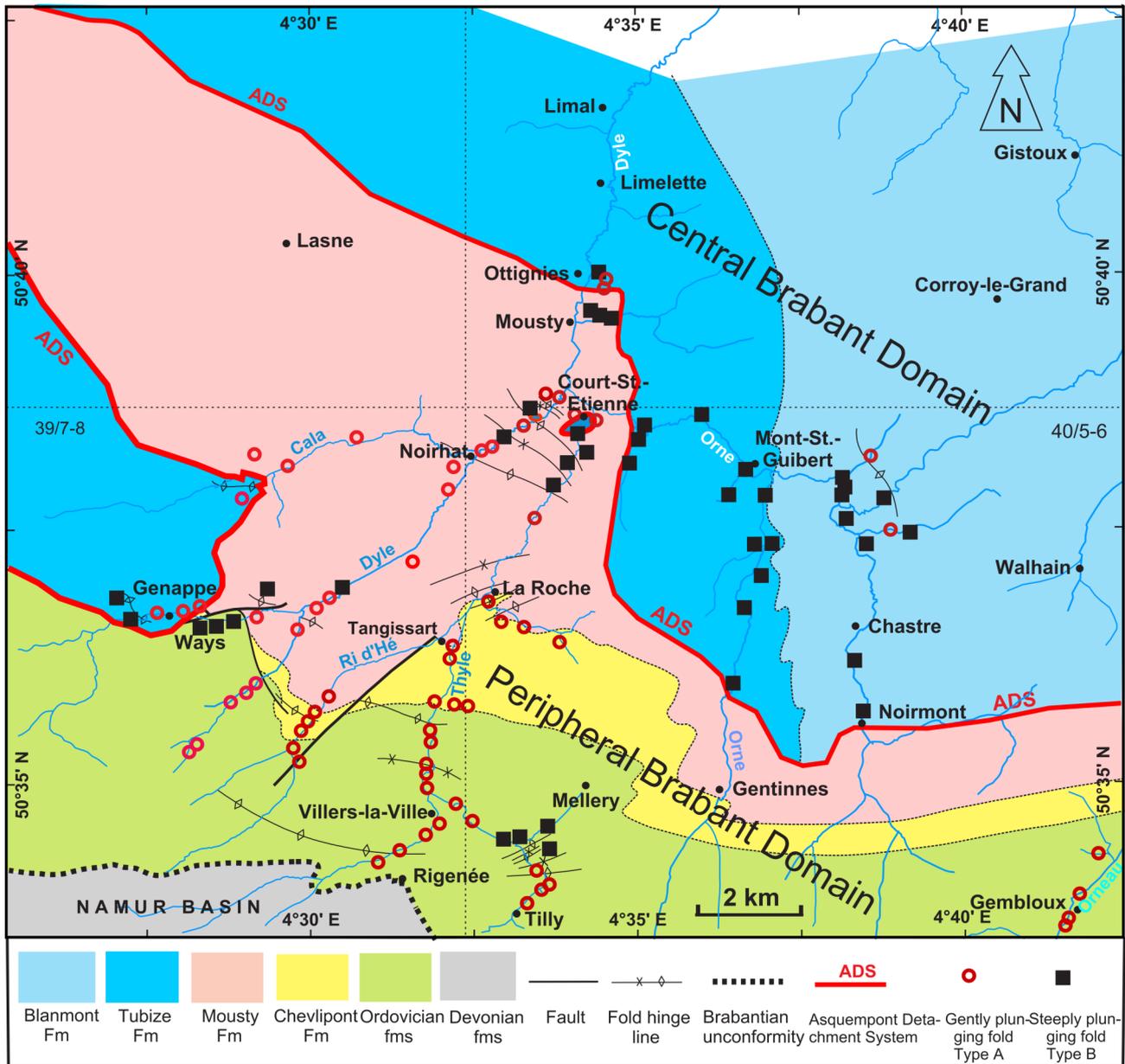

Figure 26. Simplified geological sub-crop map of the Dyle basin (from Herbosch & Lemonne, 2000; Delcambre et al., 2002; Herbosch & Blockmans, 2012) with the distribution of gently plunging folds (type A fold), and steeply plunging folds (type B fold). A divide of 35° was used (type A < 35°, type B > 35°; see § 14.2). Modified from Debacker et al. (2004a, fig.13).

the Tubize Fm into contact with the dark clayey siltstones of the Abbaye de Villers Fm (Fig. 27). The Tubize Fm is present everywhere in Genappe where it can be observed along the disused railway line (now Ravel) and in the large outcrop of the Notre-Dame de Lourdes cave. To the E, towards Ways and the Château de Thy, the contact between these two formations is clearly visible along the old railway line. Just to the N, tectonic complications bring the Tubize and Chevlipont fms into contact. As we are along the ADS, many type B folds and also some type A folds are observed (Figs 26, 27).

Figure 27. Detailed mapping of the Asquempont Detachment System (ADS) which brings the Tubize Fm into abnormal contact with the Abbaye de Villers, Chevlipont and Mousty formations in the area of Genappe (Dyle and Ri Cala valleys; location Fig. 2). See Herbosch & Debacker (2018, fig. 7B) for plotting ADS from aeromagnetic maps. Modified from Nivelles - Genappe map (Herbosch & Lemonne, 2000). Location of Photo 2 at 400 m E of the Château de Thy and Photos 5 and 17 along the brook 200 m NW of the Chapelle du Ruart.
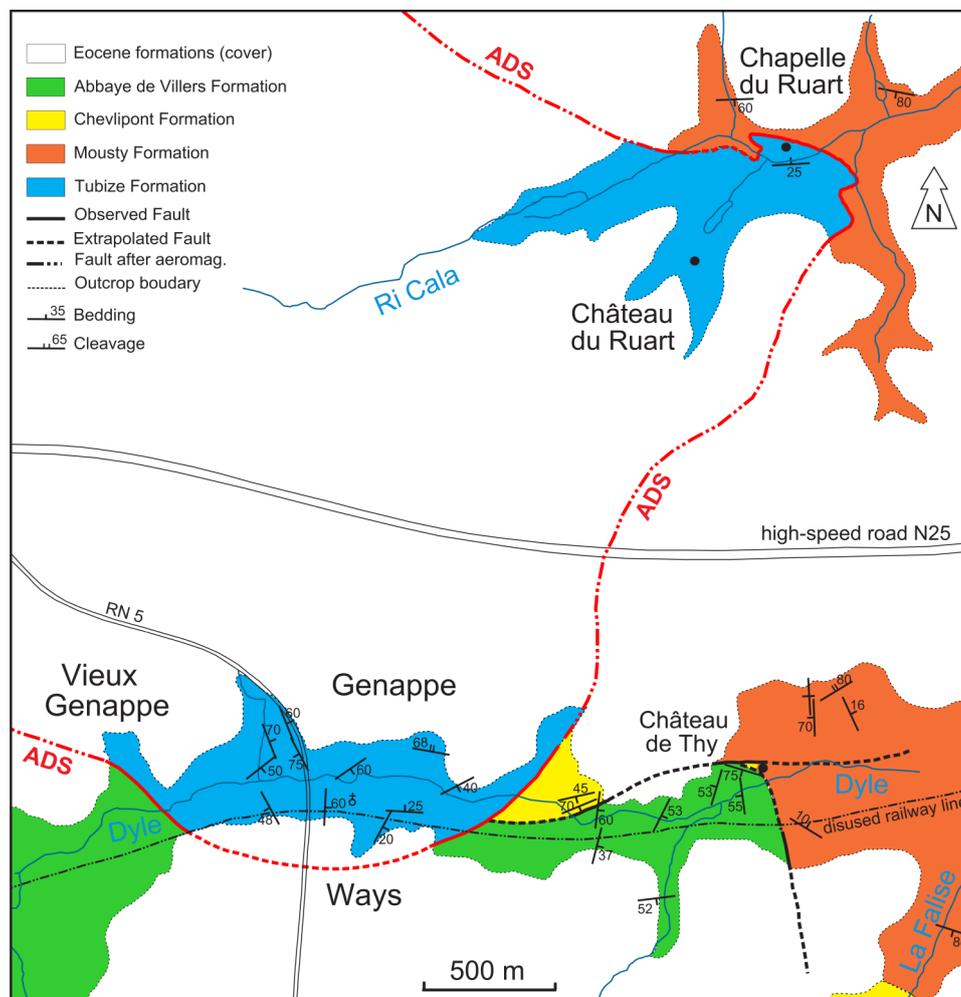
At 2 km to the N, in the upper valley of Ri Cala, the contact between the Tubize and Mousty fms can be followed on the field for about 1 km, showing a complete change of direction of the fault. The folds are of type A. The aeromagnetic map is used to link the fault trace under the cover between the two outcrops areas (Figs 3, 27; Herbosch & Debacker, 2018, fig. 7B). There is no information regarding the dip of the Genappe Fault which is part of ADS.

14. 4. The Orne Fault belongs to the Asquempont Detachment System

The E-W trace of the Orne Fault across the Dyle valley to the S of Ottignies (Fig. 2) is well constrained by the observation of Van Tassel (1986). It brings the black garnet slate of the MF, with an E-W direction and a dip of 35 to 45° S, into contact with green siltstones of close direction but with a dip of 65 to 72° N. The contact itself was never observed, thus its dip also. The folds are of type B (Fig. 26).

To the N, in the Ri Angon valley, the trace of the Orne fault, poorly constrained, has been drawn in a southerly direction about 100 metres to the W of the confluence with the Ruchaux brook, given the presence of an outcrop of Tubize Fm in the Bois de Morimont (Herbosch & Blockmans, 2012) and its known trace to the S. Further to the S, in the Orne Valley, its trace was constrained by the ground magnetic surveys conducted by de Magnée & Raynaud (1944) and the Chastre - Gembloux map work (Delcambre et al., 2002). Figure 28 shows a synthesis of all the information collected in the literature, our own field observations, as well as the different tracings

proposed for the Orne Fault (Debacker et al., 2004a, fig. 5). De Magnée & Raynaud (1944) observed an abrupt N-S trending truncation of NNE-SSW trending magnetic ridges of the Tubize Fm. They interpreted the ridge truncation as an NNE-directed thrust fault without drawing its trace to the N. They added that the magnetic signal excludes a low-slope fault dipping to the W. In consequence, the fault is either upright or with a weak slope to the E and should follow the ridge A on its W flank.

The N-S trace of the Orne Fault reported on the Chastre - Gembloux geological map disagrees with the magnetic survey because it crosses the middle of the negative magnetic anomaly zone that most likely represents the MF. A more likely trace, consistent with the magnetic survey and the fact that it is an extensional detachment fault (ADS), follows the negative anomaly zone to the E. In addition, a destructive vertical borehole of 87 m deep (BGS 40/5-527, see Fig. 28) located near the Ri Glory - Orne confluence, consists entirely of green slate with magnetite of the Tubize Fm. Considering a distance of 125 m from the easternmost documented occurrence of the MF (trench with MF fill, A. Herbosch, personal observation), the fault contact cannot have an E-ward dip of less than 35°. In the hypothesis here adopted of a curved trace along the E border of the negative magnetic anomaly, the distance between MF and the borehole is only about 50 m, which gives a much more vertical minimum slope of 60°. Given the subvertical bedding and the contact with the strongly dipping fault, it can be considered as a true cut-off.
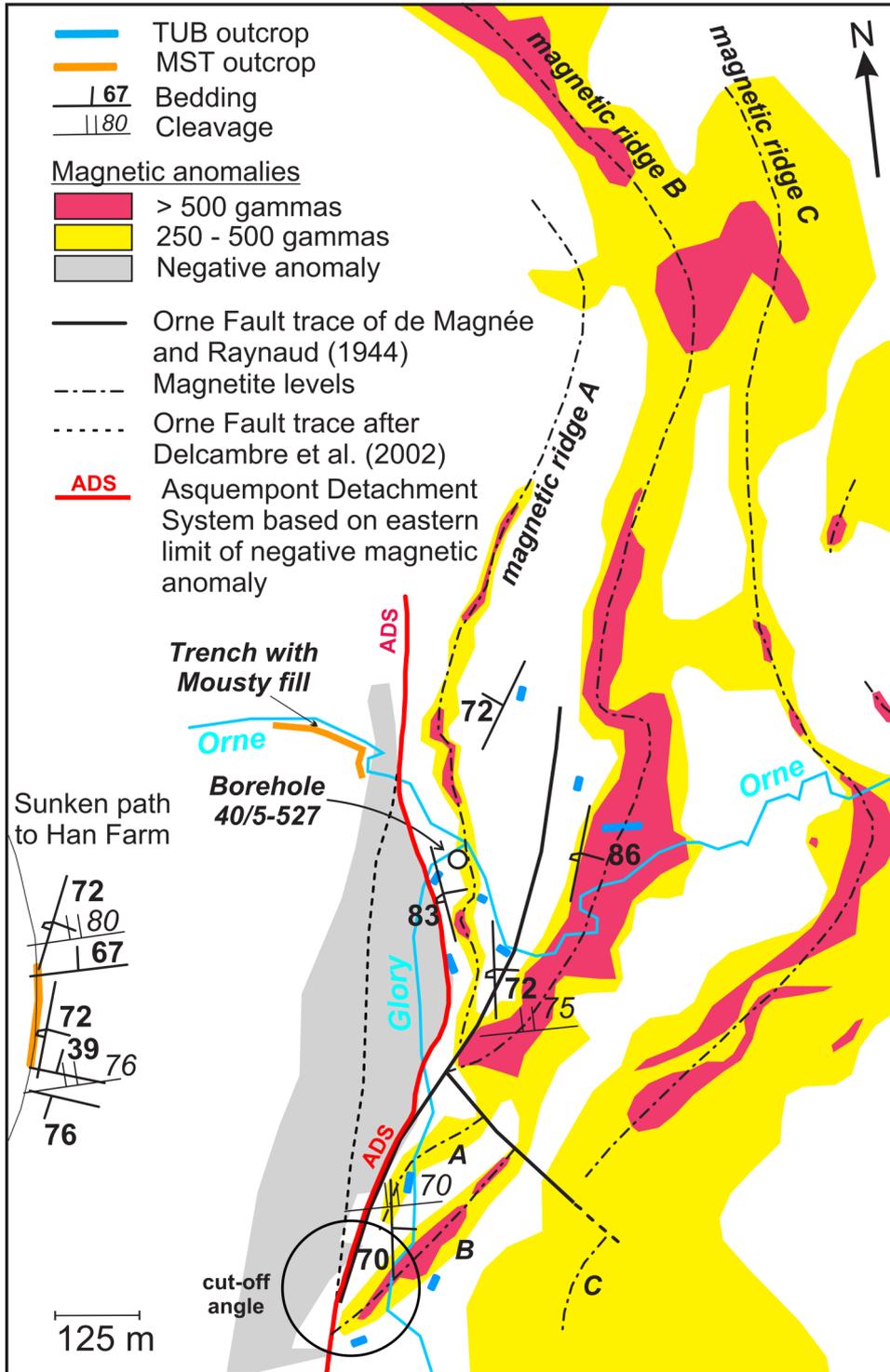
Figure 28. Ground magnetism data after de Magnée & Raynaud (1944) in the Orne valley and its tributary the Glory brook (location Fig. 2). Bedding, cleavage data and Orne fault trace taken from geological map Chastre - Gembloux (Delcambre et al., 2002). New Orne Fault trace in the hypothesis of the Asquempont Detachment System based on new personal observations and destructive borehole 40/5-527. Modified after Debacker et al. (2004a, fig 5). MST = Mousty Fm; TUB = Tubize Fm.

14.5. The Noirmont-Baudecet Fault belongs to the Asquempont Detachment System

In the Orne valley, the outcrops of the Blanmont Fm end at the Noirmont quarry, which is currently backfilled, but described by Stainier (1890) who measured a W40°N direction with a dip of 50°N. Three boreholes located a few hundred metres to the S of this quarry show the presence of MF (BGS 40/5-515, 40-5-516 and 40/5-127; location Fig. 2). These observations suggest the passage of a fault that separates the two formations. In order to clarify the position of this fault, a test hole was drilled 70 m S of the old quarry (40/5-539; Fig. 10; see Chap. 7). The latter crosses the sands of the Brussels Fm up to 20 m, then the quartzites of the Blanmont Fm up to 43.5 m and finally the

black slate of the MF up to 69 m. The cross section of Figure 29 shows the geological situation in the vicinity of Noirmont and the possible crossing zone of the fault under the assumption of an early ante-folding fault, i.e. the ADS. Its dip is unknown.

14.6. The supposed "klippe" of Court-St-Etienne is a periclinal culmination of the Asquempont Detachment System

The outcrops that can be seen on the hill formed by the southern part of Cour-St-Etienne as well as those of the railway trench that cuts it N-S have been the subject of much controversy since the early 20th century. For some, it is the MF (Fourmarier, 1920; de la Vallée Poussin, 1930) while for others it is the Tubize Fm (Anthoine & Anthoine, 1943; Mortelmans, 1955;
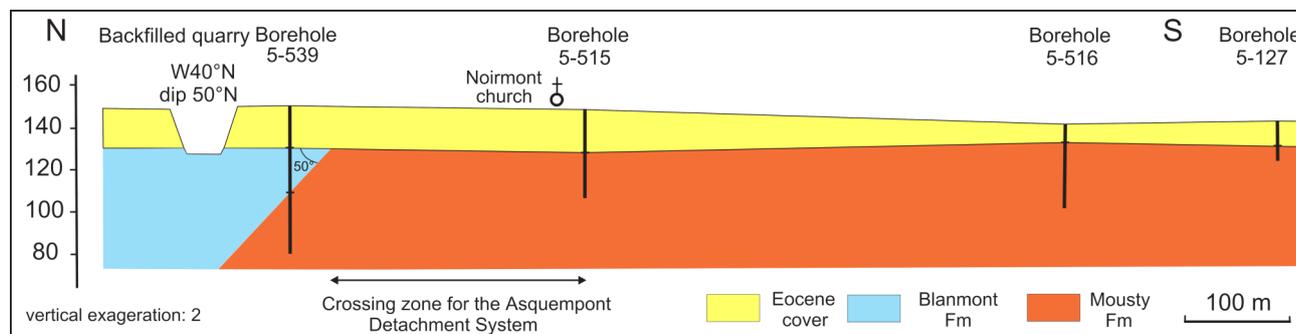
Figure 29. N-S cross-section of the Noirmont area, Orne valley (location in Figs 2, 10 Line B). The Mousty Fm was recognised on the basis of its black slate facies in the boreholes 5-539, 515, 516 and 127. The Noirmont quarry, currently backfilled, was described by Stainier (1890) who specified the direction and dip of the beds. The Asquempont Detachment System must necessarily pass between boreholes 5-539 and 5-515, but its dip is unknown.

Herbosch in André, 1991; Delcambre et al., 2002; Debacker et al., 2004a). Anthoine & Anthoine (1943) advocating a thrusting structuration, suggested the existence of a klippe for this hill surrounded on all sides by the MF.

Historically, the problem is twofold: on the one hand, it is necessary to be certain that the "klippe" is lithologically the Tubize Fm, and on the other hand, to know whether the Tubize and Mousty fms are in stratigraphic concordance. The answer to the first question has been solved by careful mapping, it is indeed the Tubize Fm (Delcambre et al., 2002; Debacker et al., 2004a). The second question will be solved only in the framework of the hypothesis of the Asquempont Detachment System (see § 14.1). In the framework of the programme of the new geological map of Wallonia, a 45° S oblique borehole was drilled in the MF in the NW flank of the supposed klippe in the hope of reaching the Tubize Fm (Fig. 5). The hole was stopped after 161 m still in the MF (see the lithological log in Fig. 6B). Following this, Delcambre & Pingot (2002, p. 47) opted for a fault contact and a klippe.

Taking all the data available in the literature and adding their own field observations, Debacker et al. (2004a) demonstrate that this is an anticlinal uplift of the Tubize Fm. Indeed, the younging direction based on sedimentological observations and bedding/cleavage relationships (see stereographic projections in Fig. 5) are directed outwards the Tubize Fm proving the dome-shaped structure. The problem of the absence of the Jodoigne and Oisquercq fms between the Mousty and Tubize fms (see Fig. 4) is solved by the fact that the fault surrounding the anticlinal uplift is the early detachment belonging to the Asquempont Detachment System (ADS). Careful and recent fieldwork combined with the examination of lidar photos (M. Laloux, pers. comm., 2020) have made it possible to better constrain the contours of the Tubize Fm (the ADS trace) despite the low number of outcrops (Fig. 5). Examination of the magnetic map (see Herbosch & Debacker, 2018, fig. 7B) shows that the anticlinal uplift coincides with a magnetic high. However, this high value occurs all around the anticline and continues towards the E to join the larger aeromagnetic high of the Tubize Fm which is exposed to the E of the Orne Fault (Figs 2, 3). These high values around the anticlinal uplift reflect deposits of the Tubize Fm below a relatively thin sequence of the MF.

In conclusion, the supposed "klippe" is currently interpreted as a periclinal culmination of the Asquempont detachment, within a fold transition zone between type A and type B folds (Debacker et al., 2004a, fig. 14). It is neither a tectonic window nor a klippe since there is no thrusting.

15. Conclusions

In this concluding chapter, we will briefly describe the main conclusions and key illustrations for each of the themes covered, with particular emphasis on new results.

- **Geological map**: four recent maps at 1/25 000 scale cover the whole Mousty Fm and a synthetic sub-crop map at 1/200 000 scale covers the entire outcrop area of the Brabant Massif southern margin (Fig. 1).
- **Area of occurrence**: its outcrops are restricted to the Dyle basin, but they are also known from boreholes under the Cenozoic cover in the same basin as well as in the Orneau basin (Fig. 2).
- **Lithology**: it is a very monotonous formation essentially formed of black graphitic slate often pyritic and sometimes manganesiferous. Sequences of low-density turbidites (Photo 15) and more rarely levels of lydite are also observed.
- **Lithostratigraphy**: due to monotonous lithology and the scarcity of outcrops, it was not possible to subdivide this thick formation into members except for its uppermost part, the already known Tangissart Member, where siltstone laminae gradually increase within the black slate. We have succeeded in identifying a section where the base of the formation is most likely present: the informal Court Unit (Fig. 7). The previously misplaced position of the Franquenies Fm now forms the informal Franquenies Unit located in the first third of the formation.
- **Bio- and chronostratigraphy**: the MF stratigraphy is only constrained by acritarchs found in two boreholes and by graptolites in the uppermost Tangissart Mbr. It extends most probably from the upper Guzhangian (~498 Ma) to the lowermost Tremadocian (~485 Ma), which represents a long period of ~13 m.y. (Figs 7, 9). The formation crosses the Cambrian–Ordovician boundary.
- **Thickness**: a new estimate based on two transversal profiles in the Gembloux - Blanmont syncline gives an estimate of the minimum thickness ranging from 1300 to 1600 m (Fig. 10). This high thickness, obtained with a few realistic assumptions, seems to be reasonable given the huge Cambrian subsidence (>9 km of sediments in a rift).
- **Sedimentology**: the black graphitic and pyritic slates forming the major part of the formation are mostly clayslates as they show a laminar structure (Photo 11). The graded mudstone-siltstone interpreted as low-density turbidites (Photo 15) are less common. The rather rare bedded lydite is interpreted as radiolarite due to the presence of elongated, clear, submillimetric (50–150 µm) microquartz-filled objects in a very fine opaque matrix (Photo 13). Numerous arguments

allow to interpret them as radiolarite ghosts. All these rocks are very dark due to the abundance of highly dispersed graphite. This attests to an anoxic environment as well as the absence of bioturbation and macrofossils.

- **Upper Tangissart Mbr** marks a gradual transition from the black slate of the Mousty Fm to the wavy-bedded siltstone of the Chevlipont Fm, interpreted as a low-density turbidite (Photo 14). This indicates a decrease in bathymetry and subsidence at the approach of Avalonia rift-drift from Gondwana.

- **Depositional environment**: all sedimentological observations indicate that pelagic to hemipelagic sediments were deposited in an anoxic deep sea, most probably located in an upwelling (Fig. 14). Palaeogeographic reconstructions (Fig. 13) show that this sea was located on the north-western rifted margin of the Gondwana continent, prior to the separation of Avalonia microplate. Comparison with the Harlech Dome (N Wales; Fig. 16) shows many similarities that have suggested to several authors that these two successions were deposited in the same aborted rift.

- **Nature of manganese protolith**: Mn is fairly common in the black slate where it is expressed by metamorphic minerals like spessartine and Mn-ilmenite. There is ample evidence that the stable phase of Mn in a deep anoxic marine environment is rhodochrosite (Fig. 12). Therefore, it is highly probable that rhodochrosite, formed during early diagenesis, was the protolith of later metamorphically formed Mn minerals.

- **Geochemistry**: major elements of Mousty Fm black slate are mainly grouped in the Shale field of lithological-geochemical classification of Herron, except for some garnet-rich slates that occur in the Fe-shale field (Fig. 17A). The many comparative shales (Brabant, Thuringia, Stavelot, Alum and Dictyonema from Baltic Basin, Shale standards) have globally the same behaviour as Mousty Fm slate. In the SiO_2/Al_2O_3 vs Fe_2O_3t diagram (Fig. 17B), the negative correlation shows that the quartz plus clay influx strongly dilutes the rather variable iron input. In the Fe_2O_3 vs MnO graph (Fig. 18A), the majority of the Mousty Fm black slate has MnO contents <1% ($mean_{26} = 0.18\%$) except four samples with $MnO \gg 1\%$. The mean major element composition of the Mousty Fm black slate is very similar to shale standards (Table 6), except for Mn which is abnormally high ($mean_{30} = 0.97\%$ sd = 2.8%) and Ca which is very low ($mean_{30} = 0.48\%$ sd = 0.46%). The Ca low values are widespread in the Cambrian and Ordovician rocks of the Brabant Massif. The hypothesis of a relationship between the high Mn content and a link with the first jolts of the opening of the Rheic Ocean as early as the Furongian is argued.

  The few major element analyses of the lydite, schistose lydite and Black Pigment of Sclayn reported in the Herron diagram (Fig. 17A) and $SiO_2 + Al_2O_3$ vs Fe_2O_3t diagram (Fig. 17B) are respectively in the Quartz Arenite field and clustered near the 100% x-axis. This proves their very siliceous nature and that the Black Pigment of Sclayn is geochemically related to lydites.

- **Radon anomaly**: the Mousty Fm outcrops are affected by high radon levels in buildings (Fig. 19; $median_{292} = 90$ bq/m^3) making it a "high radon area" according to Federal Agency for Nuclear Control regulations. Other geological units of the Brabant Massif are also affected, for example, the Silurian of the Mehaigne basin; these units are characterized by slowly deposited black shales rich in organic matter. The surprisingly low U content of the few analyses ($mean_4 = 4.3$ ppm) compared to the higher values of the Black shale standards (range 14–40 ppm; Table 7) is tentatively explained by the weathering of the field samples.

- **Metamorphic mineralogy**: the abundant minerals like muscovite, chlorite-mica stack, chlorite, ilmenite, spessartine, rutile, biotite and andalusite are often Mn-bearing. Microprobe analyses are given for the first time for these minerals and show that they are in equilibrium with the metamorphic conditions. The garnets have a fairly constant composition: $mean_{13}$ Sp 65% Al 26% Gr 7% Py 1% (Photos 20 to 22).

- **Metamorphism**: thermal maturation of organic matter by vitrinite reflection (Rmax = 6%) and Raman microspectrometry (T = 442 °C sd = 16 °C) shows that the black slates are well within the epizone. Reassessment of the precise stratigraphic assignments of illite crystallinity measurements shows that the Mousty Fm and neighbouring formations of the Dyle basin are also well within the epizone (Fig. 21). Extending the analysis to the southern margin outcrop area of the Brabant Massif show that the majority (44 from 57) of the Cambrian to Silurian rocks belong to the epizone (Fig. 22). The degree of metamorphism of Cambrian and Lower Ordovician rocks increases with age, which is typical of burial metamorphism. For 450 °C and a thickness of 9 km of Cambrian sediments, a geothermal gradient of about 50 °C/km is necessary. The measurement of the $b0$ cell dimension of the K-white mica on 121 samples from all the Brabant Massif allows to derive the burial pressure which is 2.5 kb for 400 °C and 3.3 kb for 450 °C. This is significantly higher than previous estimates. Finally, these new results show, at least for the Cambrian and Lower Ordovician rocks, that they underwent a very low grade metamorphism on a passive margin in extension of the type diastathermal metamorphism. This same burial metamorphism has been proposed to explain the metamorphism of the Harlech Dome (N Wales) which supports the hypothesis already published of a common rift basin.

- **Tectonic and the Asquempont Detachment System model**: in this last theme, specific tectonic features of the Mousty Fm are interpreted in the context of the recent low-angle extensional model called Asquempont Detachment System (ADS) which predates the Brabantian cleavage and folding. We show, with some new field observations, that the Genappe, Orne and Noirmont-Baudecet faults all belong to this detachment (Fig. 2) as well as the Court-St-Etienne supposed klippe (Fig. 5) which has recently been interpreted as a periclinal culmination of the ADS.

16. Perspectives

This summary work not only brought together all the observations made in the past but went beyond by making new field observations and proposing new perspectives. Nevertheless, there is still a lot of work to be done. In particular, the sedimentological and biostratigraphic study of the three cored boreholes and the study of the metamorphism of the Brabant Massif by extending it to the Ordovician and Silurian while specifying the precise stratigraphic attribution of the borehole samples.

In April–June 2020, ONDRAF (Organisme National des Déchets RAdioactifs et des matières Fissiles enrichies), in the announcement of a public consultation (Lambrecht, 2020), suggested using the Mousty Fm as a repository for long-lived nuclear waste. Our work clearly shows that this is not at all feasible for many reasons. In a nutshell, a notable uranium content and a high presence of radon mean a high mobility of these elements, characteristics that make this formation unsuitable for the storage of radioactive elements.

Acknowledgements

Author contribution

The interpretation and the writing of this article were performed by the author.

Data availability

All data are available online in Supplementary data.

References

Alomène, T., 1987. Etude sédimentologique et pétrographique de l'Assise de Mousty (Massif du Brabant). Unpublished Master Thesis, Université Libre de Bruxelles, Bruxelles, 70 p.

Andersson, A., Dahlman, B., Gee, D.G. & Snäll, S., 1985. The Scandinavian Alum Shales. Sveriges Geologiska Undersökning, Ca 56, 1–50.

André, L., 1983. Origine et évolution des roches éruptives du Massif du Brabant (Belgique). Implications au niveau de l'étude des roches magmatiques transformées et de la géologie calédonienne du nord-ouest de l'Europe. Unpublished Ph.D. Thesis, Université libre de Bruxelles, Bruxelles, 299 p.

André, L., 1991. The concealed crystalline basement in Belgium and the "Brabantia" microplate concept: constraints from the Caledonian magmatic and sedimentary rocks. Annales de la Société géologique de Belgique, 114, 117–139.

André, L., Deutsch, S. & Michot, J., 1981. Données géochronologiques concernant le développement tectono-métamorphique du segment calédonien brabançon. Annales de la Société géologique de Belgique, 104, 241–253.

Anthoine, R. & Anthoine, P., 1943. Les assises de Mousty et de Villers-la-Ville du bassin supérieur de la Dyle. Annales de la Société géologique de Belgique, 66, M53–M180.

Baudin, F., Tribovillard, N. & Trichet, J., 2007. Géologie de la matière organique. Vuibert et Société géologique de France, Paris, 263 p.

Beckers, R., 2004. Comparison of folds in the Chevlipont and Abbaye de Villers formations, near the Abbey of Villers, Thyle valley, Brabant Massif. Geologica Belgica, 7, 357–359.

Bergström, S.M., Chen, X., Gutierez-Marco, J.C. & Dronov, A., 2009. The new chronostratigraphic classification of the Ordovician System and its relations to major regional series and stages and to $\delta^{13}C$ chemostratigraphy. Lethaia, 42, 97–107. https://doi.org/10.1111/j.1502-3931.2008.00136.x

Beugnies, A., 1976. Structure et métamorphisme du Paléozoïque de la région de Muno, un secteur-clé du domaine hercynien de l'Ardenne. Annales des Mines de Belgique, 6, 481–509.

Bevins, R.E. & Robinson, D., 1988. Low grade metamorphism of the Welsh Basin Lower Palaeozoic succession: an example of diastathermal metamorphism? Journal of the Geological Society, 145, 363–366. https://doi.org/10.1144/gsjgs.145.3.0363

Blockmans, S., Dumoulin, V. & Herbosch, A., in press. Carte géologique de Wallonie : Uccle – Tervuren 31/7-8 et Waterloo – La Hulpe 39/3-4. 1/25 000. Service public de Wallonie, DGRNE, Namur.

Bonjean, D., Vanbrabant, Y., Abrams, G., Pirson, S., Burlet, C., Di Modica, K., Otte, M., Vander Auwera, J., Golitko, M., McMillan, R., & Goemaere, E., 2015a. A new Cambrian black pigment used during the late Middle Palaeolithic discovered at Scladina Cave (Andenne, Belgium). Journal of Archaeological Science, 55, 253–265. https://doi.org/10.1016/j.jas.2014.11.040

Bonjean, D., Vanbrabant, Y., Abrams, G., Pirson, S., Burlet, C., Di Modica, K., Otte, M., Vander Auwera, J., Golitko, M., McMillan, R., Steemans, P. & Goemaere, E., 2015b. Nouvelles données sur un pigment noir d'origine cambrienne, utilisé au Paléolithique moyen et découvert dans la grotte Scladina (Andenne, BE). Notae Praehistoricae, 35, 121–146.

Bouma, A.H., 1962. Sedimentology of some flysh deposits: a graphic approach to facies interpretation. Elsevier, Amsterdam, 168 p.

Brenchley, P.J., Rushton, A.W.A., Howells, M. & Cave, R., 2006. Cambrian and Ordovician: the early Palaeozoic tectonostratigraphic evolution of the Welsh Basin, Midland, and Mona Terranes of Eastern Avalonia. In Brenchley, P.J. & Rawson, P.F. (eds), The Geology of England and Wales. 2nd ed. The Geological Society, London, 25–74. https://doi.org/10.1144/GOEWP.3

Bucher, K. & Grapes, R., 2011. Petrogenesis of Metamorphic Rocks. 8th ed. Springer, Berlin, 428 p. https://doi.org/10.1007/978-3-540-74169-5

Caspar, J.-P., 1984. Matériaux lithiques de la Préhistoire. In Cahen, D. & Haesaerts, P. (eds), Peuples chasseurs de la Belgique préhistorique dans leur cadre naturel. Patrimoine de l'Institut royal des Sciences naturelles de Belgique, Bruxelles, 107–114.

Chester, R., 1990. Marine Geochemistry. Unwin Hyman, London, 698 p. https://doi.org/10.1007/978-94-010-9488-7

Cinelli, G. & Tondeur, F., 2015. Log-normality of indoor radon data in the Walloon region of Belgium. Journal of Environmental Radioactivity, 143, 100–109. https://doi.org/10.1016/j.jenvrad.2015.02.014

Cojan, I. & Renard, M., 2013. Sédimentologie. Dunod, Paris, 480 p.

Coombs, D.S., 1961. Some recent work on the lower grade of metamorphism. Australian Journal of Sciences, 24, 203–215.

Dahl, T.W., Boyle, R.A., Canfield, D.E., Connelly, J.N., Gill, B.C., Lenton, T.M. & Bizzarro, M., 2014. Uranium isotopes distinguish two geochemically distinct stages during the later Cambrian SPICE

event. Earth and Planetary Science Letters, 401, 313–326. https://doi.org/10.1016/j.epsl.2014.05.043

Dandois, P., 1985. Le métamorphisme des terrains paléozoïques de la partie médio-occidentale de l'Ardenne. Ph.D. Thesis, Université Catholique de Louvain, Louvain-la Neuve, 2 vol., 333 p.

Debacker, T., 1999. Folds trending at various angles to the transport direction in the Marcq area, Brabant Massif, Belgium. Geologica Belgica, 2, 159–172. https://doi.org/10.20341/gb.2014.015

Debacker, T.N., 2001. Palaeozoic deformation of the Brabant Massif within eastern Avalonia: how, when and why? Unpublished Ph.D. Thesis, Laboratorium voor Palaeontologie, Universiteit Gent, Gent, 225 p.

Debacker, T.N., 2012. Folds and cleavage/fold relationships in the Brabant Massif, southeastern Anglo-Brabant Deformation Belt. Geologica Belgica, 15, 81–95.

Debacker, T. & Herbosch, A., 2011. Field guide to the pre-cleavage deformation and stratigraphy of the Jodoigne area: Cambrian slump deformation and evidence for the Asquempont Detachment System along the N-side of the core of the Brabant Massif. Memoirs of the Geological Survey of Belgium, 57, 1–27.

Debacker, T.N., Herbosch, A., Sintubin, M. & Verniers, J., 2003. Palaeozoic deformation history of the Asquempont-Virginal area (Brabant Massif, Belgium): large-scale slumping, low-angle extensional detachment development (the Asquempont Fault redefined) and normal faulting (the Nieuwpoort-Asquempont fault zone). Memoirs of the Geological Survey of Belgium, 49, 1–30.

Debacker, T.N., Herbosch, A. & Sintubin, M., 2004a. The supposed thrust fault in the Dyle-Thyle outcrop area (southern Brabant Massif, Belgium) re-interpreted as a folded low-angle extensional detachment. Geologica Belgica, 8/3, 53–69.

Debacker, T.N., Robion, P. & Sintubin, M., 2004b. The anisotropy of magnetic susceptibility (AMS) in low-grade, cleaved pelitic rocks: influence of cleavage/bedding angle and type and relative orientation of magnetic carriers. In Martin-Hernandez, F., Lüneburg, C.M., Aubourg, C. & Jackson, M. (eds), Magnetic Fabric: Methods and Applications. Geological Society, London, Special Publications, 238, 77–107. https://doi.org/10.1144/GSL.SP.2004.238.01.08

Debacker, T.N., Dewaele, S., Sintubin, M., Verniers, J., Muchez, Ph. & Boven, A., 2005a. Timing and duration of the progressive deformation of the Brabant Massif, Belgium. Geologica Belgica, 8/4, 20–34.

Debacker, T.N., Robion, P. & Sintubin, M., 2005b. Complexity of the anisotropy of magnetic susceptibility in single-phase deformed, low-grade, cleaved mudstone. Materials Science Forum, 495-497, 45–56. https://doi.org/10.4028/www.scientific.net/MSF.495-497.45

Debacker, T.N., Dumon, M. & Matthys, A., 2009a. Interpreting fold and fault geometries from within the lateral to oblique parts of slumps: a case study from the Anglo-Brabant Deformation Belt (Belgium). Journal of Structural Geology, 31, 1525–1539. https://doi.org/10.1016/j.jsg.2009.09.002

Debacker, T.N., Hirt., A.M., Sintubin, M. & Robion, P., 2009b. Differences between magnetic and mineral fabrics in low-grade, cleaved siliciclastic pelites: A case study from the Anglo-Brabant Deformation Belt (Belgium). Tectonophysics, 466, 32–46. https://doi.org/10.1016/j.tecto.2008.09.039

Debacker, T.N., Sintubin, M. & Robion, P., 2010. On the use of magnetic techniques for stratigraphic purposes: examples from the Lower Palaeozoic Anglo-Brabant Deformation Belt (Belgium). Geologica Belgica, 13, 333–350.

Debacker, T., Herbosch, A. & Verniers, J., 2011.The presumed Upper Ordovician green rocks at Rebecq re-interpreted as a resurfacing of the Cambrian Oisquercq Formation (Senne valley, Anglo-Brabant Deformation Belt, Belgium). Geologica Belgica, 14, 249–264.

de Burtin, F.-X., 1788. Voyage et observations minéralogiques depuis Bruxelles par Wavre jusqu'à Court-St-Etienne. Mémoires de l'Académie impériale et royale des Sciences et Belles-Lettres de Bruxelles, 5, 124, 123–138.

de la Vallée Poussin, J., 1930. Contribution à l'étude du Massif « Cambrien » dans les vallées de la Dyle et de la Gette. Mémoires de l'Institut géologique de l'Université de Louvain, 6, 317–355.

Delcambre, B., Pingot, J.-L. & Herbosch, A., 2002. Carte géologique de Wallonie : Chastre – Gembloux 40/5-6.1/25 000. Ministère de la Région wallonne, DGRNE, Namur.

Delcambre, B. & Pingot, J.-L., 2002. Carte géologique de Wallonie : Chastre – Gembloux 40/5-6. Notice explicative. 1/25 000. Ministère de la Région wallonne, DGRNE, Namur, 72 p.

de Magnée, I. & Raynaud, J., 1944. Etude magnétique de la tectonique du Cambrien du Brabant à l'est de Court-St-Etienne. Annales de la Société géologique de Belgique, 67, M495–M549.

de Magnée, I. & Anciaux, P., 1945. Note préliminaire sur le métamorphisme à grenats du Brabant. Bulletin de la Société belge de Géologie, de Paléontologie et d'Hydrologie, 54, 77–85.

de Magnée, I. & Lambeau, J., 1965. Le poudingue phosphaté et manganésifère de Thy (vallée de la Dyle). Bulletin de la Société belge de Géologie, de Paléontologie et d'Hydrologie, 74, 293–300.

De Vos, W., Verniers, J., Herbosch, A. & Vanguestaine, M., 1993. A new geological map of the Brabant Massif. Geological Magazine, 130, 605–611. https://doi.org/10.1017/S0016756800020902

De Wever, P., Dumitrica, P., Caulet, J.P., Nigrini, C. & Caridroit, M., 2001. Radiolarians in the Sedimentary Record. Gordon and Breach Science Publishers, Amsterdam, 533 p. https://doi.org/10.1201/9781482283181

De Windt, J., 1897. Sur les relations lithologiques entre les roches considérées comme cambriennes des massifs de Rocroi, du Brabant et de Stavelot. Mémoires couronnés et Mémoires des Savants étrangers de l'Académie royale des Sciences, des Lettres et des Beaux-Arts de Belgique, 56, 1–96.

Domeier, M., 2016. A plate tectonic scenario for the Iapetus and Rheic oceans. Gondwana Research, 36, 275–295. https://doi.org/10.1016/j.gr.2015.08.003

Dumont, A., 1848. Mémoire sur les terrains ardennais et rhénan de l'Ardenne, du Rhin, du Brabant et du Condros (2e partie). Mémoires de l'Académie royale des Sciences, des Lettres et des Beaux-Arts de Belgique, 22, 1–451.

Dupréel, M., 1937. Recherches sur le phtanite d'Ottignies. La station paléolithique de Franquenies. Bulletin de la Société royale belge d'Anthropologie et de Préhistoire, 52, 124–129.

Edwards, C.T., 2019. Links between early Palaeozoic oxygenation and the Great Ordovician Biodiversification Event (GOBE): a review. Palaeoworld, 28, 37–50. https://doi.org/10.1016/j.palwor.2018.08.006

Everaerts, M., 2000. L'interprétation structurale de la Manche au Rhin : apport du filtrage des champs de potentiel. Unpublished Ph.D. Thesis. Université catholique de Louvain, Louvain-la-Neuve, 167 p.

Fielitz, W. & Mansy, J.-L., 1999. Pre- and synorogenic burial metamorphism in the Ardenne and neighbouring areas (Rhenohercynian zone, central European Variscides. Tectonophysics, 309, 227–256. https://doi.org/10.1016/S0040-1951(99)00141-9

Fourmarier, P., 1920. La tectonique du Brabant et des régions voisines. Mémoires de l'Académie royale de Belgique, Classe des Sciences. Collection in 4°, 2e série, 4, 94 p.

Fransolet, A.-M. & Kramm, U., 1983. Mineralogie und Petrologie Mn-reicher Metapelite des Venn-Stavelot Massivs, Ardennen, und die varistische Metamorphose im nordwestlichen Rheinischen Schild. Fortschritte der Mineralogie, 61, 31–69.

Gautneb, H. & Saether, O.M., 2009. A compilation of previously published geochemical data on the lower Cambro-Silurian sedimentary sequence, including the alum shales in the Oslo region. Geological Survey of Norway report, 2009.053, 25 p.

Geerkens, B. & Laduron D., 1996. Etude du métamorphisme dans le Massif du Brabant. Final report of project VLA/93-3.5.3.

Giese, U., Katzung, G., Walter, R. & Weber, J., 1997. The Caledonian deformation of the Brabant Massif and the Early Palaeozoic in northeast Germany: compared. Geological Magazine, 134, 637–652. https://doi.org/10.1017/S0016756897007565

Gill, B.C., Lyons, T.W., Young, S.A., Kump, L.R., Knoll, A.H. & Saltzman, M.R., 2011. Geochemical evidence for widespread euxinia in the Later Cambrian ocean. Nature, 469, 80–83. https://doi.org/10.1038/nature09700

Gill, B.C., Dahl, T.W., Hammarlund, E.U., LeRoy, M.A., Gordon, G.W., Canfield, D.E., Anbar, A.D. & Lyons, T.W., 2021. Redox dynamics of later Cambrian oceans. Palaeogeography, Palaeoclimatology, Palaeoecology, 581, 110623. https://doi.org/10.1016/j.palaeo.2021.110623

Goldman, D., Sadler, P.M. & Leslie, S.A., 2020. The Ordovician period. In Gradstein, F.M., Ogg, J.G., Schmitz, M.D. & Ogg, G.M. (eds), Geologic Time Scale 2020. Elsevier, Amsterdam, 631–694. https://doi.org/10.1016/B978-0-12-824360-2.00020-6

Gradstein, F.M., Ogg, J.G., Schmitz, M.D. & Ogg, G.M. (eds), 2020. Geologic Time Scale 2020. Elsevier, Amsterdam, 1357 p. https://doi.org/10.1016/C2020-1-02369-3

Graulich, J.-M., 1961. Le sondage de Wépion. Mémoires pour servir à l'Explication des Cartes géologiques et minières de la Belgique, 2, 1–102.

Gromet, L.P., Haskin, L.A., Korotev, R.L. & Dymek, R.F., 1984. The "North American Shale composite": Its compilation, major and trace element characteristics. Geochimica et Cosmochimica Acta, 48, 2469–2482. https://doi.org/10.1016/0016-7037(84)90298-9

Guidotti, C.V., 1984. Micas in metamorphic rocks. Reviews in Mineralogy and Geochemistry, 13, 357–467. https://doi.org/10.1515/9781501508820-014

Guidotti, C.V. & Sassi, F.P., 1976. Muscovite as a petrogenetic indicator mineral in pelitic schists. Neues Jahrbuch für Mineralogie, Abhandlungen, 127, 97–142.

Guidotti, C.V. & Sassi, F.P., 1986. Classification and correlation of metamorphic facies series by means of muscovite b_0 data from low-grade metapelites. Neues Jahrbuch für Mineralogie, Abhandlungen, 153, 363–380.

Haulotte, E., 2002. Une curiosité naturelle à Mousty. Cercle d'Histoire, d'Archéologie et de Généalogie d'Ottignies - Louvain-la-Neuve. Revue Okgni, 20, 17–19.

Herbosch, A., 2021. Stratigraphic correlations between the Brabant Massif and the Stavelot, Rocroi and Givonne inliers (Belgium) and geological implications. Geologica Belgica, 24, 137–157. https://doi.org/10.20341/gb.2021.004

Herbosch, A. & Blockmans, S, 2012. Carte géologique de Wallonie : Wavre – Chaumont-Gistoux 40/1-2.1/25 000. Ministère de la Région wallonne, DGRNE, Namur.

Herbosch, A. & Debacker, T.N., 2018. A new geological map of the outcrop areas of the Brabant Massif (Belgium). Geologica Belgica, 21, 41–58. https://doi.org/10.20341/gb.2018.003

Herbosch, A. & Lemonne, E., 2000. Carte géologique de Wallonie : Nivelles – Genappe 39/7-8. 1/25 000. Ministère de la Région wallonne, DGRNE, Namur.

Herbosch, A. & Verniers, J., 2013. Stratigraphy of the Lower Palaeozoic of the Brabant Massif, Belgium. Part 1: the Cambro-Ordovician from the Halle and Ottignies groups. Geologica Belgica, 16, 49–65.

Herbosch, A. & Verniers, J., 2014. Stratigraphy of the Lower Palaeozoic of the Brabant Massif, Belgium. Part II: The Middle Ordovician to lowest Silurian of the Rebecq Group. Geologica Belgica, 17, 115–136.

Herbosch, A. Vanguestaine, M., Degardin, J.M., Dejonghe, L., Fagel, N. & Servais, T., 1991. Etude lithostratigraphique, biostratigraphique et sédimentologique du sondage de Lessines (bord méridional du Massif du Brabant, Belgique). Annales de la Société géologique de Belgique, 114, 195–212.

Herbosch, A., Verniers, J., Debacker, T.N., Billiaert, B., De Schepper, S. & Belmans, M., 2001. The Lower Palaeozoic stratigraphy and sedimentology of the Brabant Massif in the Dyle and Orneau valleys and the Condroz Inlier at Fosses: an excursion guidebook. Pre-symposium excursion of the International Symposium on Early Palaeozoic palaeogeographies and biogeographies of Western Europe and North Africa. Université des Sciences et Technologies de Lille, Villeneuve d'Ascq, 24–26/09/2001, 59 p.

Herbosch, A., Debacker, T.N. & Piessens, K., 2008. The stratigraphic position of the Cambrian Jodoigne Formation redefined (Brabant Massif, Belgium). Geologica Belgica, 11, 133–150.

Herbosch, A., Liégeois, J.-P. & Pin, C., 2016. Coticules of the Belgian type area (Stavelot-Venn Massif): Limy turbidites within the nascent Rheic oceanic basin. Earth-Science Reviews, 159, 186–214. https://doi.org/10.1016/j.earscirev.2016.05.012

Herbosch, A., Liégeois, J.-P., Gärtner, A., Hofmann, M. & Linnemann, U., 2020. The Stavelot-Venn Massif (Ardenne, Belgium), a rift shoulder basin ripped off the West African craton: Cartography, stratigraphy, sedimentology, new U-Pb on zircon ages, geochemistry and Nd isotopes evidence. Earth-Science Reviews, 203, 103142. https://doi.org/10.1016/j.earscirev.2020.103142

Herron, M.M, 1988. Geochemical classification of terrigenous sands and shales from core or log data. Journal of Sedimentary Petrology, 58, 820–829. https://doi.org/10.1306/212F8E77-2B24-11D7-8648000102C1865D

Hey, M.H., 1954. A new review of the chlorites. Mineralogical Magazine and Journal of the Mineralogical Society, 30/224,277–292. https://doi.org/10.1180/minmag.1954.030.224.01

Ichikuni, M., 1959. Sur la dissolution des minerais sulfurés en divers milieux. II, Dissolution de la pyrite et de la chalcopyrite. Bulletin of the Chemical Society of Japan, 33, 1052–1057. https://doi.org/10.1246/bcsj.33.1052

Jodart, C., 1986. Etude cartographique et pétrologique de l'Ordovicien inférieur de la Thyle (Massif du Brabant, Belgique). Unpublished Master Thesis, Université Libre de Bruxelles, Bruxelles, 145 p.

Johnson, J.E., Webb, S.M., Ma, C. & Fisher, W.W., 2016. Manganese mineralogy and diagenesis in the sedimentary rocks record. Geochimica et Cosmochimica Acta, 173, 210–231. https://doi.org/10.1016/j.gca.2015.10.027

Kramm, U., 1973. Chloritoid stability in manganese rich low-grade metamorphic rocks, Venn-Stavelot Massif, Ardennes. Contributions to Mineralogy and Petrology, 41, 179–196. https://doi.org/10.1007/BF00375042

Kramm, U., 1982. Die Metamorphose des Venn-Stavelot-Massivs, nordwestliches Rheinisches Schiefergebirge: Grad, Alter und Ursache. Decheniana, 135, 121–178. https://doi.org/10.21248/decheniana.v135.4092

Krumbein, W.C. & Garrels, R.M., 1952. Origin and classification of chemical sediments in terms of pH and oxidation-reduction potentials. Journal of Geology, 60, 1–33. https://doi.org/10.1086/625929

Kübler, B., 1964. Les argiles, indicateurs de métamorphisme. Revue de l'Institut français du Pétrole, 19, 1093–1112.

Laibl, L., Servais, T. & Mottequin, B., 2023. Tremadocian (Ordovician) trilobites from the Brabant Massif (Belgium): Palaeogeographical and palaeoecological implications. Geobios. https://doi.org/10.1016/j.geobios.2023.04.003

Lambrecht, L., 2020. Déchets nucléaires : la polémique enfle. La Libre Belgique, 28 mai, p. 25.

Landing, E., Bowring, S.A., Davidek, K.L., Rushton, A.W.A., Fortey, R.A. & Wimbledon, W.A.P., 2000. Cambrian–Ordovician boundary age and duration of the lowest Ordovician Tremadoc Series based on U–Pb zircon dates from Avalonian Wales. Geological Magazine, 137, 485–494. https://doi.org/10.1017/S0016756800004507

Larangé F., 2002. Low-grade metamorphism and geotectonic setting of the Brabant Massif and the medio-occidental part of the Ardenne, Belgium: application of white mica crystallinity, b cell dimension and transmission electron microscope studies. Unpublished Ph.D. Thesis, Université catholique de Louvain, Louvain-la-Neuve, 213 p.

Large, R., Mukherjee, I., Danyushevsky, L., Gregory, D., Steadman, J. & Corkrey, R., 2022. Sedimentary pyrite proxy for atmospheric oxygen: evaluation of strengths and limitations. Earth-Science Reviews, 227, 103941. https://doi.org/10.1016/j.earscirev.2022.103941

Lecompte, M., 1948. Existence du Trémadocien dans le Massif du Brabant. Bulletin de l'Académie royale de Belgique, Classe des Sciences, 5ᵉ série, 34, 677–687.

Lecompte, M., 1949. Découverte de nouveaux gîtes à *Dictyonema* dans le Trémadocien du Massif du Brabant. Bulletin de l'Institut royal des Sciences naturelles de Belgique, 25/45, 1–8.

Legrand, R., 1966. Sondage de Bousval, Pl. 129E197. Service Géologique de Belgique, Professional Papers, 8, 2 p.

Legrand, R., 1968. Le Massif du Brabant. Mémoires pour servir à l'Explication des Cartes géologiques et minières de la Belgique, 9, 148 p.

Leriche, M., 1921. Compte rendu de l'excursion faite le 8 mai 1921, dans la vallée de la Dyle, aux environs d'Ottignies. Bulletin de la Société belge de Géologie, de Paléontologie et d'Hydrologie, 31, 211–216.

Li, G., Peacor, D.R., Merriman, R.J., Roberts, B. & van der Pluijm, B.A., 1994. TEM and AEM constraints on the origin and significance of chlorite-mica stacks in slates: an example from Central Wales, U.K. Journal of Structural Geology, 16, 1139–1157. https://doi.org/10.1016/0191-8141(94)90058-2

Linnemann, U., Herbosch, A., Liégeois, J.-P., Pin, C., Gärtner, A. & Hofmann, M., 2012. The Cambrian to Devonian odyssey of the Brabant Massif within Avalonia: A review with new zircon ages, geochemistry, Sm-Nd isotopes, stratigraphy and palaeogeography. Earth-Science Reviews, 112, 126–154. https://doi.org/10.1016/j.earscirev.2012.02.007

Longueville, G., 1997. Geologische kartering, litho- and biostratigrafie van het Onder-Paleozoicum in de Markvallei (Massief van Brabant). Unpublished M.Sc.-thesis, University of Gent, Gent, 72 p.

Lundegard, P.D. & Samuels, N.D., 1980. Field classification of fine-grained sedimentary rocks. Journal of Sedimentary Petrology, 50, 781–786. https://doi.org/10.1306/212F7AE5-2B24-11D7-8648000102C1865D

Malaise, C., 1873. Description du terrain silurien du centre de la Belgique. Mémoires couronnés et Mémoires des Savants étrangers de l'Académie royale des Sciences, des Lettres et des Beaux-Arts de Belgique, 37, 122 p.

Malaise, C., 1883a. Sur la composition du massif ardoisier du Brabant. Annales de la Société géologique de Belgique, 10, 19–24.

Malaise, C., 1883b. Sur la constitution du massif silurien du Brabant. Bulletin de la Classe des Sciences de l'Académie royale de Belgique, 3e série, 5, 184–211.

Malaise, C., 1909. Echelle stratigraphique du Silurien de Belgique et âge géologique des schistes noirs de Mousty. Annales de la Société géologique de Belgique, 36, M31–M39.

Mansy, J.-L., Everaerts, M. & De Vos, W., 1999. Structural analysis of the adjacent Acadian and Variscan fold belts in Belgium and northern France from geophysical and geological evidence. Tectonophysics, 309, 99–116. https://doi.org/10.1016/S0040-1951(99)00134-1

Marcilly, C.M., Torsvik, T.H. & Conrad, C.P., 2022. Global Phanerozoic sea levels from palaeogeographic flooding maps. Gondwana Research, 110, 128–142. https://doi.org/10.1016/j.gr.2022.05.011

Martin, F., 1977. Acritarches du Cambro-Ordovicien du Massif du Brabant, Belgique. Bulletin de l'Institut royal des Sciences naturelles de Belgique, 51 (1975), 1–33.

Martin, F. & Dean, W.T., 1981. Middle and Upper Cambrian and Lower Ordovician acritarchs from Random Island, Eastern Newfoundland. Geological Survey of Canada, Bulletin, 343, 1–43. https://doi.org/10.4095/124915

Maynard, J.B., 1983. Geochemistry of Sedimentary Ore Deposits. Springer, New York, 305 p. https://doi.org/10.1007/978-1-4613-9493-8

Maynard, J.B., 2003. Manganiferous sediments, rocks, and ores. In Mackenzie, F.T. (ed.), Treatise on Geochemistry. Volume 7: Sediments; Diagenesis, and Sedimentary Rocks. Elsevier, Amsterdam, 289–308. https://doi.org/10.1016/B0-08-043751-6/07099-7

Maynard, J.B., 2010. The chemistry of manganese ores through time: a signal of increasing diversity of earth-surface environments. Economic Geology, 105, 535–552. https://doi.org/10.2113/gsecongeo.105.3.535

Merriman, R.J. & Frey, M., 1999. Patterns of very low-grade metamorphism in metapelitic rocks. In Frey, M. & Robinson, D. (eds), Low-Grade Metamorphism. Blackwell Science, Oxford, 61–107. https://doi.org/10.1002/9781444313345.ch3

Merriman, R.J., 2002. Contrasting clay mineral assemblages in British Lower Palaeozoic slate belts: the influence of geotectonic setting. Clay Minerals, 37, 207–219. https://doi.org/10.1180/0009855023720041

Michel, J. & Haesaerts, P., 1975. Le site paléolithique de Franquenies. Helinium, 15, 2009–2036.

Michel, J.-P. & Fairbridge, R.W., 1992. Dictionary of Earth Science – Dictionnaire des Sciences de la Terre. 2nd ed. Masson, Paris & John Wiley & Sons, Chichester, 299 p

Michot, P., 1977. L'Ordovicien de la vallée de la Thyle (Brabant): structure tectonique, stratigraphie et lithologie. Annales de la Société géologique de Belgique, 100, 223–231.

Michot, P., 1980. Le segment tectogénique calédonien belge. Mémoires de la Classe des Sciences, Académie royale de Belgique, Collection in 8°, 2e série, 43, 1–61.

Milodowski, A.E. & Zalasiewicz, J.A., 1991. The origin and sedimentary, diagenetic and metamorphic evolution of chlorite-mica stacks in Llandovery sediments of Central Wales, UK. Geological Magazine, 128, 263–278. https://doi.org/10.1017/S0016756800022111

Mortelmans, G., 1955. Considérations sur la structure tectonique et la stratigraphie du Massif du Brabant. Bulletin de la Société belge de Géologie, de Paléontologie et d'Hydrologie, 64, 179–218.

Mourlon, M., 1893. Carte géologique de la Belgique : Waterloo – La Hulpe 116. 1/40 000. Commission géologique de Belgique, Bruxelles.

Nance, R.D., Neace, E.R., Braid, J.A., Murphy, J.B., Dupuis, N. & Shail, R.K., 2015. Does the Meguma Terrane extend into SW England? Geoscience Canada, 42, 61–76. https://doi.org/10.12789/geocanj.2014.41.056

Okita, P.M., Maynard, J.B., Spiker, E.C. & Force, E.R., 1988. Isotopic evidence for organic matter oxidation by manganese reduction in the formation of stratiform manganese carbonate ore. Geochimica et Cosmochimica Acta, 52, 2679–2685. https://doi.org/10.1016/0016-7037(88)90036-1

Peng, S.C., Babcock, L.E. & Ahlberg, P., 2020. The Cambrian period. In Gradstein, F.M., Ogg, J.G., Schmitz, M.D. & Ogg, G.M. (eds), Geologic Time Scale 2020. Elsevier, Amsterdam, 565–629. https://doi.org/10.1016/B978-0-12-824360-2.00019-X

Piessens, K., De Vos, W., Beckers, R., Vancampenhout, P. & De Ceukelaire, M., 2005. Eindverslag Project VLA03-1.1: Opmaak van de pre-Krijt subcropkaart van het Massief van Brabant voor invoering in de Databank Ondergrond Vlaanderen. Unpublished report for Ministerie van de Vlaamse Gemeenschap, Afdeling Natuurlijke Rijkdommen en Energie, 90 p.

Potdevin, J.-L., Goffette, O. & Lefèvre, C., 1993. Découverte de grenats spessartine-almandin dans l'encaissant du filon de diabase de la Grande Commune (Massif de Rocroi). Origine et implications pour le métamorphisme de l'Ardenne. Comptes rendus de l'Académie des Sciences de Paris, Série II, 316, 1763–1770.

Pingot, J.-L. & Delcambre, B., 2006. Carte géologique de Wallonie : Perwez – Eghezée 40/7-8. 1/25 000. Ministère de la Région wallonne, DGRNE, Namur.

Pothier, H.D., Waldron, J.W.F., Schofield, D.I. & DuFrane, S.A., 2015. Peri-Gondwanan terrane interactions recorded in the Cambrian–Ordovician detrital zircon geochronology of North Wales. Gondwana Research, 28, 987–1001. https://doi.org/10.1016/j.gr.2014.08.009

Pouille, L., 2012. Paléobiodiversité des radiolaires du Paléozoïque inférieur (Cambrien-Ordovicien). Aperçu à travers une étude des assemblages à radiolaires provenant des montagnes de l'Altaï (Russie), d'Aksuran (Kazakstan), du bassin de Georgina (Australie) et de la Terre Neuve occidentale (Canada). Unpublished Ph.D. Thesis, Université de Lille 1, Lille (France).

Prigmore, J.K., Butler, A.J. & Woodcock, N.H., 1997. Rifting during separation of Eastern Avalonia from Gondwana: Evidence from subsidence analysis. Geology, 25, 203–206. https://doi.org/10.1130/0091-7613(1997)025<0203:RDSOEA>2.3.CO;2

Quinby-Hunt, M.S., Wilde, P., Orth, C.J. & Berry, W.B.N., 1989. Elemental geochemistry of black shales–Statistical comparison of low-calcic shales with other shales. In Grauch, R.I. & Leventhal, J.S. (eds), Metalliferous Black Shales and Related Ore Deposits—Program and Abstracts. U.S. Geological Survey Circular, 1037, 8–15.

Ribecai, C. & Vanguestaine, M., 1993. Latest Middle–Late Cambrian acritarchs from Belgium and northern France. Special papers in Palaeontology, 48, 45–55.

Robb, L., 2005. Introduction to Ore-Forming Processes. Blackwell, Malden, MA, 373 p.

Roberts, B., Merriman, R.J., Hirons, S.R., Fletcher, C.J.N. & Wilson, D., 1996. Synchronous very low-grade metamorphism, contraction and inversion in the central part of the Welsh Lower Palaeozoic Basin. Journal of the Geological Society, London, 153, 277–285. https://doi.org/10.1144/gsjgs.153.2.0277

Robinson, D., 1987. Transition from diagenesis to metamorphism in extensional and collision settings. Geology, 15, 866–869. https://doi.org/10.1130/0091-7613(1987)15<866:TFDTMI>2.0.CO;2

Robinson, D. & Bevins, R.E., 1989. Diastathermal (extensional) metamorphism at very low grades and possible high grade analogues. Earth and Planetary Science Letters, 92, 81–88. https://doi.org/10.1016/0012-821X(89)90022-8

Robinson, D., Reverdatto, V.V., Bevins, R.E., Polyansky, O.P. & Sheplev, V.S., 1999. Thermal modelling of convergent and extensional tectonic settings for the development of low-grade metamorphism in the Welsh Basin. Journal of Geophysical Research, B104, 23069–23079. https://doi.org/10.1029/1999JB900172

Rogers, J.J.W. & Adams, J.A.S., 1969. Uranium. In Wedepohl, K.H. (ed.), Handbook of Geochemistry. Vol. II, chap. 92. Springer, Berlin.

Römer, R.L. & Hahne, K., 2010. Life of the Rheic Ocean: scrolling through the shale record. Gondwana Research, 17, 236–253. https://doi.org/10.1016/j.gr.2009.09.004

Ronov, A.B. & Migdisov, A.A., 1996. Time variations in the abundance of rocks, minerals and elements in the Russian platform sediment cover. Geochemistry International, 33, 30–63.

Roth, S., 2007. Geochemical signature of rocks and weathering products in Luxembourg. Publications du Service géologique du Luxembourg, 31, 139 p.

Saltzman, M.R., Edwards, C.T., Adrain, J.M. & Westrop, S.R., 2015. Persistent oceanic anoxia and elevated extinction rates separate the Cambrian and Ordovician radiations. Geology, 43, 807–810. https://doi.org/10.1130/G36814.1

Sassi, F.P. & Scolari, A., 1974. The b_0 value of the potassic white micas as a barometric indicator in low-grade metamorphism of pelitic schists. Contribution to Mineralogy and Petrology, 45, 143–152. https://doi.org/10.1007/BF00371166

Schovsbo, N.H., 2002. Uranium enrichment shorewards in black shales: A case study from the Scandinavian Alum Shale. Journal of the Geological Society of Sweden, 124, 107–115. https://doi.org/10.1080/11035890201242107

Schreyer, W., Bernhardt, H.-J. & Medenbach, O., 1992. Petrologic evidence for a rhodochrosite precursor of spessartine in coticules of the Venn-Stavelot Massif, Belgium. Mineralogical Magazine, 56, 527–532. https://doi.org/10.1180/minmag.1992.056.385.08

Schulz, H-M., Yang, S., Schovsbo, N.H., Rybacki, E., Ghanizadeh, A., Bernard, S., Mahlstedt, N., Krüger, M., Amann-Hildebrandt, A., Krooss, B.M., Meier, T. & Reinicke, A., 2021. The Furongian to Lower Ordovician Alum Shale Formation in conventional and unconventional petroleum systems in the Baltic Basin – A review. Earth-Science Reviews, 218, 103674. https://doi.org/10.1016/j.earscirev.2021.103674

Sintubin, M., 1997. Structural implications of the aeromagnetic lineament geometry in the Lower Paleozoic Brabant Massif (Belgium). Aardkundige Mededelingen, 8, 165–168.

Sintubin, M., 1999. Arcuate fold and cleavage patterns in the southeastern part of the Anglo–Brabant Fold Belt (Belgium): tectonic implications. Tectonophysics, 309, 81–97. https://doi.org/10.1016/S0040-1951(99)00133-X

Stainier, X., 1890. Compte rendu de la réunion extraordinaire de la Société géologique de Belgique dans le Brabant méridional, du 7 au 10 septembre 1889. Annales de la Société géologique de Belgique, 17, 29–55.

Stow, D.A.V. & Piper, D.J.W., 1984. Deep-water fine-grained sediments: facies models. In Stow, D.A.V. & Piper, D.J.W. (eds), Fine-grained sediments: Deep-water processes and facies. Geological Society, London, Special Publications, 15, 611–646. https://doi.org/10.1144/GSL.SP.1984.015.01.38

Stow, D. & Smillie, Z., 2020. Distinguishing between deep-water sediments facies: turbidites, contourites and hemipelagites. Geosciences, 10, 68. https://doi.org/10.3390/geosciences10020068

Stryckmans, O., 1989. Etude géochimique du Massif du Brabant (Belgique). Unpublished Master Thesis, Université Libre de Bruxelles, Bruxelles, 116 p.

Theunissen, K., 1970. L'andalousite et ses phases de transformation dans la région de Vielsalm. Annales de la Société géologique de Belgique, 93, 363–382.

Theye, T., Schreyer, W. & Fransolet, A.-M., 1996. Low-temperature, low-pressure metamorphism of Mn-rich rocks in the Lienne Syncline, Venn–Stavelot Massif (Belgian Ardennes), and the role of carpholite. Journal of Petrology, 37, 767–783. https://doi.org/10.1093/petrology/37.4.767

Tolmacheva, T.J., Danelian, T. & Popov, L.E., 2001. Evidence for 15 m.y. of continuous deep-sea biogenic siliceous sedimentation in early Paleozoic oceans. Geology, 29, 755–758. https://doi.org/10.1130/0091-7613(2001)029<0755:EFMYOC>2.0.CO;2

Tondeur, F., 1998. Mesures de radon dans les bâtiments par les laboratoires belges : résultats d'intercomparaisons et de campagnes de mesures menées depuis 1993. Annales de l'Association belge de Radioprotection, 23, 175–201.

Tondeur, F., Gerardy, I., Couwenbergh, C., Herbosch, A. & Festraets, M., 2001. Search and mapping of small radon-prone areas in Walloon Brabant (Belgium) on a geological basis. Proceedings of the 3rd Eurosymposium on Protection against Radon. AIM, Liège, 171–174.

Tondeur, F., Cinelli, G. & Dehandschutter, B., 2014. Homogenity of geological units with respect to the radon risk in the Walloon region of Belgium. Journal of Environmental Radioactivity, 136, 140–151. https://doi.org/10.1016/j.jenvrad.2014.05.015

Tondeur, F., Cinelli, G. & Dehandschutter, B., 2015. High radon areas in the Walloon region of Belgium. Radiation Protection Dosimetry, 164, 563–568. https://doi.org/10.1093/rpd/ncv312

Vandenberghe, N., Laga, P., Steurbaut, E., Hardenbol, J. & Vail, P.R., 1999. Tertiary sequence stratigraphy at the southern border of the North Sea Basin in Belgium. In de Graciansky, P.-C., Hardenbol, J.,

Jacquin, T. & Vail, P.R. (eds), Mesozoic and Cenozoic Sequence Stratigraphy of European Basins. SEMP Society for Sedimentary Sedimentology, Special Publications, 60, 119–154. https://doi.org/10.2110/pec.98.02.0119

Vander Auwera, J. & André, L., 1985. Sur le milieu de dépôt, l'origine des matériaux et le faciès métamorphique de l'Assise de Tubize (Massif du Brabant, Belgique). Bulletin de la Société belge de Géologie, 94, 171–184.

Van der Sluys, J., 1990. Onderzoek naar mogelijk herkomstgebieden en studie van oppervlaktekenmerken van enkele zware mineralen uit belgische Meso-Cenozoische sedimenten. Unpublished Ph.D. Thesis. Rijksuniversiteit Gent, Gent, 110 p.

Van der Sluys, J., 1991. Detrital heavy minerals as provenance indicators of Belgian Mezo-Cenozoic sediments. Bulletin de la Société belge de Géologie, 100, 177–193.

Van Grootel, G., Verniers, J., Geerkens, B., Laduron, D., Verhaeren, M., Hertogen, J. & De Vos, W., 1997. Timing of magmatism, foreland basin development, metamorphism and inversion in the Anglo-Brabant fold belt. Geological Magazine, 134, 607–616. https://doi.org/10.1017/S0016756897007413

Vanguestaine, M., 1974. Espèces zonales d'acritarches du Cambro-Trémadocien de Belgique et de l'Ardenne française. Review of Palaeobotany and Palynology, 18, 63–82. https://doi.org/10.1016/0034-6667(74)90010-4

Vanguestaine, M., 1977. Données palynologiques nouvelles dans l'Ordovicien inférieur du bassin de la Senne, Massif du Brabant, Belgique. Annales de la Société géologique de Belgique, 100, 193–198.

Vanguestaine, M., 1992. Biostratigraphie par acritarches du Cambro-Ordovicien de Belgique et des régions limitrophes : synthèse et perspectives d'avenir. Annales de la Société géologique de Belgique, 115, 1–18.

Vanguestaine, M., Chakir, A. & Servais, T., 1989a. Cambrian (?) and Ordovician acritarchs from the Thyle valley. International Meeting of the Caledonides of the Midlands and the Brabant Massif, Brussels, 20–23 sept. 1989. Abstracts, 45.

Vanguestaine, M., Servais, T. & Steemans, Ph., 1989b. Biostratigraphy of 28 boreholes in the Brabant Massif. International Meeting of the Caledonides of the Midlands and the Brabant Massif, Brussels, 20–23 sept. 1989. Abstracts, 46.

Van Tassel, R., 1986. Contribution à la lithologie du segment calédonien des vallées de la Dyle et de la Thyle, Brabant, Belgique. Aardkundige Mededelingen, 3, 239–268.

Verniers, J., Herbosch, A., Vanguestaine, M., Geukens, F., Delcambre, B. Pingot, J.-L., Belanger, I, Hennebert, M., Debacker, T., Sintubin, M. & De Vos, W., 2001. Cambrian-Ordovician-Silurian lithostratigraphic units (Belgium). Geologica Belgica, 4, 5–38. https://doi.org/10.20341/gb.2014.042

Verniers, J., Pharaoh, T.C., Andre, L., Debacker, T., De Vos, W., Everaerts, M., Herbosch, A., Samuelsson, J., Sintubin, M. & Vecoli, M., 2002. The Cambrian to mid Devonian basin development and deformation history of Eastern Avalonia, east of the Midlands Microcraton: new data and a review. In Winchester, J.A., Pharaoh, T.C. & Verniers, J. (eds), Palaeozoic Amalgamation of Central Europe. The Geological Society, London, Special Publications, 201, 47–93. https://doi.org/10.1144/GSL.SP.2002.201.01.04

Vine, J.D. & Tourtelot, E.B., 1970. Geochemistry of black shale deposits—A summary report. Economic Geology, 65, 253–272. https://doi.org/10.2113/gsecongeo.65.3.253

Waldron, J.W.F., Schofield, D.I., White, C.E. & Barr, S.M., 2011. Cambrian successions of the Meguma Terrane, Nova Scotia, and Harlech Dome, North Wales: dispersed fragment of a peri-Gondwanan basin? Journal of the Geological Society, London, 168, 83–98. https://doi.org/10.1144/0016-76492010-068

Walraevens, P., 1982. Levé magnétique du compartiment de schistes à magnétite devilliens de Ways-Ruart. Unpublished Master Thesis, Université Libre de Bruxelles, Bruxelles, 104 p.

Wang, W. & Servais, T., 2015. A re-investigation of the *Rhabdinopora flabelliformis* fauna from the early Tremadocian 'Dictyonema Shale' in Belgium. Geologica Belgica, 18, 66–77.

Warr, L.N., Primmer, T.J. & Robinson, D., 1991. Variscan very low-grade metamorphism in southwest England: a diasthermal and thrust-related origin. Journal of Metamorphic Geology, 9, 751–764. https://doi.org/10.1111/j.1525-1314.1991.tb00563.x

Webby, B.D., Cooper, R.A., Bergström, S.M. & Paris, F., 2004. Stratigraphic framework and time slices. In Webby, B.D., Paris, F., Droser, M.L. & Percival, I.G. (eds), The Great Ordovician Biodiversification Event. Columbia University Press, New York, 41–47. https://doi.org/10.7312/webb12678-003

Woodcock, N.H., 1990. Sequence stratigraphy of the Palaeozoic Welsh Basin. Journal of the Geological Society, London, 147, 537–547. https://doi.org/10.1144/gsjgs.147.3.0537

Woodcock, N.H., 1991. The Welsh, Anglian and Belgian Caledonides compared. Annales de la Société géologique de Belgique, 114, 5–17.

Woodcock, N.H. & Soper, N.J., 2006. The Acadian Orogeny: the mid-Devonian phase of deformation that formed slate belts in England and Wales. In Brenchley, P.J. & Rawson P.F. (eds), The Geology of England and Wales. 2nd ed. Geological Society, London, 131–146.

Yavuz, F., Kumral, M., Karakaya, N. & Karakaya, M.C., 2015. A Windows program for chlorite calculation and classification. Computers & Geosciences, 81, 101–113. https://doi.org/10.1016/j.cageo.2015.04.011

Zane, A. & Weiss, Z., 1998. A procedure for classifying rock-forming chlorites based on microprobe data. Rendiconti Lincei, Scienze Fisiche e Naturali, 9, 51–56. https://doi.org/10.1007/BF02904455

Appendix 1. Cored borehole information

Bousval borehole 39/8-197
Drilling: vertical, May 1966.
Location: Ri Cala valley, to the NW of "ferme de l'Alfère". N 50°38'02"/ E 4°30'06" Z 108 m.
Depth: 50 m of which 13.2 m in the Bruxelles Fm and 36.8 m in the Mousty Fm.
Description: see log in Legrand (1966). The dip in the first 13 m is about 70°. Mainly grey-black "quartzophyllades", "phyllades", "phyllades zonaires", slate, pyritic black "phyllades", quartzites. The rocks are highly weathered even at a depth of 50 m.
Biostratigraphy: "Acritarchs compatible with Mousty Fm lithology have been found but are of no stratigraphic significance" (Vanguestaine, 1992, p. 8).
Storage: partial in Geological Survey of Belgium, Brussels.

Tangissart Borehole 39/8-419
Drilling: vertical, May 1995.
Location: 10 m E of Tangissart railway crossing, E-side of the Thyle valley.
Lambert coordinates: X 161800 Y 143920. N 50°36'21.83"/E 4°32'14.87 Z 88 m.
Depth: 49.60 m; upper part of MF in the anticlinal dome of "Bois Ste Catherine".
Storage: complete in the Belgian Geological Survey, Brussels.
Description: short description by A. Herbosch, 1995, unpublished:
  - 3.05–2.40 m: black slate severely altered. Dip subvertical
  - 16.47–17.90 m: finely laminar black slate with pyrite, severely altered. Dip 30–40°
  - 19.40–20.90 m: black slate particularly dark, weathered patches. Dip 30–40°
  - 25.50–27.00 m: zoned black slate with black filaments. Dip subvertical
  - 27.00–28.42 m: black slate with cm rhythmic laminations. Quartz vein 1 cm. Broken and weathered. Dip vertical
  - 28.42–29.90 m: cm laminar black slate with black filaments and pyrite. Dip 45°
  - 29.90–31.40 m: black slate with low-density turbidite structure, locally brecciated. Some slump. Dip 30–40°
  - 31.40–32.95 m: black slate with low-density turbidite structure. Dip 30°
  - 32.95–34.45 m: black slate with low-density turbidite structure, pyrite. Dip horizontal
  - 34.45–35.95 m: black slate particularly dark, cm pyrite layers. Dip heckled 40–60°
  - 35.95–37.45 m: black slate with cm layers of pyrite. Dip 50–60°
  - 37.45–38.95 m: black slate with pyrite then low-density turbidite. Dip 10–20°
  - 38.95–40.45 m: black slate with low-density turbidite structure. Dip 30–40°
  - 40.45–41.95 m: particularly dark black slate. Quartz vein 5 cm. Dip low
  - 41.95–42.95 m: particularly dark massive black slate
  - 42.95–44.15 m: particularly dark massive black slate. Dip low
  - 44.15–45.80 m: dark massive black slate with pyrite
  - 45.80–48.00 m: dark grey-black slate, some brecciation. Dip low
  - 48.00–49.60 m: black slate with alternating black and grey facies. Some slump.

Noirhat borehole 39/8-418
Drilling: vertical, September 1996.
Location: in "Bois de Noirhat" E-side of the Dyle valley. Along a parallel path W of the Ravel.
Lambert coordinates: X 161890 Y 146630. N 50°37'48"/E 4°32'09" Z 79 m.
Depth: 50 m in the middle (?) part of the Mousty Fm.
Description: not done.
Storage: complete in the Belgian Geological Survey, Brussels.

Court-St-Etienne borehole 40/5-540
Drilling: oblique drilling at 45° S, November–December 1998.
Location: Court-St-Etienne, in meadows on the hill 50 m S of the Avenue des Prisonniers de Guerre, almost opposite to the Institut St Etienne. See Fig. 5 for location. N 50°38'38"/E 4°33'44" Z 83 m.
Description: Simplified lithological log (Fig. 6B) made for this paper from a detailed description by Delcambre, Herbosch & Pingot (2000, unpublished).
Storage: complete in the Université Catholique de Louvain, Louvain-la-Neuve, Belgium.